UNIVERSITY OF SOUTHAMPTON

FACULTY OF ENGINEERING, SCIENCE & MATHEMATICS

OPTOELECTRONICS RESEARCH CENTRE

DEVELOPMENT OF GERMANIUM BASED SULPHIDE GLASS BY CHEMICAL VAPOUR DEPOSITION (CVD)

by

Chung-Che Huang

Thesis submitted for the degree of Doctor of Philosophy

June 2005

UNIVERSITY OF SOUTHAMPTON

ABSTRACT

FACULTY OF ENGINEERING, SCIENCE & MATHEMATICS

OPTOELECTRONICS RESEARCH CENTRE

Doctor of Philosophy

DEVELOPMENT OF GERMANIUM BASED SULPHIDE GLASS BY CHEMICAL VAPOUR DEPOSITION (CVD)

by Chung-Che Huang

Chalcogenide glasses, especially sulphide glasses, are becoming more and more important for the fabrication of optoelectronic devices in part because of the high nonlinearity, strong photosensitivity and several other unique properties they have. Chalcogenide glasses are normally fabricated by a conventional melt-quenching method. The glasses are then further processed to form, for example, thin films, optical fibre and optoelectronic devices.

Germanium sulphide glass thin films have been directly deposited on a variety of substrates by means of chemical vapour deposition (CVD). The deposition rate of germanium sulphide glass film by this CVD process is estimated to be about 12 μm/hr at 500°C. These films have been characterized by micro-Raman spectroscopy, X-ray diffraction (XRD), and scanning electron microscopy (SEM). The refractive index of germanium sulphide glass film, measured by both the prism coupling technique and the single transmission technique were 2.093±0.008 at 632.8nm and 2.107±0.003 at 642nm respectively. The propagation loss of a germanium sulphide waveguide on a Schott N-PSK58 substrate, measured at 632.8nm by a He-Ne laser was 2.1±0.3 dB/cm. Germanium sulphide glass planar waveguide with rib structures have been fabricated by a photolithography and argon ion-beam milling process. Germanium sulphide glass films have also been deposited on some commercial silicon wafers with buffer layers such as SiO_2 and GeO_2. In addition, Ag-doped germanium sulphide glass channel waveguides, fabricated by the thermal evaporation, photolithography, and photo-dissolution process, with the propagation loss of 0.67±0.05 dB/cm at 632.8nm have been demonstrated.

High purity germanium sulphide bulk glass has also been fabricated by this CVD process. The optical and thermal properties of this glass have been investigated. The transmission range of this glass extends from 0.5 μm to 10.5 μm, as measured by UV-VIS-NIR and FT-IR spectroscopy. The thermal properties, studied by DTA and TMA, certify that this stable glass has a glass transition temperature (T_g) of 456 °C, an onset of crystallization temperature (T_x) of 620 °C, a melting temperature (T_m) of 715 °C, and a coefficient of thermal expansion (CTE) of 12.9×10^{-6}/°C. The purity of germanium sulphide bulk glass bas been determined by a glow discharge mass spectrometry (GDMS) technique and an exceptionally low level of transition metal impurities in this glass have been achieved.

Table of Contents

DECLARATION OF AUTHORSHIP

I, **CHUNG-CHE HUANG,** declare that the thesis entitled

"DEVELOPMENT OF GERMANIUM BASED SULPHIDE GLASSES BY CHEMICAL VAPOUR DEPOSITION (CVD)"

and the work presented in it are my own. I confirm that:

- this work was done wholly or mainly while in candidature for a research degree at this University;
- where any part of this thesis has previously been submitted for a degree or any other qualification at this University or any other institution, this has been clearly stated;
- where I have consulted the published work of others, this is always clearly attributed;
- where I have quoted from the work of others, the source is always given. With the exception of such quotations, this thesis is entirely my own work;
- I have acknowledged all main sources of help;
- where the thesis is based on work done by myself jointly with others, I have made clear exactly what was done by others and what I have contributed myself;
- parts of this work has been published before submission as:

Publications:

[1] C. C. Huang, D. W. Hewak, and J. V. Badding, "Deposition and characterization of germanium sulphide glass planar waveguides", Optics Express, **12** (2004) 2501-2505.

[2] C.C. Huang, D.W. Hewak, "High purity germanium sulphide glass for optoelectronic applications synthesized by chemical vapour deposition", Electronics Letters, **40** (2004) 863-865.

[3] C.C. Huang, D.W. Hewak, and J.V. Badding, "Direct synthesis of germanium sulphide glass planar waveguides by chemical vapour deposition (CVD)", CLEO/IQEC 2004 San Francisco 16-21 May 2004.

[4] R.J. Curry, A.K. Mairaj, C.C. Huang, R.W. Eason, C. Grivas, J.V. Badding, D.W. Hewak, "Chalcogenide glass thin films and planar waveguides", Journal of American Ceramic Society, 2004 (accepted).

[5] R.J. Curry, C.C. Huang, A.K. Mairaj, R.E. Simpson, D.W. Hewak, "Advancing the application of planar chalcogenides", AcerS. Glass & Optical Materials Div., Fall 2004 Meeting Florida Nov 2004.

[6] A.K. Mairaj, C.C. Huang, R.J. Curry, R.W. Eason, C. Grivas, J.V. Badding, D.W. Hewak, "Through thick and thin: recent developments with chalcogenide films", The American Ceramic Society: Glass and Optical Materials Division Fall Meeting Corning 12-15 Oct 2003 (invited).

[7] C. C. Huang, D. W. Hewak, and J. V. Badding, "Properties and application of germanium sulphide glass", PREP 2003 Exeter 14-16 Apr 2003.

Patents:

[1] D.W. Hewak, C.C. Huang, J.V. Badding, "Synthesis of germanium sulphide and related compounds", (filed).

Signed: .....

Date: .....

ACKNOWLEDGEMENTS

I would like to sincerely thank my supervisor, Dr. Dan Hewak, for his support, patience and guidance through my research project and for the opportunity to work in such a stimulating environment. I am also grateful to Dr. John Badding for his help on the CVD experiments and all the members who have helped me at the Optoelectronics Research Centre. A particular thank must go to Dr. Eleanor Tarbox for her suggestions on my thesis.

Finally, I am grateful to have my family accompanying me during the study of my PhD. The encouragement and the endless love from my wife, Grace Hsiu-Mei LIU, have made me carefree regarding my two children, Mike and Emmy, and my research. Also, I would like to thank my parents for their fully support.

Chapter 1

Introduction

1.1 Motivation

Telecommunications has proved itself as one of the key technologies to emerge out of the 20th century. The pressure to fully exploit the bandwidth capability of silica optical fibre remains intense and devices such as optical switches, modulators, transmitters and receivers are required to realise this. The ultimate goal is to produce all optical integrated circuits (OICs) that contain the above devices on a single substrate, enabling high functionality and low cost [1-2].

An optical integrated circuit is a thin-film-type optical circuit designed to perform a function by integrating a laser diode light source, functional components such as switches/modulators, interconnecting waveguides, and photodiode detectors, all on a single substrate. Through integration, a more compact, stable, and functional optical system can be produced. Since the key components are slab or channel waveguides for OICs applications, a key objective of this thesis is to discover how to design and fabricate good waveguides using the right materials and processes.

There are several approaches aimed at producing OICs, using materials that include silica, silicon and optically active polymers. To date there is no ideal solution to the problem. All glass OICs have advantages over silicon and polymer approaches including an increased transparency and a high optical damage threshold. However, finding a suitable glass with the properties required, such as the ability

to host rare earth ions or provide a high non-linearity, has proved difficult.

One such family of glasses, providing glass that appears to be a suitable candidate for producing OICs, are the chalcogenides, and in particular, a germanium sulphide glass investigated by this research work. This glass is an amorphous semiconductor with an absorption edge at ~425nm (2.9 eV). Its properties include a low-phonon energy, the ability to incorporate rare earth ions, low-toxicity, high glass transition temperature, and superb photo-modification characteristics. These properties, together with high non-linearity and well documented spectroscopic properties make it an excellent candidate for research into planar channel waveguide structures and active telecommunications devices.

Another application for planar germanium sulphide devices utilises the low phonon energy of this glass, which enables transmission from 0.5µm through to 10.5µm. The optical third-order nonlinearity of germanium sulphide glass (~7.5×10^{-5} cm^2/GW) was measured by D. Marchese *et al.* [3], making this glass one of the best candidates for ultra-fast nonlinear optical applications.

Chalcogenide glasses are normally fabricated by a conventional melt-quenching method [4, 5]. The glasses are then further processed to form, for example, thin films, optical fibre and optoelectronic devices. Thin films of chalcogenide glass can also be deposited by a number of methods including evaporation [6], sputtering [7] and ablation [8]. These techniques in general suffer from difficulties associated with the incorporation of impurities or non-stoichiometry. Sol-gel techniques can be used for the fabrication of sulphide glass

waveguides [9], but these materials are often contaminated by oxide impurities.

Chemical vapour deposition (CVD) has proved to be highly advantageous for the fabrication of ultra high purity silica glass fiber preforms. It would be desirable to find an analogous approach for the fabrication of chalcogenide materials and there has been considerable work devoted to this objective [10], although no suitable process has been reported. Reaction between germanium chloride ($GeCl_4$) and hydrogen sulphide (H_2S) to form germanium sulphide (GeS_2), for example, was reported to be unsatisfactory for the fabrication of planar or preform structures because of a low reaction rate and a low yield of deposited product. Another approach to form germanium sulphide films by plasma-enhanced CVD [11] reported the production of unstable films, easily oxidized in air, fabricated through the reaction between GeH_4 and H_2S.

The synthesis of chalcogenide glass using CVD techniques has not been widely reported. Therefore, with an available source of the high purity germanium chloride (99.9999%) and the ability to melt in a reactive atmosphere of H_2S available in our laboratory, we began to review the reaction between $GeCl_4$ and H_2S to form GeS_2. A thermodynamic analysis indicates that this reaction should be favoured and therefore preliminary tests were undertaken. The ability to fabricate thin films of chalcogenide is increasingly of interest, and the promise of practical planar integrated devices motivated this work [12-13].

1.2 Project aim

The objective of this research work is to develop waveguide devices for planar or fibre applications directly by means of chemical vapour deposition (CVD). The challenges in the research required encompassed materials science, mechanical engineering, semiconductor fabrication, and characterization techniques.

Germanium sulphide glass with the excellent properties, such as non-toxicity, high transition temperature, good rare-earth solubility, low phonon energy, high refractive index, high non-linearity, photo-modification characteristics, and well documented spectroscopy, make it an outstanding candidate for research into fibre and planar waveguide applications [4, 5]. However, to date, there is still no reported chalcogenide planar waveguide fabricated directly by means of CVD. Therefore, the main objective is to develop a reliable CVD process for the fabrication of a germanium sulphide glass planar waveguide. In addition, it would be more desirable to apply the CVD process to the fabrication of high purity germanium sulphide bulk glasses or, ultimately, fibre preforms.

1.3 Thesis synopsis

This thesis describes the original research in design, fabrication, and characterization of germanium based sulphide glass planar waveguide and bulk glass by means of chemical vapour deposition (CVD). This chapter has presented the motivation and aims of the project.

Chapter 2 reviews the literature including the planar waveguide fabrication techniques, channel waveguide fabrication techniques, and applications based on chalcogenide glasses.

Chapter 3 discusses the attempt to fabricate chalcogenide based glass by a sol-gel technique. However, with the success in the CVD process, the sol-gel work has been suspended and the research will focus on the CVD technique.

Chapter 4 reviews the fundamentals of CVD techniques, including the thermodynamics of CVD, kinetics and mass-transport mechanisms, CVD systems, precursors, and gas purification systems.

Chapter 5 discusses the fabrication and characterization of germanium sulphide glass planar waveguides by CVD. First, the thermodynamic analysis of the formation of germanium sulphide glass from the reaction between $GeCl_4$ and H_2S has been investigated, which reveals that the CVD process is feasible and has a higher yield at higher temperatures. The parameters, such as flow rate, temperature, molar ratio of $H_2S/GeCl_4$, and substrate selection, of CVD experiments have been optimized. The germanium sulphide glass films have been characterization by micro-Raman, X-ray diffraction (XRD), and scanning electron microscopy (SEM) with energy dispersion X-ray analysis (EDX). The refractive index of germanium sulphide glass films have been investigated by the prism coupling and the single transmission techniques. The first planar waveguide based on chalcogenide glass made by the CVD technique and the propagation loss of the germanium sulphide glass planar waveguide have been studied. Besides, a germanium sulphide glass waveguide with channel

structures has been fabricated using the CVD, photolithography, and dry-etching techniques.

Chapter 6 involves the fabrication and characterization of germanium sulphide bulk glass by the CVD process. The original design of the CVD reactor has been presented and the yield of the CVD process has been estimated. The optical properties of germanium sulphide bulk glass have been studied by UV-VIS-NIR and FT-IR spectroscopy. The thermal properties of germanium sulphide bulk glass have been investigated by DTA and TMA techniques. The purity of this glass fabricated by the CVD process has been measured by glow discharge mass spectrometry (GDMS) by an independent laboratory.

Chapter 7 reports an extended application based on germanium sulphide glass planar waveguides. With the incorporation of silver into germanium sulphide glass film by a photo-dissolution process, the increased refractive index of Ag-doped germanium sulphide glass films have been measured by a single transmission technique. In addition, the Ag-doped germanium sulphide glass channel waveguides have been fabricated by photolithography, thermal evaporation, and photo-dissolution technique and the propagation loss of the channel waveguides has been estimated.

Chapter 8 is a comprehensive summary of the contents of this thesis and suggests the possible areas for future research and advancement of the technology.

1.4 References

[1] S.E. Miller, “Integrated Optics: An Introduction”, The Bell System Technical Journal, **48** (1969) 2059.

[2] Chao-Yi Tai, PhD thesis, “Tantalum Pentoxide Waveguides for Photonic Crystal Circuits”, 2004, University of Southampton.

[3] D. Marchese, M. De Sario, A. Jha, A. K. Kar, E. C. Smith, "Highly nonlinear GeS_2-based chalcogenide glass for all-optical twin-core-fibre switching", J. Optical Society of America, **15** (1998) 2361.

[4] T. Katsuyama and H. Matsumura, “Infrared Optical Fibers”, Adam Hilger, 1989.

[5] J.S. Sanghera and I.D. Aggarwal, “Infrared Fiber Optics”, CRC Press, 1998.

[6] E. Marquez, T. Wagner, J.M. Gonzalez-Leal, A.M. Bernal-Oliva, R. Prieto-Alcon, R. Jimenez-Garay, P.J.S. Ewen, "Controlling the optical constant of thermally-evaporated $Ge_{10}Sb_{30}S_{60}$ chalcogenide glass films by photodoping with silver", J. Non-Cryst. Solids, **274** (2000) 62-68.

[7] S. Ramachandran, S.G. Bishop, "Excitation of Er^{3+} emission by host glass absorption in sputtered films of Er-doped $Ge_{10}As_{40}Se_{25}S_{25}$ glass", Appl. Phys. Lett. **73**, (1998) 3196-3198.

[8] D.S. Gill, R.W. Eason, C. Zaldo, H.N. Rutt, N.A. Vainos, "Characterisation of Ga-La-S chalcogenide glass thin-film optical waveguides, fabricated by pulsed laser deposition", J. Non-Cryst. Solids, **191** (1995) 321-326.

[9] J. Xu and R.M. Almeida, "Preparation and Characterization of Germanium Sulphide Based Sol-Gel Planar Waveguides", J. Sol-Gel Science and Technology, **19** (2000) 243-248.

[10] P. J. Melling, "Alternative Methods of Preparing Chalcogenide Glasses", Ceramic Bulletin, **63** (1984) 1427-1429.

[11] E. Sleeckx, P. Nagels, R. Callaerts and M. Vanroy, "Plasma-enhanced CVD of amorphous Ge_xS_{1-x} and Ge_xSe_{1-x} films", J. de Physique IV, **3** (1993) 419-426.

[12] Keiji Tanaka, "Photoinduced process in Chalcogenide glass", Current Opinion in Solid State & Materials Science, **1** (1996) 567.

[13] A.V. Kolobov, "Photo-induced Metastability in Amorphous Semiconductors", Wiley-VCH, 2003.

Chapter 2

Literature Review

The optical integrated circuit (OIC) has attracted increasing attention, originally as the key component in an optical computer and laser beam circuitry for telecommunications [1, 2] and today for an increasingly wide range of devices, for example, optical sensors, amplifier and laser, and nonlinear switches. An optical integrated circuit is a thin-film-type optical circuit designed to perform a function by integrating a laser diode light source, functional components such as switches/modulators, interconnecting waveguides, and photodiode detectors, all on a single substrate. Through integration, a more compact, stable, and functional optical system can be produced. The key components are slab [two-dimensional (2-D)] or channel [three dimensional (3-D)] waveguides. Therefore, the important point, and a key objective of this thesis, is how to design and fabricate reliable waveguides using the right materials and processes.

In order to investigate the potential of the planar waveguide applications and develop improved materials and processes, the fabrication techniques of planar waveguides and channel waveguides will first be reviewed. We will focus on applications based on chalcogenide glasses, whose properties are particularly promising for the next generation of optoelectronic devices. These glasses are low-phonon-energy materials and are generally transparent from the visible up to infrared. Chalcogenide glasses can be doped by rare-earth elements, such as Er, Nd, Pr, etc., and hence numerous applications of active optical devices have been proposed. These glasses are optically highly non-linear and could therefore be useful for all-optical switching

(AOS). Chalcogenide glasses are sensitive to the absorption of electromagnetic radiation and show a variety of photoinduced effects as a result of illumination [3].

2.1 Planar/Slab optical waveguides fabrication techniques for glass

Thin-film science and technologies play an important role in many industries, not only in optoelectronics, but also in many high technology deposition processes which had their origin in such basic technologies as anti-reflection coatings and anti-wear coatings. There are two main processes, physical deposition and chemical deposition, to make a glass thin-film on a substrate. This chapter is divided into sections, physical and chemical deposition, which provides a convenient method of categorising the wide range of processes. In the physical deposition section, thermal evaporation, sputtering, pulsed laser deposition (PLD) or laser ablation, and spin & dip coating will be reviewed. In chemical deposition section, the sol-gel process (Sol-Gel), liquid-phase deposition (LPD), flame hydrolysis deposition (FHD), and chemical vapour deposition (CVD) will also be discussed.

2.1.1 Physical depositions

Physical deposition techniques including thermal evaporation, sputtering, pulsed laser deposition (PLD) or laser ablation, and spin & dip coating, will be discussed in the context of their use in the preparation of planar optical waveguides.

2.1.1.1 Thermal evaporation technique

Deposition of thin films by evaporation is very simple and convenient, and is one of the most widely used techniques. It is only necessary to produce a vacuum environment in which a sufficient amount of heat is given to the evaporant to attain the vapour pressure required for evaporation; the evaporated materials are then allowed to condense on a substrate kept at a suitable temperature.

A normal thermal deposition process consists of three distinguishable steps.

1. Transition of the condensed phase (solid or liquid) into the gaseous state.
2. Transport of vapour from the source to the substrate.
3. Deposition of these evaporated particles on the substrate.

Substrates are made from a wide variety of materials and may be kept at a temperature that depends on the film properties that are required. When evaporation is made in vacuum, the evaporation temperature will be considerably lowered and the formation of oxides and incorporation of impurities in the growing layer will be reduced. The most commonly used heating method for evaporation is resistive heating. The material to be evaporated is raised in temperature by electrical resistance heating within the wire spirals, or a crucible, made of tungsten, tantalum, or molybdenum. The pressure used for normal evaporation work is about 10^{-5} torr. This also ensures a straight line path for most of the emitted vapour atoms, for a substrate-to source distance of approximately 10-50 cm in a vacuum system.

Many compounds, such as SiO_2, MgF_2, Si_3N_4, HfC, SnO_2, BN, PbS, and VO_2, often vaporize with a range of species from atoms, to clusters of molecules, to dissociated or partially dissociated molecules. For example, in the thermal evaporation of SiO_2, a number of species are formed in addition to SiO_2, for example, $(SiO_2)_x$, SiO_{2-x}, SiO, Si, O, etc. The degree of dissociation is strongly dependent on the temperature and composition of the compound [4]. Furthermore, thermal evaporation is one of the most common techniques to prepare thin-film chalcogenide materials. A wide range of chalcogenide thin films have been prepared by this technique in [5-14].

2.1.1.2 Sputtering technique

It has long been known that when a surface is bombarded with high velocity positive ions, it is possible to cause the ejection of atoms. This process of ejecting atoms from the surface by the bombardment of positive ions, usually inert, is commonly known as sputtering or sputter deposition. The ejected atoms can be made to condense on a substrate to form a thin film. Some of sputtering systems typically used are ion beam sputtering, magnetron sputtering, unbalanced magnetron sputtering, and RF sputtering [15].

Sputter deposition can be used to deposit films of compound materials either by sputtering from a compound or by sputtering from an elemental target in a partial pressure of a reactive gas (i.e., reactive sputter deposition). In most case, sputter deposition of a compound material from a compound target results in a loss of some of the more volatile material (e.g., oxygen from SiO_2, sulphur from S-based chalcogenides) and this loss is often compensated by deposition in an atmosphere containing a partial pressure of the reactive gas in a

process called quasi-reactive sputter deposition. In this technique, the partial pressure of reactive gas that is needed is less than that used for reactive sputter deposition. The technique also has been applied to fabricate oxide-based planar waveguides [16-21] and chalcogenide thin films [22] and waveguides [23].

2.1.1.3 Pulsed laser deposition (PLD) or laser ablation technique

Pulsed laser deposition (PLD) has been extensively studied within the past decade because it is a relatively fast, simple, and flexible technique for growing thin films of a variety of materials. This method is based on rapid evaporation by means of high power laser pulses and the subsequent condensation of the ablated material onto a substrate. Amorphous, polycrystalline, and single crystal layers are grown, depending on experimental parameters that included target composition, substrate temperature, target-substrate distance, and the presence of a reactive/inert gas. Recent successes in crystalline growth by PLD have permitted the demonstration of efficient lasing action in a 2-10 μm thick layer of gadolinium gallium garnet, GGG, grown on YAG [24 ,25], and also Ti:sapphire, grown on undoped sapphire [26]. The loss reported by Anderson *et al.* [25] is 0.3-0.5 dB/cm. However, glasses are more difficult to grow by using PLD. Several early attempts to grow both silicate and phosphate glasses resulted in films which were opaque and diffuse in character, and under microscopic examination, revealed a structure composed of few μm sized particles. No smooth, continuous and transparent films could be grown by PLD. The underlying reasons for this are likely to be due to the extremely non-equilibrium nature of PLD, when compared to other existing methods for glass fabrication. The PLD technique has been applied to the gallium lanthanum sulphide (GLS) glass thin films deposition [27-

29]. The loss reported in ref. [29] was ~6 dB/cm. Chalcogenide thin films with different compositions also have been fabricated by this PLD technique [30-33]. The loss of an As_2S_3 waveguide reported by Rode *et al.* [30] was 0.2 dB/cm measured at 1.55 μm.

2.1.1.4 Spin & dip coating technique

This technique has been developed by D. W. Harwood *et al.* at the ORC, University of Southampton [34]. At temperatures above the liquidus temperature, compound glasses, such as the fluorides, sulphides and phosphates, have viscosities comparable to those of spin coating solutions. A neodymium-doped fluoroaluminate (AlF) glass, with a viscosity of 0.1 poise at 1000 ^{o}C, has been successfully spin coated into a waveguide geometry directly from its liquid phase. Laser operation around 1050 nm has been observed in a 20 micron thick, 0.5% Nd-doped glass waveguide fabricated using this technique. Performance is consistent with propagation losses of 0.5dB/cm, which have been independently measured by imaging the scattered light from the waveguide surface. Other materials including sulphide and heavy metal oxide glasses are also being studied.

Recently, the spin & dip coating technique for GLSO planar waveguide applications has been developed by A.K. Mairaj *et al.* and the waveguide loss of the GLSO planar waveguide was 0.3 dB/cm at 1.064 μm [35].

2.1.2 Chemical depositions

There are two main categories of chemical deposition techniques, liquid phase and gas phase, used for the fabrication of planar

waveguides. Both will be discussed in this section. First the sol-gel technique and liquid phase deposition (LPD) in the liquid phase chemical deposition section and then flame hydrolysis deposition (FHD), chemical vapour deposition (CVD) and plasma enhanced chemical vapour deposition (PECVD) in gas phase deposition will be discussed in the following section.

2.1.2.1 Sol-gel technique

The sol-gel technique has been extensively investigated for the fabrication of optical waveguides because it is a convenient and flexible way to deposit oxide films on a variety of substrates. A key application for glass waveguides is integrated optics or photonics, especially planar waveguide devices for use in fibre communication systems. The use of silicon as a substrate to make silica-on-silicon is one of the most important photonic technologies. The sol-gel technique also has been applied to form optical fibre preforms [36].

Sol-gel has become a flexible method for fabricating silica-on-silicon components, since its key difficulty of crack failure has been overcome by two approaches: the use of interactive spin coating and flash annealing [37], and the use of organic-inorganic composite materials [37]. Both techniques have now been used to make waveguides with low propagation loss (<0.3dB/cm) at the telecommunications wavelengths, especially 1550 nm, and passive devices such as Y-junction splitters have been demonstrated [37].

For silica-based glasses, two other techniques have been used to fabricate silica-on-silicon components – flame hydrolysis deposition (FHD) and plasma-enhanced chemical vapour deposition (PECVD), and

both have reached a significantly higher level of development than sol-gel for this application. While sol-gel offers potential cost advantages, deposition of glass does not contribute a very large proportion of overall component costs. Therefore, for sol-gel to gain commercial acceptance it must compete based on some performance advantage [38].

Sol-gel does indeed offer great performance possibilities, because of the ease of introducing a wide variety of dopants, and the possibility of controlling the molecular structure through chemistry. Consequently, the development of erbium doped planar waveguide amplifiers is highly attractive. This technique also has been applied to fabricate chalcogenide planar waveguides by forming an oxide based material on a substrate and then making a conversion, under H_2S, to a sulphur based material [39-41].

2.1.2.2 Liquid phase deposition (LPD) technique

Liquid phase deposition (LPD, also known as chemical bath deposition) of an oxide film was first realized by Nagayama et al. [42], who used the technique to prepare SiO_2 coatings on silicon wafers. The processes have been extended to the formation of other oxides, including those of Ti, Sn, Zr, V, Fe, Ni, Zn and Cd [43]. The method involves immersion of a substrate in an aqueous solution containing a precursor species (commonly a fluoro-anion) which hydrolyzes slowly to produce a super-saturated solution of a desired oxide, which then precipitates preferentially on the substrate surface, producing a conformal coating. LPD of SiO_2 has received considerable attention in the semiconductor industry, and many modifications of the deposition conditions have been explored to optimize the electronic properties,

which are affected by the crystallinity and by residual fluoride or hydroxide content.

Liquid phase deposition of SiO_2 is based on the reaction of H_2SiF_6 with water to form hydrofluoric acid and solid SiO_2, as shown in the Eq. (2.1).

$$H_2SiF_6 + 2\,H_2O \longleftrightarrow SiO_2 + 6\,HF \qquad (2.1)$$

This model shows the increased super-saturation and hence the increased deposition of SiO_2 by the addition of water to the growth solution.

2.1.2.3 Flame hydrolysis deposition (FHD) technique

Flame hydrolysis deposition (FHD) is one of the most important fabrication techniques for glass optical waveguides, especially for silica optical waveguides. This technique is a process for forming a film structure by using an oxy-hydrogen flame to produce glass soot particles to deposit subsequently on a substrate [44]. The process is developed to fabricate a film structure for an optical waveguide having under and over cladding layers and a core layer surrounded by them, as showed in figure 2.1. Layer 1 is a first cladding layer, a porous vitreous layer (SiO_2+B_2O_3+P_2O_5), to become the under cladding layer made by oxidation from $SiCl_4$, BCl_3, and $POCl_3$ on a substrate. Layer 2 is a second porous vitreous layer (SiO_2+B_2O_3+P_2O_5+GeO_2) to become the core layer formed by oxidation from $SiCl_4$, BCl_3, $POCl_3$, and $GeCl_4$. Layer 3 is the over cladding layer which is made by the same process as layer 1. After deposition, all the porous vitreous layers are sintered

to a transparent film. The FHD technique has been intensively applied to the fabrication of silica based planar lightwave circuits [45].

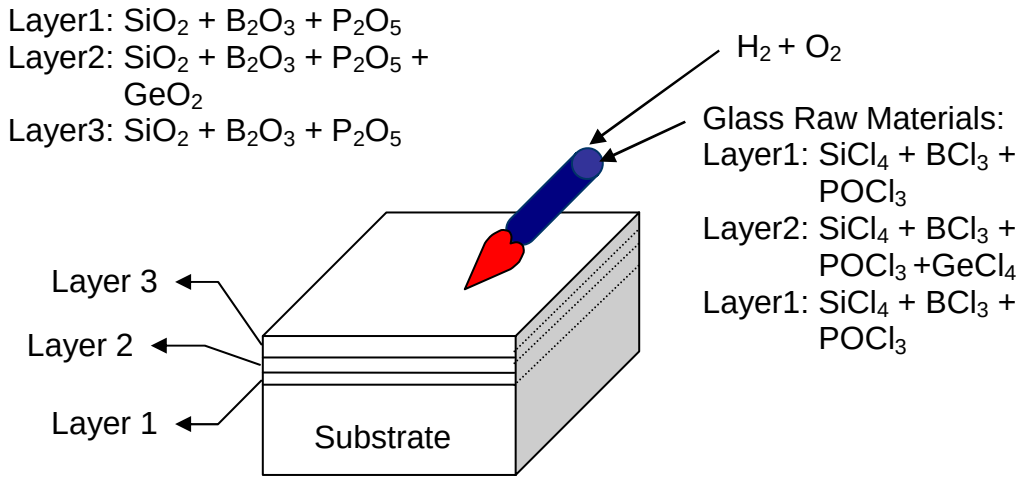

Figure 2.1 Flame hydrolysis deposition (FHD) for silica base planar waveguides

2.1.2.4 Chemical vapour deposition (CVD) technique

Chemical vapour deposition (CVD) is an important and popular technique for the preparation of thin films on a wide variety of materials – elements as well as compounds – on different substrates. CVD offers many advantages over other methods of thin film deposition. For example, films with a high degree of purity and good quality, with accurately controllable stoichiometric compositions and doping levels, can be prepared. Because of the good throw power attainable with CVD, the coating of complex shapes is possible. Since many reactions can be accomplished at ambient pressure, the need for expensive high vacuum equipment can be avoided.

On the other hand, an obvious disadvantage associated with CVD is that many coating reactions require high temperatures and the vapour may react with substrates or apparatus. Also, the apparatus used in CVD can be complex, and there are many control variables.

The main application of CVD is in semiconductor integrated electronic circuits. Epitaxial deposition of silica on silicon wafers and the deposition of dielectric films such as silicon dioxide and silicon nitride for passivation in integrated circuitry are made possible by CVD. For example, silicon dioxide films are usually prepared by the oxidation of silane (SiH_4). Silane is mixed with oxygen together with an inert gas dilutant at atmospheric pressure. The reaction is as following Eq. (2.2):

$$SiH_{4(g)} + O_{2(g)} \longleftrightarrow SiO_{2(s)} + 2\,H_{2(g)} \qquad (2.2)$$

The reaction can be processed at temperature as low as 450 ^{o}C. Operation at atmospheric pressure is advantageous in the sense that it allows a simpler and less expensive system than that required with vacuum environment. When operating at atmospheric pressure, the gas phase nucleation is reduced by the degree of inert gas diluent used.

Other processes used for the deposition of SiO_2 are as follows:

$$SiH_{4(g)} + 2\,N_2O_{(g)} \longleftrightarrow SiO_{2(s)} + 2\,H_{2(g)} + 2\,N_{2(g)} \qquad (2.3)$$

$$SiH_2Cl_{2\,(g)} + 2\,N_2O_{(g)} \longleftrightarrow SiO_{2(s)} + 2\,HCl_{(g)} + 2N_{2(g)} \qquad (2.4)$$

The temperatures required for these reactions are approximately 850 and 900 ^{o}C, respectively.

The direct oxidation of silicon tetrachloride and germanium tetrachloride requires very high deposition temperatures (approximately 1500 - 1800 ^{o}C), as in the following equations:

$$SiCl_{4(g)} + O_{2(g)} \longleftrightarrow SiO_{2(s)} + 2\,Cl_{2(g)} \quad (2.5)$$

$$GeCl_{4(g)} + O_{2(g)} \longleftrightarrow GeO_{2(s)} + 2\,Cl_{2(g)} \quad (2.6)$$

The above reactions are also applied to the modified chemical vapour deposition (MCVD) process for the silica preform preparation.

The metal halide precursors are very important not only in oxide glass formation, but also in sulphide glass formation. For example, germanium tetrachloride can react with hydrogen sulphide to form germanium sulphide glass, as shown in the Eq. (2.7)

$$GeCl_{4(g)} + 2H_2S_{(g)} \longleftrightarrow GeS_{2(s)} + 4HCl_{(g)} \quad (2.7)$$

Although the above reaction was reported to be unsatisfactory for the fabrication of planar or preform structures because of a low reaction rate and a low yield of deposited product [46], our thermodynamic calculation in chapter 5 reveals that this reaction is feasible and indeed practical for thin film deposition.

The main CVD techniques are thermal CVD, plasma CVD and laser CVD. With the introduction of metal-organic precursors, the metal-organic CVD (MOCVD) is becoming more and more important, especially in GaN based light emitting laser diode applications [47]. Moreover, plasma enhanced CVD and metal-organic CVD have been applied to form chalcogenide thin films.

2.1.2.5 Plasma enhanced chemical vapour deposition (PECVD)

The plasma enhanced chemical vapour deposition (PECVD) technique has been widely used in microelectronics, modern optics, and photovoltaic applications in recent years. PECVD is a versatile technique for depositing a wide variety of film materials. Dielectric and semiconductor films such as SiO_2, amorphous hydrogenated silicon, polycrystalline silicon, and silicon carbide have become increasingly important, since many such elemental and compound material films can be prepared at much lower temperatures than are possible with conventional CVD. In the majority of the work reported, the plasma is produced by an RF field, although DC and microwave fields have also been used. The primary role of the plasma is to promote chemical reactions, the average electron energies (1-20 eV) in the plasma being sufficient to ionize and dissociate most types of gas molecule. An important aspect in this substitution of electron kinetic energy for thermal energy is that the substrate degradation due to excessive heating is avoided and a variety of thin film materials can be formed on temperature-sensitive substrates such as polymers. Although electrons are the ionizing source, collisions involving excited species can lead to the formation of free radicals and can also assist the ionization process [48].

Chalcogenide glass films formed by PECVD have been described by P. Nagels *et al.* [9, 49-55], however no details of waveguide characterization were reported.

2.1.2.6 Metal-organic chemical vapour deposition (MOCVD)

Metal-organic chemical vapour deposition (MOCVD) is a recently developed technique that is increasingly used for preparing high quality epitaxial films for applications in optoelectronics and microwave devices. Since the first demonstration of the deposition onto insulator substrates of single-crystal films of GaAs by MOCVD [56] using trimethylgallium (TMG) and AsH_3 as the sources of Ga and As, respectively, many reports have been published on the growth of compound semiconductor films by this vapour phase materials technology. The basic reaction for GaAs formation is as Eq. (2.8):

$$Ga(CH_3)_3 + AsH_3 \longleftrightarrow GaAs + 3\ CH_4 \qquad (2.8)$$

In the MOCVD process, the metal-organic precursors are very important not only to help to reduce the formation temperature, but also to make it possible to incorporate rare earth elements in the CVD processes.

Furthermore, some chalcogenide glass films formed on quartz substrates by the MOCVD process have been reported [57], however no formal paper has been reported on this method.

2.1.3 Summary

Thin film deposition techniques described above can be broadly classified as either physical deposition or chemical deposition, as shown in Fig.2.2.

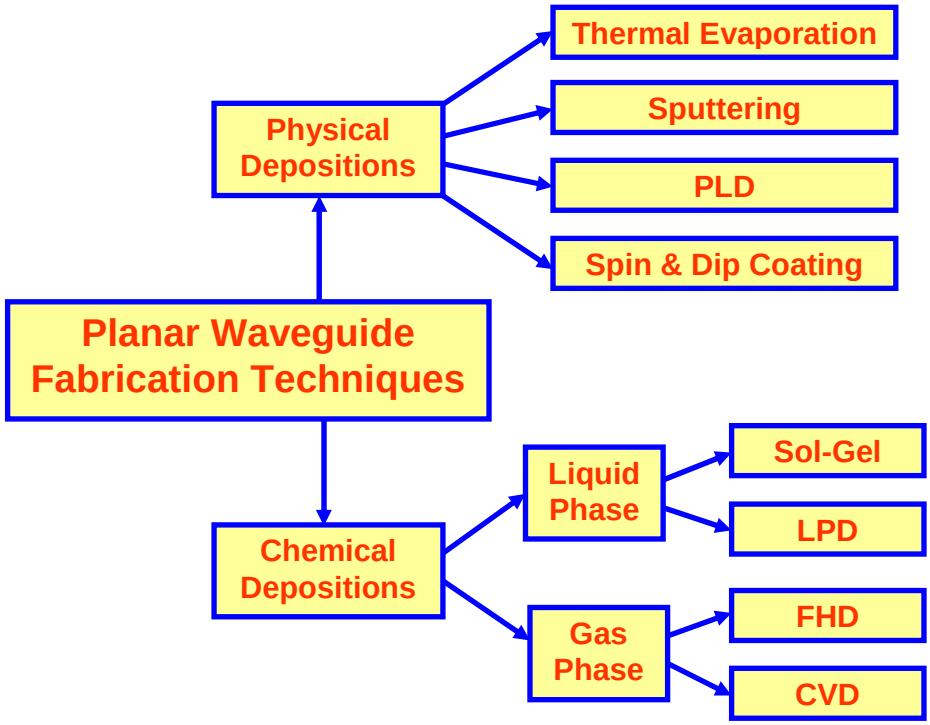

Fig 2.2 Broad classification of thin-film deposition techniques

In physical deposition, the thermal evaporation is a simple and cost effective way to form thin film materials on a substrate but suffers from the difficulty of stoichiometric control. The sputtering technique is an alternative way to prepare thin film materials on a substrate but the cost is relatively high compared to thermal evaporation. Although this technique suffers from the dissociation of volatile elements during the deposition process, the dissociation can be compensated for by adding reactive gas into the system. The PLD technique requires a high vacuum environment and the cost of the system is extremely high. Finally, the spin & dip coating technique is a cost effective and simple way to get a glass thin film from a wide variety of optical glasses.

In the chemical deposition techniques, LPD is an inexpensive and simple method to form a thin film on a substrate, but its use is limited to some specific materials. The sol-gel technique is a flexible and inexpensive method to fabricate oxide-based glass thin films on a

substrate. An in-direct sol-gel method has been successfully applied to chalcogenide glass thin film fabrication. FHD is a very practical method to fabricate a silicate based glass thin film waveguide and this technique is well-established. CVD is one of the most versatile methods to fabricate a glass thin film waveguide. With this method it is possible to control the stoichiometry of the materials and directly form the materials on the substrates. Therefore, the use of the CVD method to form chalcogenide glass planar waveguide has attracted more and more research.

2.2 Channel waveguide fabrication techniques

Channel waveguides can be made by several methods, including ion-exchange, diffusion, direct writing, photolithography, and dry-etching. Photolithography, widely used in semiconductor fabrication, has become one of the most important methods to fabricate channel waveguides. Direct writing techniques have been successfully used in photosensitive glass materials, especially in the chalcogenide glasses. The ion-exchange method is limited by the ion selection for a selected glass material. Diffusion is not commonly used to fabricate a channel waveguide, but is applied for special materials.

2.2.1 Ion-exchange

The ion-exchange technique has been used to improve the surface-mechanical properties of glass and, more importantly, create a waveguiding region in the glass. Since Izawa and Nakagome [58] reported the first ion-exchanged waveguide made by Tl^+-Na^+ exchange from a mixture of molten nitrate salts. The Na^+ ions of a glass substrate were exchanged by a diffusion process with ions (Tl^+, K^+,

Ag^+, Cs^+, Rb^+, or Li^+). The local modification of the chemical composition of the glass increased the refractive index at the glass surface.

2.2.2 Diffusion

The diffusion technique has been used to fabricate, for example, Ti-diffused $LiNbO_3$ and Zn-diffused $LiNbO_3$ waveguides by vapour phase deposition. The refractive index change is typically $5x10^{-3}$ in the Zn-diffused $LiNbO_3$ waveguide [59]. Apostolopoulos *et al*. have reported a gallium-diffused waveguide in sapphire by heating the gallium oxide on the sapphire substrate at 1600°C. The refractive index change was $6x10^{-3}$ in this waveguide [60].

2.2.3 Direct writing

Direct writing techniques have been widely used to create channel waveguides on the surface of photosensitive materials and silica based glasses modified by photosensitive elements [61], and has been more recently applied to chalcogenide glasses [62]. These materials experience a permanent change in their refractive index when exposed to sub-bandgap light. Direct UV-light writing is one of the most popular methods to generate a well-structured waveguide. Mairaj *et al.* has applied this technique to the gallium lanthanum sulphide glass and obtained a channel waveguide with a low propagation loss of <0.3 dB/cm at 1.3 μm [62]. Moreover, a recently developed micro-machining technique using a fs-laser resulting in less damage on the structures and less thermal diffusion, a commercial instrument is now available. This technique has been applied to fabricate waveguides in bulk glasses [61, 63-67].

2.2.4 Photolithography

Photolithography is an optical means for transferring patterns onto a substrate [68]. It is an essential technique used to define the shape of micromachined structures. The process is shown schematically in Figure 2.3.

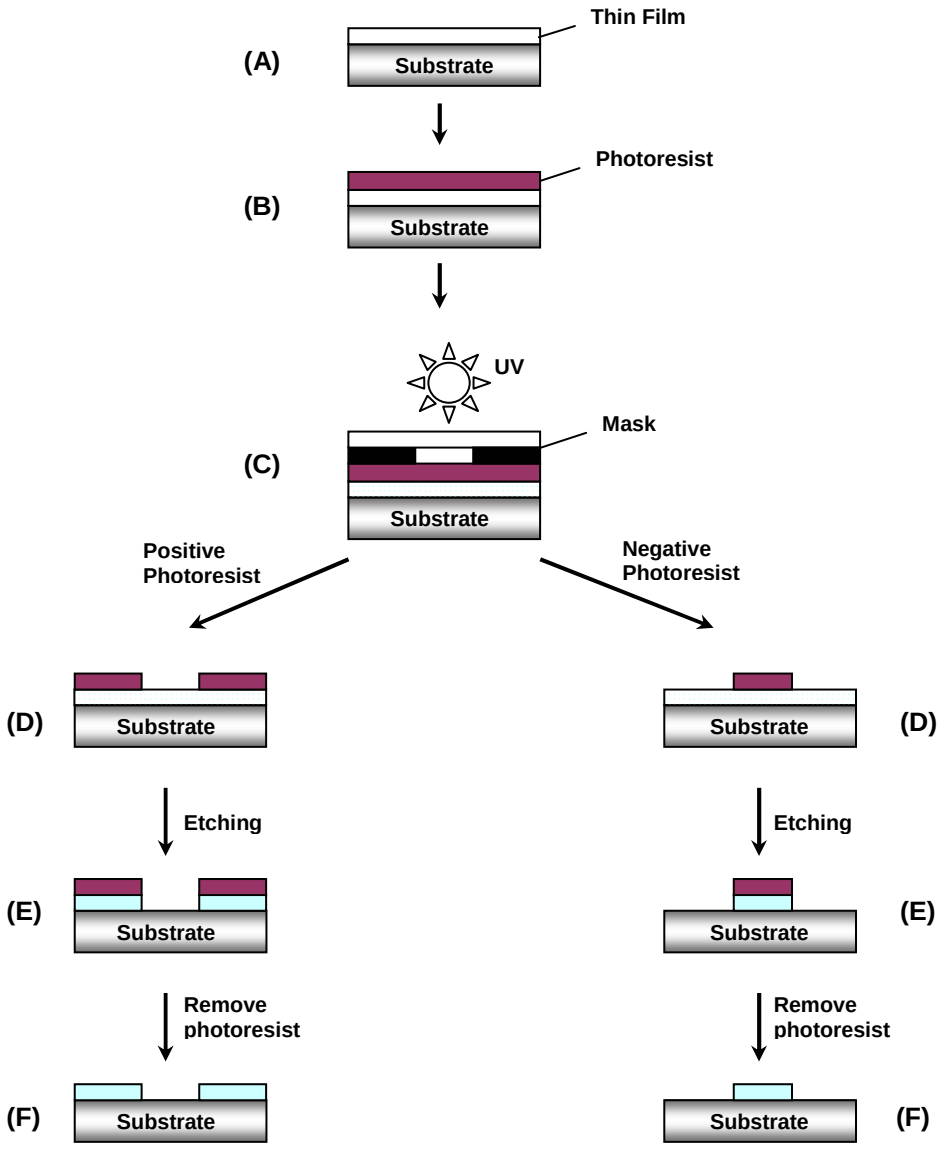

Fig. 2.3 Typical photolithography process

In the process step A, a thin film is coated on a substrate by any method of thin film formation. The thin film is then coated with a UV sensitive polymer, photoresist, in the process step B. After that, a UV light source illuminates a patterned mask onto the photoresist (process step C) transferring the pattern on the mask to the photoresist layer (process step D).

There are two types of photoresist, termed positive and negative. Where the UV light strikes the positive resist it weakens the polymer, so that when the image is developed the resist is easily washed away in any area exposed thereby transferring a positive image of the mask to the resist layer. The opposite occurs with negative resist, where the UV light strengthens the polymer, so that when developed the resist that was not exposed to UV light is washed away – a negative image of the mask is thus transferred to the resist.

A chemical or physical process is then used to remove the thin film layer, i.e. etching process, where it is exposed through the openings the resist (process step E). These are described in detail in the following section. Finally, the resist is removed leaving the patterned thin film (process step F).

2.2.5 Dry-etching

After a photoresist image has been formed on the surface of a substrate, the next process usually involves transferring that image into the layer under the photoresist by etching. Dry etching processing using a plasma is one of the most important processes for integrated circuit manufacturing. Plasma-driven chemical reactions and/or reactive ion beams are used to remove material in dry etching. Dry

etch processing has become popular in semiconductor manufacturing because of advantages over wet etching, particularly in improved vertical pattern transfer, better uniformity, higher reproducibility and improved controllability [69].

All dry etch processes and reactors are basically alike in that the wafer is placed in a vacuum chamber, gases are admitted to the chamber, and a plasma is initiated in the gas. For an etch process to proceed successfully there are four required conditions. The first is that the plasma must generate species. The second is that the reactant radicals must be transferred to the sample surface. The third is the atoms on the sample must react with the radicals in the plasma, and finally the by-products must be moved away from the surface of sample. Of these four events, the slowest step primarily determines the etch rate, which may be diffusion or chemical-reaction limited.

Etching mechanisms can be characterized by physical damage, chemical attack, or some combination of the two. In the remainder of this section, plasma etching, reactive ion etching (RIE), and ion beam milling techniques will be discussed.

2.2.5.1 Plasma Etching

Until the 1970's, pure plasma etching was known as one of the most popular etching techniques, together with wet etching. Typically, plasma etching is performed at a pressure over 100 millitorr, and is purely chemical in nature, meaning and there is no charged particle bombardment of the surface to enhance the etch rate or to promote directionality. Today, this technique is usually used to strip the photo

resist mask layer after patterning transfer, in a process refered to as plasma ashing.

Reactive species generated in the plasma react with the sample surface and create volatile etch products that are then swept away. If the gases were carefully selected, then it is possible to achieve very high selectivity through this process. Pure plasma etching has significant advantages, such as reducing the damage to the samples during the etching process. Also, plasma etching is frequently used for dry cleaning of damaged wafers after high energy ion bombardment. For example, deep contact hole formation, trench etching and gate material etching for field effect transistors is performed without surface treatment after ion assisted bombardment etching.

In spite of the great advantages of plasma etching there is the critical issue that the films tend to etch in all directions at once, so vertically fine sub-micron patterning cannot be achieved using a pure plasma type etching process. The result is an isotropic etch, therefore, this process is limited to isotropic pattern transfer in semiconductors.

2.2.5.2 Reactive Ion Etching (RIE)

In contrast to plasma etching, with reactive ion etching (RIE) ions from the plasma bombard the surface to be etched at normal incidence and with an energy of hundreds of volts, so it is easy to achieve an anisotropic pattern transfer.

For reactive ion etching, the sample is put on a powered electrode (negatively biased cathode) and accelerated ions bombard the samples and anisotropic pattern transfer can be achieved. RIE takes advantage of a synergism between the physical and chemical

etching mechanism and achieves etch rates that are faster than the sum of the two components. However, this technique has a serious disadvantage which is damage to the samples because of the high energy ion bombardment. In order to decrease the sample damage and increase the etch rates, much lower ion energy need to be used and a high density plasma technique, therefore new techniques are needed to solve those kinds of problems.

2.2.5.3 Ion beam Milling

Ion beam milling is a purely physical technique, with no chemical reactive etching factor. A relatively high energy (500-800 eV) inert ion beam transfers large amounts of energy and momentum to the substrate. If the force is strong enough, these ions can physically remove material from the sample surface. Usually, the pressure used in ion milling is under 0.1 millitorr. Since the pressure is low, the mean free path of the particle is long and the ejected sputtered material can cross the reactor vessel and reach opposing walls. When a uniform ion beams bombards a sample, it provides an anisotropic profile in pattern transfer. But, poor selectivity, low etch rate and severe damage on the sample are critical disadvantages to the wide use of the ion milling process, these occur because of physical sputtering, and the etch rates strong dependence on the beam angle.

2.2.6 Summary

In this section, ion-exchange and diffusion have been discussed in some applications. However these two techniques suffer from limitations. Direct writing is a very powerful technique to write channel structures and even some complicated structures. The damage and

thermal effects can be controlled by using a f-s laser. Furthermore, photolithography is a well-established technique to transfer patterns on the planar waveguides. Combined with the dry-etching technique, it is becoming more and more attractive to fabricate planar devices in versatile structures.

2.3 Applications based on chalcogenide glasses

For over two decades, optical engineers have dreamt of the day when the large scale integration applied to microelectronics could be applied to optical components. The primary limitation is a suitable material. Today, there is no optical equivalent of silicon, nothing with the same ability to embody multiple-complex-functionality in the optical domain.

There are however, contenders for this role; glasses such as silica on silicon, semiconductors including gallium arsenide and indium phosphide; crystals, in particular lithium niobate and a wide range of polymers, all may be the next "optical" silicon. Markets for devices based on these materials are predicted to grow by a factor of over 200 over the next 3-5 years [70].

From the early days of research on integrated optical waveguides, glasses have played a key role, and silica glass waveguides, as thin films on silicon substrates, remain a top choice for optical integration on a substrate. However, the very nature of silica, the properties that have made it perhaps the ultimate optical waveguide in the form of optical fibre, considerably reduce its applications in thin film form. Silica is stable and inert, the perfect passive waveguide. For active applications, for functionality rather than simply transmission, silica

glass has its limitations. An example is switching, where the switching effect in silica is based on its thermo-optic properties. Using thermal methods, switching is slow, millisecond switch times are typical, large powers are required and complex thermal controls are needed. Widespread use of a silica-based optical switch is unlikely [70].

Other glasses have been considered as integrated optical materials; heavy metal oxides, in which for example, the silicon in a silica glass is replaced by heavy elements such as lead, tellurium or bismuth, offer many improvements over silica. Here an enhanced nonlinearity opens up nonlinear switching regimes, with switching speeds in the terahertz range predicted. Halide-based glasses, in which the oxygen in silica glass is replaced by a halide, like fluorine, offer roles as more efficient light sources. When doped with the rare earth elements, visible red-green-blue light, emission in each of the telecommunication windows, around 0.8, 1.3 and 1.55 microns, and infrared emission up to wavelengths of about 4 microns, can be realized in a fluoride glass. A third family of glasses based on the chalcogenide elements, sulphur, selenium and/or tellurium have also been intensely studied, but are probably the least understood [70].

The term "glass" requires some definition. A glass is defined in American Society of Testing and Materials (ASTM) as 'an inorganic product of fusion which has been cooled to a rigid condition without crystallization'. According to this definition, a glass is a non-crystalline material obtained by a melt-quenching process. Nowadays, non-crystalline materials that can not be distinguished from melt-quenched glasses of the same composition are obtained by using various techniques such as chemical vapour deposition, sol-gel process, etc. Therefore, most glass scientists regard the term 'glass' as covering 'all

non-crystalline solids that show a glass transition' regardless of their preparation methods [71].

Glass can be made with excellent homogeneity in a variety of forms and sizes, from small fibres to meter-sized pieces. Furthermore, glass can be doped with rare earth ions and micro-crystallites for a wide range of properties which can be chosen to meet the needs of various applications. These advantages over crystalline materials are based on the unique structural and thermodynamic features of glass materials. The macroscopic properties of a glass such as optical transmission and absorption, refraction of light, thermal expansion, etc. are observed always equally in all directions, provided that the glass is free from stress and strain. That is, a glass is an isotropic material, whereas crystalline materials are generally anisotropic [72].

Glasses have several unique physical properties that distinguish them from other materials. A material gradually transforms from a supercooled liquid to a glassy state over the glass transition range of temperatures. This is indicated on the volume-temperature diagram shown in Figure 2.4. The temperature at which the glass transition takes place can vary according to how slowly the material cools. If it cools slowly it has a longer time to relax, the transition occurs at a lower temperature and the glass formed is more dense. If it cools very slowly it will crystallize. A liquid to crystal transition is a thermodynamic one; i.e. the crystal is energetically more favourable than the liquid when below the melting point. The glass transition is purely kinetic: i.e. the disordered glassy state does not have enough kinetic energy to overcome the potential energy barriers required for movement of the molecules past one another. The molecules of the glass take on a fixed but disordered arrangement. Glasses and

supercooled liquids are both metastable phases rather than true thermodynamic phases like crystalline solids [72].

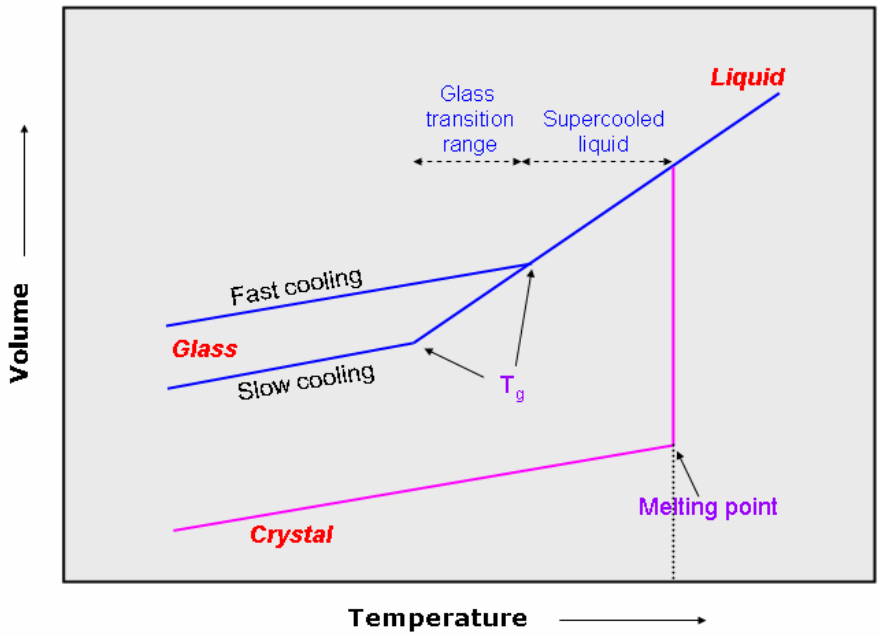

Fig. 2.4 Volume-temperature diagram for glass forming melts (cooling) [72]

2.3.1 Optical properties of chalcogenides

A chalcogenide glass can be regarded as a "soft semiconductor", soft because its atomic structure is flexible and viscous and a semiconductor because it processes a bandgap energy (~2 eV) which is characteristic of semiconductors. For other semiconductor properties, for example, electron mobility, a chalcogenide glass appears to possess intermediate properties between a crystalline material and a polymer.

As an optical material, chalcogenides offer a wide range of properties that have been exploited or have the potential for new, relatively unexplored applications. Chalcogenide glasses are a group of non-oxide vitreous materials. Instead of oxygen, these glasses contain

other elements from group VI of the periodic table; namely sulphur, selenium or tellurium as glass-forming anions. Most chalcogenide glasses are opaque in the visible with the exception of some sulphide glasses. They transmit from approximately 1μm to longer infrared wavelengths than oxide or fluoride glasses. Sulphide glasses are transparent up to 12μm, selenide glasses up to 15μm and telluride glasses transmit to 20μm. These glasses are able to transmit further into the infrared than silica, by using heavy ions, and weak bonding between ions. The lower phonon energy of the resulting amorphous structure shifts the multi-phonon edge (IR limit of the transmission window) to longer wavelengths. In addition to giving MIR transmission in these glasses the reduced maximum phonon energy leads to reduced non-radiative decay rates and increased radiative quantum efficiency for electronic transitions of dopants introduced to the glasses (rare-earth) [73].

Chalcogenide glasses are becoming increasingly important for the fabrication of optoelectronic devices in part because of their high nonlinearity, strong photosensitivity and other unique properties [74]. Of particular interest are the following:

2.3.1.1. Nonlinearity

The interaction of an electromagnetic field with an atomic system has been reviewed with emphasis on nonlinear optics. The polarization (P) induced in a medium by an intense light beam is proportional, in addition to the linear response, to the higher order terms of the applied electric field (E) of frequency (ω) as shown in the Eq. (2.9) [75].

$$P(\omega) = \chi^{(1)}(\omega)E(\omega) + \chi^{(2)}(\omega = \omega_1 + \omega_2)E(\omega_1)E(\omega_2) + \chi^{(3)}(\omega = \omega_1 + \omega_2 + \omega_3)E(\omega_1)E(\omega_2)E(\omega_3) + \ldots \quad \text{(Eq. 2.9)}$$

where $\chi^{(n)}$, the complex dielectric susceptibilities, are tensors of rank (n+1) and are related to the microscopic (electronic and nuclear) structure of the material. Classic or linear optics are concerned with the first order linear term $\chi^{(1)}$. The real part of $\chi^{(1)}$ gives rise to the linear refractive index n_0 whilst absorption is proportional to the imaginary part of $\chi^{(1)}$.

The second order nonlinearity is important in materials having no centre of inversion, which is typical for some crystals, for example $LiNbO_3$. In isotropic materials that possess inversion symmetry, such as glasses, the second order contributions vanish.

The third-order contributions to the total polarization are given by the Eq. (2.10)

$$\chi_i^{(3)}(\omega_4) = \sum_{jkl} \chi_{jkl}^{(3)}(-\omega_4, \omega_1, \omega_2, \omega_3) \times E_j(\omega_1)E_k(\omega_2)E_l(\omega_3) \quad \text{(Eq. 2.10)}$$

where $\omega_4=\omega_1+\omega_2+\omega_3$ and E_j, E_k, and E_l are three separately applied electric fields, each having its own frequency (ω_1, ω_2, ω_3) and polarization direction. In the case of third order nonlinearities, many different processes are possible because of the three incoming electric fields involved. Processes involving $\chi^{(3)}$ are third harmonic generation ($\chi^{(3)}(-3\omega,\omega,\omega,\omega)$) Raman and Brillouin scattering ($\chi^{(3)}(-\omega_1,\omega_2,-\omega_2,\omega_1)$) and a large number of three and four wave mixing processes, the most common of which is degenerate four-wave mixing ($\chi^{(3)}(-\omega,\omega,\omega,-\omega)$).

The optical Kerr effect is a four wave process and results in an intensity-dependent contribution to the refractive index. The total index of refraction is given by the following equation (Eq. 2.11)

$$n = n_0 + n_2 < E^2 > \qquad \text{(Eq. 2.11)}$$

where n_0 is the linear index of refraction, $<E^2>$ is the time-averaged square of the electric field of the incident optical beam in esu, and n_2 is the nonlinear refractive index. In SI units (Eq. 2.12)

$$n = n_0 + n_2 I \qquad \text{(Eq. 2.12)}$$

where I is the intensity (W/m^2) of the incident beam. The relationship between the nonlinear index in SI and *esu* units is (Eq. 2.13)

$$n_2(m^2/W) = 40\frac{\pi}{cn_0} n_2(cm^2/erg) = 4.19\times10^{-7} n_2(esu) \qquad \text{(Eq. 2.13)}$$

For a linear polarized monochromatic beam of frequency ω and an isotropic medium the nonlinear index of refraction $n_2\,(esu)$ is related to the real part of $\chi^{(3)}$ via. (Eq. 2.14)

$$n_2 = \frac{12\pi}{n_0} \mathrm{Re}\,\chi^{(3)}_{1111}(-\omega,\omega,\omega,-\omega) \qquad \text{(Eq. 2.14)}$$

All-optical switches based on highly non-linear materials are probably the key device required for high speed optical data processing and optical telecommunications. There are also applications in all-optical bistablity and optical limiting devices. Practical devices require a large and fast third-order nonlinear optical response and suitable

materials include heavy metal oxide, chalcogenide and metal-nanoparticle dispersed glasses. The sulphide family of glasses also has a large third order nonlinear response ($\chi^{(3)}$) under a strong electromagnetic field because of the high hyperpolarisability of the sulphide ion. Moreover, two-photon absorption (TPA) limits the optical power that can be transmitted and hence the attainable nonlinear phase shift in all-optical switching. When the TPA is large, structure changes and damage can occur, which is clearly undesirable for device applications. The nonlinearity properties of a selection of chalcogenide glasses are summarized in Table 2.1 [76-78].

Glass	λ_{meas} **(μm)**	n_o	n_2 $(10^{-14}\ cm^2/W)$	β (cm/GW)	**FOM** $(n_2/\beta\lambda)$	**Absorption edge (nm)**
$Ge_{10}As_{10}Se_{80}$	1.06	-	22	2.7	0.77	760
$Ge_{30}Se_{70}$	1.06	-	21	1.1	1.8	705
$Ge_{0.28}Se_{0.60}Sb_{0.12}$	1.5	2.6	9.4	0.2	3.13	690
As_2Se_3	1.5	2.8	13.0	0.4	2.16	700
As_2S_3	1.06	2.6	5.7	0.26	2.07	520
GNS	1.52	2.14	1.01	<0.01	6.64	473
GLS	1.52	2.41	2.16	<0.01	14.21	545
GLSO	1.52	2.25	1.77	<0.01	11.64	500
GLSOF	1.52	2.26	1.39	<0.01	9.14	497

Table 2.1 Nonlinear properties of some chalcogenide glasses. Here λ_{meas} is the wavelength used for each measurement, n_o is the linear index, n_2 the nonlinear index, β is the two photon absorption (TPA)

The refractive nonlinearity results for Ga:La:S glasses show values close to a hundred times that of silica glasses (~$2.8x10^{-16}$

cm^2/W). This demonstrates that Ga:La:S glasses have larger off-resonant nonlinearities than oxide and heavy metal oxide glasses, however they are not the highest nonlinear chalcogenide glass. On the other hand, the small TPA of Ga:La:S glasses is one of their most outstanding features. When considering practical all-optical switching devices, both the nonlinear refractive index and the two-photon absorption coefficient must be taken into account. The required phase shift for a Mach–Zehnder-based switch is $\Phi_{NL}=\pi$. We define a figure of merit (FOM) = $n_2/\beta\lambda$. In this case for example, a 10% non-linear loss requires a FOM of approximately 5. The goal in engineering the nonlinear material should be a large value of n_2 and a small value of β. This, in turn, implies that ideally the photon energy corresponding to the wavelength of operation should be less than half the energy gap of the material, where TPA is negligible. The wavelength of operation that is of interest in optical communication is approximately λ=1.55 μm (0.8 eV), and therefore we should aim for a material with an energy gap larger than 1.6 eV [79].

2.3.1.2 Low Phonon Energy

Phonon energy is a quantum of vibration energy in the acoustic vibrations of a crystalline lattice. Chalcogenide glasses are composed of heavy ions that are weakly bonded. This gives the glass a low phonon energy and hence its extended infrared transparency. The transmission window for chalcogenide glass is approximately from 1μm to longer infrared wavelengths as compared with oxide and fluoride glass. In general, sulphide, selenide, and telluride glasses are transparent up to 12 μm, 15 μm and 20 μm respectively [73]. It also gives rise to large numbers of vacancies and dangling bonds on the amorphous lattice, which gives a large density of states in the bandgap

(mobility gap). These states are not available for conduction, but can have electrons excited to them from the valence band, which gives rise to absorption even for photons with small energies [72]. The enhanced mid-IR transmission in chalcogenide glass, with reduced maximum phonon energy leads to lower non-radiative decay rates and increased radiative quantum efficiency for electronic transitions of rare-earth dopants introduced into the glass [80].

Although the low phonon energy materials seem to have excellent properties, there are still some drawbacks in these materials. Most infrared materials suffer from thermo-mechanical degradation, poor resistance to air and moisture and are especially prone to crystallization [81].

2.3.1.3 Photoinduced phenomena

At least seven distinct photoinduced phenomena are observed in amorphous chalcogenides [74]. These include photo-crystallization (or conversely photo-amorphization), photo-polymerization, photode-composition, photo-contraction or expansion, photo-vaporization, photo-dissolution of metals such as Ag into the chalcogenide and light-induced changes in local atomic configuration. These changes are accompanied by changes in the optical constants, i.e., changes in the electronic band gap, refractive index and optical absorption coefficient. These light-induced changes are favoured in chalcogenide glasses due to their structural flexibility (low coordination of chalcogens) and also due to the high-lying lone-pair p states in their valence bands. Annealing chalcogenide glasses can affect the photoinduced changes, in particular irreversible effects occur in as-deposited films, while reversible effects occur in well-annealed films as well as bulk glasses.

Changes in local atomic structure are observed on illumination with light having a photon energy near the optical band gap of the chalcogenide. Although light-induced effects can also be observed at longer wavelengths, they generally necessitate much higher intensities. Photodarkening is sensitive to hydrostatic pressure and can be thermally erased by annealing near the glass-transition temperature. Photoinduced anisotropy (PA) is induced when the glass or film is exposed to plane-polarized light and can be removed by exposure to unpolarized light or thermal annealing. When chalcogenide glasses are exposed to short laser pulses, large Kerr-type nonlinearities are induced. Table 2.2 shows some of the photoinduced effects exhibited by typical chalcogenide compositions which can be used for the fabrication of devices such as gratings, waveguides, etc [30, 82-86].

Composition	**Nature of edge shift**	**$\Delta n/n$ (%)**	**Ref.**
$As_{42}S_{58}$	photodarkening	4	82
$As_{39}S_{58}Tl_3$	photodarkening	3	82
$As_{10}S_{60}Ge_{30}$	photobleaching	-	82
$Ge_{31}S_{63}Bi_6$	photobleaching	8	82
$Ge_{31}S_{63}Tl_6$	photobleaching	3	82
As_2S_3	photodarkening	1.5	30
GaLaS	photodarkening	-	82
Ge-S-Bi(Tl,In)	photobleaching	0.5-3	84
GeS_2	photobleaching	3	84-86

Table 2.2 Photoinduced phenomena in some chalcogenide glasses

2.3.2 Passive applications

2.3.2.1 Waveguide fabrication

Planar channel waveguides with very low losses (<0.3 dB/cm) have been fabricated in different compositions of chalcogenide glasses e.g., Ga–La–S, As_2S_3, Ge–As–Se–S, etc. These channel waveguides have been fabricated using the photo-darkening effect in thermally evaporated, sputtered, pulsed-laser-deposited and spin & dip coated films [35]. Moreover, as described later in this work, a germanium sulphide planar waveguide was directly fabricated on a Schott N-PSK58 substrate by CVD with a propagation loss of 2.1 dB/cm at 632.8nm demonstrated [87]. Table 2.3 shows the compositional dependence of propagation loss measured in some typical chalcogenide glasses.

Composition	Preparation method	Film treatment	λ (μm)	Loss (dB/cm)	Ref.
As_2S_3	Evaporation	As-deposited	1.3	0.5	11
As_2S_3	PLD	As-deposited	1.55	<0.3	26
$As_{24}S_{38}Se_{38}$	Evaporation	As-deposited	1.3	1	11
$Ge_{10}As_{40}S_{25}Se_{25}$	Sputtering	Rapid thermally annealed	1.566	<0.3	19
Ga:La:S	PLD	As-deposited	0.6328	6	25
Ga:La:S:O	Spin & dip coating	Annealed	1.064	0.3	31
GeS_x	CVD	Annealed	0.6328	2.1	This work

Table 2.3 Compositional dependence of waveguide loss in some typical chalcogenide glass films

2.3.2.2 Grating devices

Diffraction gratings have been fabricated in chalcogenide glasses using the photoinduced effects which occur in them. Both photodarkening and the metal-photodissolution effect have been used to fabricate transmissive gratings, especially for use at IR wavelengths. A variety of techniques have been used to fabricate these gratings, including holographic, mask exposure or etching methods. These gratings can be used as efficient beam combiners, couplers and have significant applications in monochromators, laser-tuning devices, shapers, coupling of optical fibres, etc. [88, 89].

2.3.3 Active applications

2.3.3.1 Fibre fabrication

Chalcogenide glasses based on sulphides have attracted considerable interest for their possible role as new optical fibre materials. When doped with rare earths, these glasses, by virtue of their low phonon energy and high refractive index, open up the possibility of new transitions and significantly increased pumping efficiencies. A variety of sulphide glass systems have been studied based on gallium and germanium sulphides [90, 91], arsenic trisulphide and $Ge_{30}As_{10}Se_{30}Te_{30}$ [92]. However arsenic trisulphide glasses suffer from poor rare-earth solubility and signs of crystallization are observed coinciding with the temperature for fibre-drawing. Hewak *et al.* [93] reported an optical fibre fabricated from the gallium–lanthanum glass system. This material provides an ideal host for the rare earths, which substitute directly for lanthanum ions, while

at the same time providing a wide transmission range and a relatively stable and non-toxic glass matrix. Both rods and preforms of gallium–lanthanum sulphide glasses have been drawn into fibres. Transmission loss was estimated by the cutback method over a 63 cm section of praseodymium doped multimode fibre. A loss of <5 dB/m was measured at 1.34 μm and 4.9 dB/m at 4.7 μm. Moreover, with a further purification of raw materials, optimization of the composition of GLSO glass, and well-controlled fibre drawing conditions, the loss of 1.5 dB/m measured at 4 μm has been achieved by Hewak *et al.* at the ORC, University of Southampton.

Recent developments in the production of As–S glass fibres [94] have shown that an increase in the degree of purity of the As–S glasses allows optical fibres to be drawn with minimum losses for multimode optical fibres of 23–45 dB/km at 2.2–2.7 μm, 50–70 dB/km at 3.2–3.6 μm and 300–500 dB/ km at 5–5.5 μm. $As_{40}S_{60}$ and $As_{38}S_{62}$ were used as core and cladding compositions.

Further increases in the degree of purity of glasses should be considered as the main way to improve the optical properties of the fibres. Long lengths (>150 m) of single-mode chalcogenide optical fibre have been fabricated by a double-crucible technique [95]. The core and cladding glass compositions used were $As_{40}S_{58}Se_2$ and $As_{40}S_{60}$, respectively. The optical loss of this fibre measured by a standard cutback technique was slightly less than 1 dB/m at 2.7 μm. These authors reported that the double-crucible process had an advantage over the rod-in-tube method, especially for less stable glasses that will devitrify during the stretching and over-cladding process. Scattering theory has been used [96] to determine the effect of various defects on the scattering loss of As_2S_3 glass fibres. The scattering loss is related to the particle shape, size, relative refractive index and wave-

length of light. Bubbles cause the highest relative refractive-index difference and therefore the highest scattering loss. The scattering decreases in the order: bubbles > carbon > SiO_2 >Al_2O_3 >As_2S_3 crystallites. Therefore, purification techniques and fibre-drawing processes need to address and minimize the carbon and bubble concentrations, as well as the other defects, in order to produce low-loss fibres. Minimum-loss predictions and measurements in gallium lanthanum sulphide-based glasses and fibres have also been presented [97].

The theoretical minimum loss for GaLaS is 0.5 dB/km at 3.5 μm while for the GaLaSO glass it is 0.1 dB/km at 2.6 μm. Some of the causes of loss in these materials have been identified as being impurities in the raw materials and scattering centers introduced during fibre drawing.

2.3.3.2 Fibre amplifiers and lasers

Optical amplification at 1.083 μm with neodymium-doped chalcogenide fibres was observed [98] in a glass composition of Ge–As–Ga–Sb–S. A maximum internal gain of 6.8 dB was achieved for a pump power of 180 mW. The first amplified spontaneous emission in a chalcogenide glass fibre was also reported [98].

A selenide glass has been developed that can be doped with rare-earth ions and is stable against crystallization during the fibre drawing process [99]. The glass is based on GeAsGaSe and can be doped with Pr^{3+} and Dy^{3+} for near-and mid-IR applications. The doped glasses have been drawn into fibres with core-only losses of 0.8 dB/m at 6 μm and 1.5 dB/m at 2.5 μm. Single-mode fibres have been drawn

with a measured core loss of 3 dB/m at 1.55 μm.

Schweizer *et al.* [100] found that the absorption spectrum of a 9.7 mol% Er^{3+}-doped GaLaS glass showed excellent rare-earth solubility and the potential for high doping concentrations and hence short devices; this represents a major advantage of GaLaS glass compared with conventional chalcogenide glasses, which suffer from very low rare-earth solubilities. Moreover, the radiative properties of Er^{3+}-doped Ga–La–S lend themselves to several applications. Radiation at 2 μm has application in LIDAR systems, radiation at 2.75 μm coincides with a strong water absorption in tissue and is used for medical applications, the 3.6 μm transition could be useful for H_2S, NO, and SO_2 sensing or remote sensing and the 4.5 μm transition could find use in CO and O_3 gas sensors when tuned to 4.7 μm. Finally, laser action in a rare-earth-doped GaLaS chalcogenide glass has been demonstrated, showing that this class of glasses is suitable for active applications such as amplifiers and lasers [101]. A neodymium-doped GaLaS glass laser operated under continuous-wave conditions at a wavelength of 1.08 μm when pumped with a Ti:sapphire laser at either 0.815 or 0.890 μm [101]. The reasonably low laser threshold indicated acceptable glass losses, but the laser performance was worse in comparison with conventional Nd-lasers.

2.3.3.3 Switching devices

Among the various kinds of materials, glass is the easiest material to use in fabricating a long fibre-type waveguide. Thus glass is suitable for non-resonant applications. Due to its low-loss characteristics, conventional silica fibre has been one of the most commonly used non-resonant non-linear media in all-optical switching

[102]. However, the low non-linearity of silica glass requires that the fibre be extremely long, for example a few kilometers in length. To overcome this problem, a glass is needed with a higher non-linearity. As discussed in the previous section (Table 2.1), among various glasses studied, chalcogenide glasses have a higher level of non-linearity (two orders of magnitude higher than that of silica glass) [103]. One of the significant features of chalcogenide glasses is that they possess a very high non-linearity at a nonresonant wavelength. Among the various types of chalcogenide glass, As_2S_3 possesses one of the highest $\chi^{(3)}$ values and is one of the most well known. Recent progress in studying non-linear optical properties of chalcogenide glass fibres and their applications to AOS have been reviewed [103].

Single mode As_2S_3-based fibres have been fabricated and the non-linear optical properties have been investigated. The non-linear refractive index and Raman-gain coefficient were measured to be two orders of magnitude higher than those of silica fibres. A sub-picosecond response of the non-linear refractive-index change and a small two-photon absorption (TPA) at the communication wavelength were confirmed [103].

All-optical switching using As_2S_3-based fibres has been demonstrated in the Kerr shutter and non-linear optical loop mirror (NOLM) configuration [103]. The switching power was reduced to 0.4 W using a 4-m-long low-loss fiber in a NOLM configuration. The large group-velocity dispersion (GVD) of the fibre might restrict the applicable length of the fibre. To overcome this problem, fabrication of As_2S_3-based fibre gratings has been demonstrated [103].

2.3.4 Other potential applications

Recently supercontinuum (SC) generation in microstructured and tapered optical fibres as well as highly nonlinear fibres has attracted considerable interest. Supercontinuum generation is a complex nonlinear phenomenon that is characterized by the dramatic spectral broadening of intense light pulses passing through a nonlinear material [104]. It was first observed in 1970 [105]. Since then, it has been shown to occur in various nonlinear media and has been extensively used in numerous applications ranging from spectroscopy to ultrashort pulse generation [104].

Most of the work on this topic has dealt with supercontinua seeded by pulsed sources. For instance, octave-spanning supercontinuum generation has been successfully demonstrated by launching femtosecond laser pulses into the cores of these fibres. Applications for supercontinuum generation include spectral slicing for wavelength division multiplexing, optical coherence tomography, sensing, and device characterization. The spectral slicing of supercontinuum laser sources has also been proposed as a means to make a multi-wavelength source for wavelength-multiplexed optical telecommunications [106] and, more recently, an ultra-broadband SC spanning more than an octave from the ultraviolet to the infrared has been applied to high precision optical frequency metrology [107].

Most of the research on supercontinuum generation is based on the microstructured optical fibre [108, 109]. However, supercontinuum generating planar devices have been demonstrated by Mesophotonics Ltd [110]. As described in the previous section, chalcogenide glasses

with excellent nonlinear properties give them great potential in the supercontinuum generation application area.

2.3.5 Summary

Chalcogenide glasses are novel materials with very promising properties. Low phonon energy makes these glasses transparent to the mid-infrared range. Moreover, low losses and photoinduced effects make these glasses suitable candidates for the fabrication of devices such as gratings and waveguides. Excellent rare-earth solubility in chalcogenide glasses make them suitable for amplifier and laser applications. Chalcogenide glasses are materials with high optical non-linearities which make them attractive for all-optical switching applications at telecommunication wavelengths. Another potential application for chalcogenide glasses could be the supercontinuum generation application. Future trends would be toward fabricating materials with optimum properties for the production of efficient passive and active devices.

2.4 References

[1] S. E. Miller, "Integrated Optics: An Introduction", Bell System Technical Journal, **49** (1969) 2059-2069.

[2] A. Yariv, "Guided Wave Optics", Scientific American, **240** (1979) 64-91.

[3] A.V. Kolobov, "Photo-induced metastability in amorphous semi-conductors", Wiley-VCH, 2003.

[4] S. Otani, T. Tanaka, and Y. Ishizawa, "Evaporation from molten TiC_x", Journal of Materials Science, **21**(1986)176-178.

[5] M. M. El-Nahass, A.A.M. Farag, E.M. Ibrahim, S. abd-El-Rahman, "Structural, optical and electrical properties of thermally evaporated Ag_2S thin films", Vacuum, **72** (2004) 453-460.

[6] N. Sulitanu, "Thermoelectrical properties and memory switch phenomenon in amorphous $Ge_{46}S_{54}$ films", Materials Science and Engineering, **B83** (2001) 84-88.

[7] A. A. Othman, M. A. Osman, H. H. Amer, and A. Dahshan, "Annealing dependence of optical properties of $Ga_{20}S_{75}Sb_5$ and $Ga_{20}S_{40}Sb_{40}$ thin films", Thin Solid Films, **457** (2004) 253-257.

[8] J. Dheepa, R. Sathyamoorthy, S. Velumani, A. Subbarayan, K. Natarajan, P.J. Sebastian, "Electrical resistivity of thermally evaporated bismuth telluride thin films", Solar Energy Materials & Solar Cell, **81** (2004) 305-312.

[9] P. Nagels, R. Mertens, L. Tichy, "Reversible photodarkening in amorphous As_xS_{100-x} films prepared by thermal evaporation and plasma-enhanced chemical vapour deposition", Materials Letters, **57** (2003) 2494-2500.

[10] H.J. Yuan, S.S. Xie, D.F. Liu, X.Q. Yan, Z.P. Zhou, L.J. Ci, J.X. Wang, Y. Gao, L. Song, L.F. Liu, W.Y. Zhou, G. Wang,

"Formation of ZnS nanostructures by a simple way of thermal evaporation", Journal of Crystal Growth, **258** (2003) 225-231.

[11] H. S. Metwally, "Optical parameter studies of as-deposited and annealed $Ge_{30}Sb_{10}S_{60}$ thin films", Vacuum, **62** (2001) 345-351.

[12] E. Marquez, T. Wagner, J.M. Gonzalez-Leal, A.M. Bernal-Oliva, R. Prieto-Alcon, R. Jimenez-Garay, P.J.S. Ewen, "Controlling the optical constants of thermally-evaporated $Ge_{10}Sb_{30}S_{60}$ chalcogenide glass films by photodoping with silver", Journal of Non-Crystalline Solids, **274** (2000) 62-68.

[13] J. Fick, E. J. Knystautas, A. Villeneuve, F. Schiettekatte, S. Roorda, and K. A. Richardson, "High photoluminescence in erbium-doped chalcogenide thin films", Journal of Non-Crystalline Solids, **272** (2000) 200-208.

[14] J. Viens, C. Meneghini, A. Villeneuve, K.A. Richardson, and T. Cardinal, "Fabrication and characterization of integrated optical waveguides in sulphide chalcogenide glasses", Journal of Lightwave Technology, **17** (1999) 1184-1191.

[15] D.M. Mattox, "Handbook of physical vapour deposition (PVD) processing", Noyes Publications, 1998.

[16] A. Chiasera, M. Montagna, C. Tosello, S. Pelli, G.C. Righini, M. Ferrari, L. Zampedri, A. Monteil, P. Lazzeri, "Enhanced spectroscopic properties at 1.5μm in Er^{3+}/Yb^{3+}-activated silica-titania planar waveguides fabricated by RF-sputtering", Optical Materials, **25** (2004) 117-122.

[17] G.C. Righini, S. Pelli, M. Ferrari, C. Armellini, L. Zampedri, C. Tosello, S. Ronchin, R. Rolli, and S.J.L. Ribeiro, "Er-doped silica-based waveguides prepared by different techniques: RF-sputtering, sol-gel and ion-exchange", Optical and Quantum Electronics, **34** (2002) 1151-1166.

[18] C.Y. Tai, C. Grivas, and J.S. Wilkinson, "UV photosensitivity in a Ta_2O_5 rib waveguide Mach-Zehnder interferometer", IEEE Photonics Technology Letters, **16** (2004) 1522-1524.

[19] C. Tosello, F. Rossi, S. Ronchin, R. Rolli, G.C. Righini, F. Pozzi, C. Duverger, A. Chiappini, C. De Bernardi, "Erbium-activated silica-titania planar waveguides on silica-on-silicon substrates prepared by RF-sputtering", Journal of Non-Crystalline Solids, **284** (2001) 230-236.

[20] S. Kashimura, M. R. Islam, M. Takeuchi, A. Hongo, K. Ohira, K. Imoto, S.Kuma, "Refractive-index-adjustment of SiO_2-GeO_2 films deposited by radio frequency magnetron sputtering", Applied Surface Science, **142** (1999) 58-62.

[21] H. Nagata, T. Fujino, N. Mitsugi, M. Tamai, "Effect of substrate heating on elimination of pinholes in sputtering deposited SiO_2 films on $LiNbO_3$ single crystal substrates", Thin Solid Films, **335** (1998) 117-121.

[22] A. Jdanov, J. Pelleg, Z. Dashevsky, R. Shneck, "Growth and characterization of PbTe films by magnetron sputtering", Materials Science and Engineering, **B106** (2004) 89-94.

[23] S. Ramachandran and S. G. Bishop, "Low loss photoinduced waveguides in rapid thermally annealed films of chalcogenide glasses", Applied Physics Letters, **74** (1999) 13-15.

[24] C.L. Bonner, A.A. Anderson, R.W. Eason, D.P. Shepherd, D.S. Gill, C. Grivas, N. Vainos, "Performance of a low pulsed laser deposited Nd:$Gd_3Ga_5O_{12}$ waveguide laser at 1.06μm and 0.94μm", Optics Letters, **22** (1997) 988-990.

[25] A.A. Anderson, C.L. Bonner, D.P. Shepherd, R.W. Eason, C. Grivas, D.S. Gill, N. Vainos,"Low loss (0.5dB/cm) Nd:$Gd_3Ga_5O_{12}$ waveguide layers grown by pulsed laser deposition", Optics Communications, **144** (1997) 183-186.

[26] A.A. Anderson, R.W. Eason, L.M.B.Hickey, M. Jelinek, C. Grivas, D.S. Gill, N.A. Vainos, "A Ti:sapphire planar waveguide laser grown by pulsed laser deposition", Optics Letters, **22** (1997) 1556-1558.

[27] D.S. Gill, R.W. Eason, C. Zaldo, H.N. Rutt, N.A. Vainos, "Characterization of Ga-La-S chalcogenide glass thin-film optical waveguides, fabricated by pulsed laser deposition", Journal of Non-Crystalline Solids, **191** (1995) 321-326.

[28] R. Asal, H.N. Rutt, "Optical properties of laser ablated gallium lanthanum sulphide chalcogenide glass thin films prepared at different deposition laser energy densities", Optical Materials, **8** (1997) 259-268.

[29] K.E. Youden, T. Grevatt, R.W. Eason, H.N. Rutt, R.S. Deol, G. Wylangowski, "Pulsed laser deposition of Ga-La-S chalcogenide glass thin film optical waveguides", Applied Physics Letters, **63** (1993) 1601-1603.

[30] A.V. Rode, A. Zakery, M. Samoc, R.B. Charters, E.G. Gamaly, B. Luther-Davies, "Laser-deposited As_2S_3 chalcogenide films for waveguide applications", Applied Surface Science, **197-198** (2002) 481-485.

[31] A.P. Caricato, M. De Sario, M. Fernandez, M. Ferrari, G. Leggieri, A. Luches, M. Martino, M. Montagna, F. Prudenzano, A. Jha, "Chalcogenide glass thin film waveguides deposited by excimer laser deposition", Applied Surface Science, **208-209** (2003) 632-637.

[32] P. Nemec, J. Jedelsky, M. Frumar, M. Stabl, M. Vlcek, "structure, thermally and optically induced effects in amorphous As_2Se_3 films prepared by pulsed laser deposition", Journal of Non-Crystalline Solids, **65** (2004) 1253-1258.

[33] P. Nemec, M. Frumar, J. Jedelsky, M. Jelinek, J. Lancok, I. Gregora, "Thin amorphous chalcogenide films prepared by pulsed laser deposition", Journal of Non-Crystalline Solids, **299-302** (2002) 1013-1017.

[34] D.W. Harwood, E.R. Taylor, R. Moore, D.N. Payne, "Fabrication of fluoride glass planar waveguides by hot dip spin coating", Journal of Non-Crystalline Solids, **332** (2003) 190-198.

[35] A.K. Mairaj, R.J. Curry, D.W. Hewak, "Chalcogenide glass thin films through inverted deposition and high velocity spinning", Electronics Letters, **40** (2004) 421-422.

[36] L.C. Klein, "Sol-Gel technology for thin film, fiber preforms, electronics, and specialty shaped", Noyes Publications, 1988.

[37] R.R.A. Syms, V. Schneider, W. Huang, and M.M. Ahmad, "High-Δn silica-on-silicon channel waveguides based on sol-gel germano-phosphosilicate glass", Electronics Letters, **33** (1997) 1216.

[38] C.J. Brinker, and G.W. Scherer, "The physics and chemistry of sol-gel processing", Academic Press, 1990.

[39] J. Xu and R.M. Almeida, "Preparation and characterization of germanium sulphide based sol-gel planar waveguides", Journal of Sol-Gel Technology, **19** (2000) 243-248.

[40] J. Xu, and R.M. Almeida, "Sol-gel derived germanium sulphide planar waveguides", Materials Science in Semiconductor Processing, **3** (2000) 339-344.

[41] O. M. Martins, J. Xu, and R. M. Almeida, "Sol-gel processing of germanium sulphide based films", Journal of Non-Crystalline Solids, **256&257** (1999) 25-30.

[42] H. Nagayama, H. Honda, H. Kawahara, "A new process for silica coating", J. Electrochem. Soc., **135** (1988) 2013-2015.

[43] T.J. Richardson, and M.D. Rubin, Electrochimica Acta, "Liquid phase deposition of electrochromic thin films", **46** (2001) 2119-2123.

[44] Kanamori *et al.*, "Method for fabricating an optical waveguide", US Patent 5556442, Sept.17 (1996)

[45] Tetsuo Miya, "Silica-based planar lightwave circuits: passive and thermally active devices", IEEE Journal of Selected Topics in Quantum Electronics", **6** (2000) 38-45.

[46] P. J. Melling, "Alternative methods of preparing chalcogenide glasses", American Ceramic Society Bulletin, **63** (1984) 1427-1429.

[47] S. Nakamura, "Introduction to nitride semiconductor blue lasers and light emitting diodes", CRC Press, 2000.

[48] Bazylenko *et al.*, "Fabrication method of making silica-based optical devices and opto-electronic devices", US Patent 6154582, Nov. 28 (2000).

[49] H. Ticha, L. Tichy, P. Nagels, E. Sleeckx, and R. Callaertsm, "Temperature dependence of the optical gap in thin amorphous films of As_2S_3, As_2Se_3 and other basic non-crystalline chalcogenides", Journal of Physics and Chemistry of solids, **61** (2000) 545-550.

[50] E. Marquez, P. Nagels, J.M. Gonzalez-Leal, A.M. Bernal-Oliva, E. Sleeckx, R. Callaerts, "On the optical constants of amorphous Ge_xSe_{1-x} thin films of non-uniform thickness prepared by plasma-enhanced chemical vapour deposition", Vacuum, **52** (1999) 55-60.

[51] P. Nagels, L. Tichy, R. Mertens, R. Callaerts, "Low-temperature photodarkening of As_xSe_{100-x} system prepared by PECVD, Materials Letters, **46** (2000) 234-238.

[52] P. Nagels, E. Sleeckx, R. Callaerts, E. Marquez, J.M. Gonzalez, and A. M. Bernal-Oliva, "Optical properties of amorphous Se films prepared by PECVD", Solid State Communication, **102** (1997) 539-543.

[53] V. Boev, E. Sleeckx, M. Mitkova, P. Markovsky, P. Nagels, and K. Zlatanova, "Holographic investigation of photoinduced changes in PECVD Ge-Se thin films", Vacuum, **47** (1996) 1211-1213.

[54] P. Nagels, E. Sleeckx, R. Callaerts, and L. Tichy, "Structural and optical properties of amorphous selenium prepared by plasma-enhanced CVD", Solid State Communication, **94** (1995) 49-52.

[55] E. Sleeckx, P. Nagels, R. Callaerts, and M. Vanroy, "Plasma-enhanced CVD of amorphous Ge_xS_{1-x} and Ge_xSe_{1-x} films", Journal de Physique IV, **3** (1993) 419-426.

[56] H. M. Manasevit, "Sigle-crystal gallium arsenide on insulating substrates", Applied Physics Letters, **12** (1968)156-159.

[57] Fujiura Kazuo, "Production of chalcogenide glass containing rare earth metal ion", Japanese Patent 6122523, May 06 (1994).

[58] T. Izawa and H. Nakagome, "Optical waveguide formed by electrically induced migration of ions in glass plates", Applied Physics Letters, **21** (1972) 584-586.

[59] G. Lifante, E. Cantelar, J. A. Munoz, R. Nevado, J. A. Sanz-Garcia, and F. Cusso, "Zn-diffused $LiNbO_3:Er^{3+}/Yb^{3+}$ as a waveguide laser material", Optical Materials, **13** (1999)181-186.

[60] V. Apostolopoulos, L.M.B. Hickey, D. A. Sager, and J. S. Wilkinson, "Gallium-diffused waveguides in sapphire", Optics Letters, **26** (2001) 1586-1588.

[61] D. Homoelle, S. Wielandy, A. L. Gaeta, N. F. Borrelli, and C. Smith, "Infrared photosensitivity in silica glasses exposed to femtosecond laser pulses", Optics Letters, **24** (1999) 1311-1313.

[62] A.K. Mairaj, P. Hua, H.N. Rutt, D.W. Hewak, "Fabrication and characterization of continuous wave direct UV (λ=244nm) written channel waveguides in chalcogenide (Ga:La:S) glass", Journal of Lightwave Technology, **20** (2002) 1578-1584.

[63] J.W. Chan, S.H. Risbud, J.S. Hayden, D.M. Krol, "Waveguide fabrication in phosphate glasses using femtosecond laser pulses", Applied Physics Letters, **82** (2003) 2371-2373.

[64] R. Osellame, S. Taccheo, M. Marangoni, R. Ramponi, and P. Laporta, "Femtosecond writing of active optical waveguides with astigmatically shaped beams", J. Opt. Soc. Am. B, **20** (2003) 1559-1567.

[65] R. Osellame, S. Taccheo, G. Cerullo, M. Marangoni, D. Polli, R. Ramponi, P. Laporta, S. De Silvestri, "Optical gain in Er-Yb doped waveguides fabricated by femtosecond laser pulses", Electronics Letters, **38** (2002) 964-965.

[66] D. M. Krol, "Waveguide fabrication in glasses using femto-second laser pulses", Glass Science and Technology, **75** (2002) 164-180.

[67] O.M. Efimov, L.B. Glebov, K.A. Richardson, E. Van Stryland, T. Cardinal, S.H. Park, M. Couzi, J.L. Bruneel, "Waveguide writing in chalcogenide glasses by a train of femtosecond laser pulses", Optical Materials, **17** (2001)379-386.

[68] S.A. Campbell, "The Science and Engineering of Microelectronic Fabrication", 2nd, Oxford University Press, 2001.

[69] S.J. Pearton, "Wide bandgap semiconductors: Growth, Pro-cessing and Applications", William Andrew Publishing/Noyes, 2000.

[70] D.W. Hewak, private communication (12/09/2003).

[71] Yamame Masayuki, Yoshiyuki Asahara, "Glasses for Photonics", Cambridge University Press, 2000.

[72] D.J. Brady, "Gallium lanthanum sulphide based glasses for mid-infrared optical fibres", PhD. Thesis, University of Southampton, 2000.

[73] L.B. Shaw, B. Cole, P.A. Thielen, J.S. Sanghera, and I.D. Aggarwal, "Mid-wave IR and long-wave IR laser potential of rare-earth doped chalcogenide glass fiber", IEEE Journal of Quantum Electronics, **48** (2001) 1127-1137.

[74] Keiji Tanaka, "Photoinduced processes in chalcogenide glasses", Current Opinion in Solid State & Materials Science, **1** (1996) 567-571.

[75] E. M. Vogel, M. J. Weber, and D. M. Krol, "Nonlinear optical phenomena in glass", Physics and Chemistry of Glasses, **32** (1991) 231-254.

[76] J. Requejo-Isidro, A.K. Mairaj, V. Pruneri, D.W. Hewak, M.C. Netti, J.J. Baumberg, "Self refractive non-linearities in chalcogenide based glasses", Journal of Non-Crystalline Solids, **317** (2003) 241-246.

[77] F. Smektala, C. Quemard, V. Couderc, A. Barthelemy, "Non-linear optical properties of chalcogenide glasses measured by Z-scan", Journal of Non-Crystalline Solids, **274** (2000) 232-237.

[78] G. Lenz, J. Zimmermann, T. Katsufuji, M.E. Lines, H.Y. Hwang, S. Spalter, R.E. Slusher, and S.-W. Cheong, "Large Kerr effect in bulk Se-based chalcogenide glasses", Optics Letters, **25** (2000) 254-256.

[79] J. M. Harbold, F. O. Ilday, F. W. Wise, J. S. Sanghera, V. Q. Nguyen, L. B. Shaw, I. D. Aggarwal, "Highly nonlinear As-S-Se glasses for all-optical switching", Optics Letters, **27** (2002) 119-121.

[80] D.W. Hewak, "Properties, processing and applications of glass and rare earth-doped glasses for optical fibres", INSPEC, 1998.

[81] A.K. Mairaj, "Optical waveguides and lasers in improved gallium lanthanum sulphide glass", PhD. Thesis, University of Southampton, 2003.

[82] K. Petkov, P.J.S Ewen, "Photoinduced changes in the linear and nonlinear optical properties of chalcogenide glasses", Journal of Non-Crystalline Solids, **249** (1999) 150-159.

[83] M. Petrovich, A.K. Mairaj, D.W. Hewak, H.N. Rutt, "Temperature dependence of reversible photodarkening in Ga:La:S and Ga:La:S:O glass fibres", XIX International Congress on Glass, Edinburgh 1-6 Jul. 2001, **2** (2001) 951-952.

[84] R. Todorov, Tz. Iliev, K. Petkov, "Light-induced changes in the optical properties of thin films of Ge-S-Bi(Tl,In) chalcogenides", Journal of Non-Crystalline Solids, **326&327** (2003) 263-267.

[85] Q. Liu, and F. Gan, "Photobleaching in amorphous GeS_2 thin films", Materials Letters, **53** (2002) 411-414.

[86] E. Marquez, A.M. Bernal-Oliva, J.M. Gonzalez-Leal, R. Prieto-Alcon, R. Jimenez-Garay, "On the reversible photo-bleaching phenomenon in obliquely-evaporated GeS_2 glass films", Journal of Non-Crystalline Solids, **222** (1997) 250-257.

[87] C.C. Huang, D.W. Hewak, and J.V. Badding, "Deposition and characterization of germanium sulphide glass planar waveguides", Optics Express, **12** (2004) 2501-2506.

[88] A. V. Stronski, M. Vlcek, A. Sklenar, P. E. Shepeljavi, S. A. Kostyukevich, T. Wagnar, "Application of $As_{40}S_{60-x}Se_x$ layers for high-efficiency grating production", Journal of Non-Crystalline Solids, **266-269** (2000) 973-978.

[89] T. Wagner, and P.J.S. Ewen, "Photo-induced dissolution effect in $Ag/As_{33}S_{67}$ multilayer structures and its potential application", Journal of Non-Crystalline Solids, **266-269** (2000) 979-984.

[90] D. Marchese and A. Jha, "The structural aspects of the solubility of Pr^{3+} in GeS_2-based glasses", Journal of Non-Crystalline Solids, **213&214** (1997) 381-387.

[91] D. R. Simons, A. J. Faber, and H. de Waal, "GeS_x glass for Pr^{3+} - doped fiber amplifiers at 1.3 μm", Journal of Non-Crystalline Solids, **185** (1995) 283-288.

[92] J. S. Sanghera, and I. D. Aggarwal, "Active and passive chalcogenide glass optical fibers for IR applications: a review", Journal of Non-Crystalline Solids, **256&257** (1999) 6-16.

[93] D.W. Hewak, J.A. Medeiros Neto, B. Samson, R.S. Brown, K.P. Jedrzejewski, J. Wang, E. Tayler, R.I. Laming, G. Wylangowski, and D.N. Payne, "Quantum-efficiency of praseodymium doped Ga:La:S glass for 1.3 μm optical fibre amplifiers", IEEE Photonics Technology Letters, **6** (1994) 609-612.

[94] G. G. Devyatykh, M. F. Churbanov, I. V. Scripachev, G. E. Snopatin, E.M. Dianov, V.G. Plotnichenko, "Recent developments in As-S glass fibres", Journal of Non-Crystalline Solids, **256&257** (1999) 318-322.

[95] R. Mossadegh, J.S. Sanghera, D. Schaafsma, B.J. Cole, V.Q. Nguyen, R.E. Miklos, and I.D. Aggarwal, "Fabrication of single-mode chalcogenide optical fiber", Journal of Lightwave Technology, **16** (1998) 214-217.

[96] J.S. Sanghera, L.E. Busse, and I.D. Aggarwal, "Effect of scattering centers on the optical loss of As_2S_3 glass fibers in the infrared", Journal of Applied Physics, **75** (1994) 4885-4891.

[97] D.J. Brady, T.Schweizer, J. Wang, D.W. Hewak, "Minimum loss predictions and measurements in gallium lanthanum sulphide based glasses and fibre", Journal of Non-Crystalline Solids, **242** (1998) 92-98.

[98] A. Mori, Y. Ohishi, T. Kanamori, and S. Sudo, "Optical amplification with neodymium-doped chalcogenide glass fiber", Applied Physics Letters, **70** (1997) 1230-1232.

[99] B. Cole, L.B. Shaw, P.C. Pureza, R. Mossadegh, J.S. Sanghera, I.D. Aggarwal, "Rare-earth doped selenide glasses and fibers for active applications in the near and mid-IR", Journal of Non-Crystalline Solids, **256&257** (1999) 253-259.

[100] T. Schweizer, D.J. Brady, and D.W. Hewak, "Fabrication and spectroscopy of erbium doped gallium lanthanum sulphide glass fibres for mid-infrared laser applications", Optics Express, **1** (1997) 102-107.

[101] T. Schweizer, B.N. Samson, R.C. Moore, D.W. Hewak, and D.N. Payne, "Rare-earth doped chalcogenide glass fibre laser", Electronics Letters, **33** (1997) 414-416.

[102] S. Kawanishi, H. Takara, K. Uchiyama, M. Saruwatari, and T. Kitoh, "Fully time-division-multiplexed 100 Gbit/s optical transmission experiment", Electronics Letters, **29** (1993) 2211-2212.

[103] M. Asobe, "Nonlinear optical properties of chalcogenide glass fibers and their application to all-optical switching", Optical Fiber Technology, **3** (1997) 142-148.

[104] R.R. Alfano, "The Supercontinuum Laser Source", Springer-Verlag, 1989.

[105] R.R. Alfano and S.L. Shapiro, "Emission in the region 4000 to 7000 angstrom via four-photon coupling in glass", Phys. Rev. Lett., **24** (1970) 584-587.

[106] T. Morioka, K. Mori, and M. Saruwatari, "More than 100-wavelength-channel picosecond optical pulse generation from single laser source using supercontinuum in optical fibres", Electronics Letters, **29** (1993) 862-864.

[107] D.J. Jones, S.A. Diddams, J.K. Ranka, A. Stentz, R.S. Windeler, J.L. Hall, and S.T. Cundiff, "Carrier-envelope phase control of femtosecond mode-locked lasers and direct optical frequency synthesis", Science, **288** (2000) 635-639.

[108] J.K. Ranka, R.S. Windeler, and A.J. Stentz, "Visible continuum generation in air-silica microstructure optical fibres with anomalous dispersion at 800nm", Optics Letters, **25** (2000) 25-27.

[109] S. Coen, A.H.L. Chau, R. Leonhardt, J.D. Harvey, J.C. Knight, W.J. Wadsworth, and P.St.J. Russell, "White light supercontinuum generation with 60-ps pulses pump in a photonic crystal fiber", Optics Letters, **26** (2001) 1356-1358.

[110] Mesophotonics Ltd., Southampton, U.K. (www.mesophotonics.com)

Chapter 3

Sol-Gel process for planar waveguides

3.1 Introduction

Glass preparation by the sol-gel process has been extensively studied since H. Dislich [1] reported the formation of borosilicate glass by hot-pressing granules of dehydrated gel in 1971. The sol-gel process begins with formation of a sol, consisting of colloids dispersed in a liquid medium. A sol turns into a porous gel by the coagulation of these colloids while standing in a mold or on a substrate which is used as a coating film base. The gel thus obtained is dried and sintered into a pore-free dense glass, or glass film, at a temperature slightly above the glass transition temperature of the eventual glass [2-5].

The sol-gel process is a versatile solution process for making advanced materials, including ceramics and organic-inorganic hybrids. In general, the sol-gel process involves the transition of a solution system from a liquid "sol" (mostly colloidal) into a solid "gel" phase. Utilizing the sol-gel process, it is possible to fabricate advanced materials in a wide variety of forms: ultrafine or spherical shaped powders, thin film coatings, fibers, porous or dense materials, and extremely porous aerogel materials.

The starting materials used in the preparation of the "sol" are usually inorganic metal salts or metal organic compounds such as metal alkoxides. In a typical sol-gel process, the precursor is subjected to a series of hydrolysis and polymerization reactions to form a

colloidal suspension, or a "sol". Further processing of the "sol" makes it possible to make materials in different forms.

There are various ways of preparing a sol which depend on the material to be made. In the case of the formation of bulk glass, the most widely used method is the hydrolysis and poly-condensation of silicon alkoxide or its mixture with the alkoxides of Ti, Al, Zr, Ge, etc. Representative metal alkoxides employed in the glass preparation by hydrolysis and poly-condensation are shown in Table 3.1 [6].

The hydrolysis and condensation reactions of these metal alkoxides are schematically expressed by following equations.

$$\mathbf{M}(OR)_n + n\,H_2O \longleftrightarrow \mathbf{M}(OH)_n + n\,ROH \qquad (3.1)$$

$$m\,\mathbf{M}(OH)_n \longleftrightarrow m\,\mathbf{M}O_{n/2} + (mn/2)\,H_2O \qquad (3.2)$$

where **M** is Si, Al, Ti, Ge, B, Zr, etc.,
R is CH_3, C_2H_5, C_3H_7, C_4H_9, etc.

Table 3.1 Representative metal alkoxides employed in glass preparation [6]

Alkoxides	Formula	Boiling point (°C/mmHg)
Boron *n*-butoxide	$B(OBu^n)_3$	128/760
Aluminium *n*-propoxide	$Al(OPr^n)_3$	205/1.0, 245/10.0
Aluminium *n*-butoxide	$Al(OBu^n)_3$	242/0.7, 284/10.0
Aluminium *tert*-butoxide	$Al(OBu^t)_3$	151/1.3, 185/10.0
Silicon ethoxide (TEOS)	$Si(OEt)_4$	168/760

Silicon methoxide (TMOS)	$Si(OMe)_4$	153/760
Germanium ethoxide	$Ge(OEt)_4$	86/12.0
Titanium ethoxide	$Ti(OEt)_4$	103/0.1
Titanium *tert*-butoxide	$Ti(OBu^t)_4$	93.8/5.0
Zirconium ethoxide	$Zr(OEt)_4$	190/0.1

Me: CH_3, Et: C_2H_5, Pr: C_3H_7, *n*-Bu: C_4H_9, *tert*-Bu: $(CH_3)_3C$

The basic procedure to form, for example, a silica glass rod using silicon methoxide as the starting material is schematically illustrated in Figure 3.1 [2, 3].

It should be noted that the highest temperature required to obtain a silicate glass is 1000°C, which is lower by about 1000°C than the temperature required for the melt-quenching and MCVD techniques. Thus the sol-gel process has great advantages over the melt-quenching technique for the preparation of glasses containing a large amount of refractory materials such as Al_2O_3, TiO_2, ZrO_2, GeO_2, etc. In addition, unlike the CVD process it is possible to prepare glasses containing alkali, alkali-earth, and rare-earth elements, etc. by using aqueous solutions of their salts instead of water in the process shown in Figure 3.1. Another advantage of this low-temperature process is that it is possible to incorporate thermally unstable compounds such as non-oxide semiconductors into a glass to develop a glass with special properties such as high optical nonlinearity.

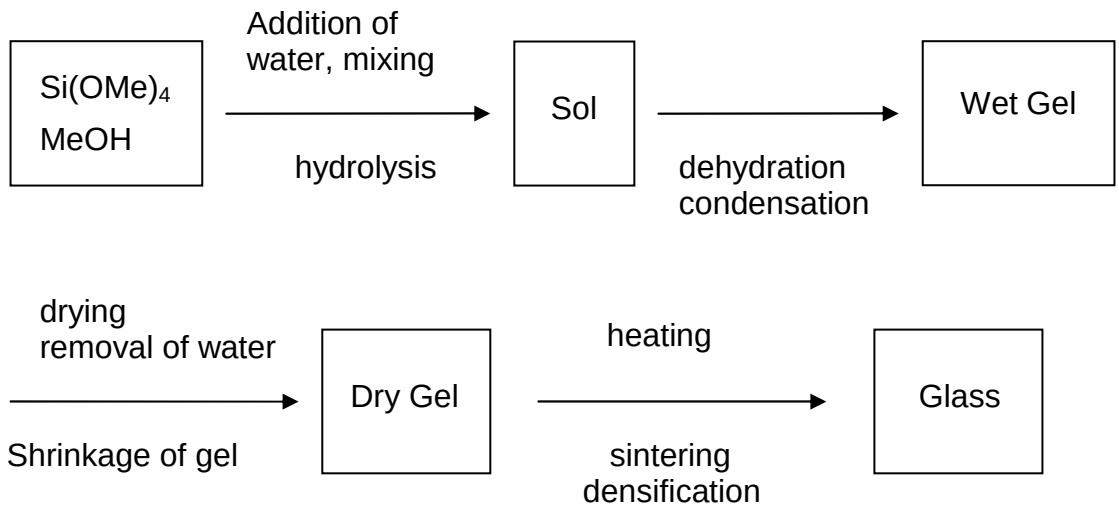

Fig. 3.1 Schematic illustration of sol-gel process for glass preparation.

High purity metal alkoxides are commercially available because most alkoxide precursors are in a liquid state and they are easily purified by repeated distillation. Moreover, in contrast to melt-quenching techniques, the sol-gel process is conducted in the solution and there is no possibility of contamination from a container because this is a process that does not use a crucible. With these advantages, it is also possible to obtain glasses of very high purity such as those used for fabrication of optical fibre.

There are of course some drawbacks or disadvantages compared with the two other processes discussed above. The biggest drawback of the sol-gel process is the large amount of shrinkage of a wet gel upon drying, which often leads to fracture. The other big problems which have to be overcome are the preferential precipitation of a particular oxide during sol formation, for multi-component glasses made from alkoxide precursors, and the heterogeneous precipitation of

metal salts on the surface during the drying of a gel which was made using aqueous solutions of metal salts as the source of alkali, alkali-earth oxide, etc [2].

The sol-gel technique has been widely used in oxide based glasses, especially in silica glass, but with limited application in the sulphide glasses. However, an indirect sol-gel technique for chalcogenide glass (germanium sulphide) has also been developed [7-9].

As described in Chapter 2, chalcogenide glasses are particularly promising for the next generation of optoelectronic devices. The GaLaS or GaLaSO glasses have been developed in our previous research work by melt-quenching technique [11]. Since the sol-gel technique is a low-temperature, flexible, high volume, high purity and low cost method to make a slab waveguide, it would be desirable to fabricate chalcogenide, particularly GaLaS or GaLaSO, thin film or bulk glass by using this indirect sol-gel technique.

The idea here is to fabricate Ga-O-Ga and La-O-La wet gels from gallium ethoxide and lanthanum ethoxide respectively. After mixing a suitable stoichiometric ratio of Ga-O-Ga and La-O-La wet gels, a Ga-O-Ga / La-O-La thin film can be formed on a substrate by a spinning & coating method. Then this thin film can be placed in a furnace, with H_2S gas flow, for heat treatment and then converted to a GaLaS/GaLaSO glass thin film on the substrate.

3.2 Apparatus and experimental methods

In the sol-gel process, the precursors, metal alkoxides, play the key roles in the reaction. Therefore, in our plan, we will use germanium ethoxide as the starting precursor for Ge-O-Ge sol-gel formation, gallium ethoxide for Ga-O-Ga sol-gel formation, and lanthanum ethoxide for La-O-La sol-gel formation.

For GaLaS/GaLaSO, Ga-O-Ga and La-O-La wet gels can be synthesized by the following possible equations.

Hydrolysis: $Ga(OEt)_3 + 3\ H_2O \longleftrightarrow Ga(OH)_3 + 3\ EtOH$

Condensation: $2\ Ga(OH)_3 \longleftrightarrow 2\ GaO_{3/2} + 3\ H_2O$ (3.3)

Hydrolysis: $La(OEt)_3 + 3\ H_2O \longleftrightarrow La(OH)_3 + 3\ EtOH$

Condensation: $2\ La(OH)_3 \longleftrightarrow 2\ LaO_{3/2} + 3\ H_2O$ (3.4)

where Et is C_2H_5

3.2.1 Ge-O-Ge gel fabrication

With the source available and the approved process [7-9], germanium ethoxide was used as the starting material to form Ge-O-Ge gel for our first trial; the process is schematically shown in Figure 3.2. 2ml germanium ethoxide (99.995% pure from Alfa Aesar) was dissolved in 40ml propanol (99.9+% pure from Aldrich). 100μl propionic acid (99.5+% pure from Aldrich) was added into the above

solution. Then 100μl deionised water was added slowly to the solution. The solution was aged at room temperature in a covered flask for 3 days under continuous stirring.

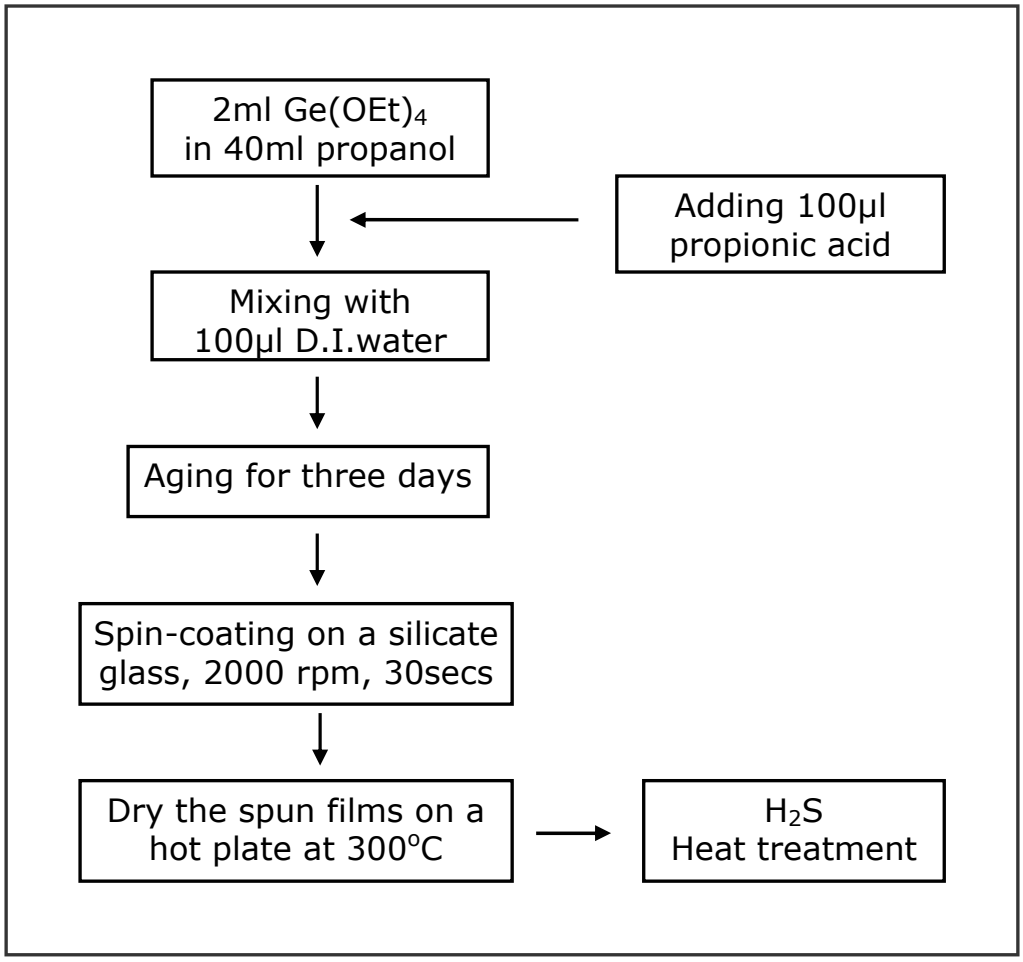

Fig. 3.2 Sol-gel processes for germanium sulphide glassy films

3.3 Results

By following the sol-gel process in Figure 3.2, a transparent white Ge-O-Ge wet gel solution was fabricated in the flask. This solution was then filtered by 0.2μm filter and then used for the deposition of a Ge-O-Ge thin film on a borosilicate glass substrate. The deposited Ge-O-Ge thin film was then dried on a hot plate at about 300 °C. Moreover,

the filtered Ge-O-Ge wet gel solution was dried by a hot plate to remove the solvent and then to produce Ge-O-Ge dry gel powders.

3.4 Characterization

3.4.1 Raman Analysis

A Raman technique was used to characterize the Ge-O-Ge thin film and gel powders. The Raman analyzer used is RENISHAW Ramascope equipped with a CCD camera. A 633nm He-Ne laser was used to excite the sample and the Raman shifted spectrum was measured from 1000cm^{-1} to 100cm^{-1} with a resolution of 1cm^{-1}.

The Ge-O-Ge thin film was too thin to get a Raman shift spectrum with an identifiable intensity. However, the Ge-O-Ge dry gel powders can be measured by the Raman technique and the Raman shifted spectrum (Figure 3.3) reveals some significant peaks although there are a few spike peaks in the spectrum due to the powder sample.

From Martins *et al.* [9], the absorption peaks of the Ge-O bond are at 870 and 560 cm^{-1}. More than two peaks can be found in the Raman shifted spectrum of Ge-O-Ge powders (Figure 3.3), and another strong peak at 770cm^{-1} was also found in the spectrum. From Sigaev *et al.* [10], the peak is assigned to the Ge-O bonding in octahedral GeO_6 structure. Therefore, the Ge-O-Ge gels we have fabricated are mixtures with different structures.

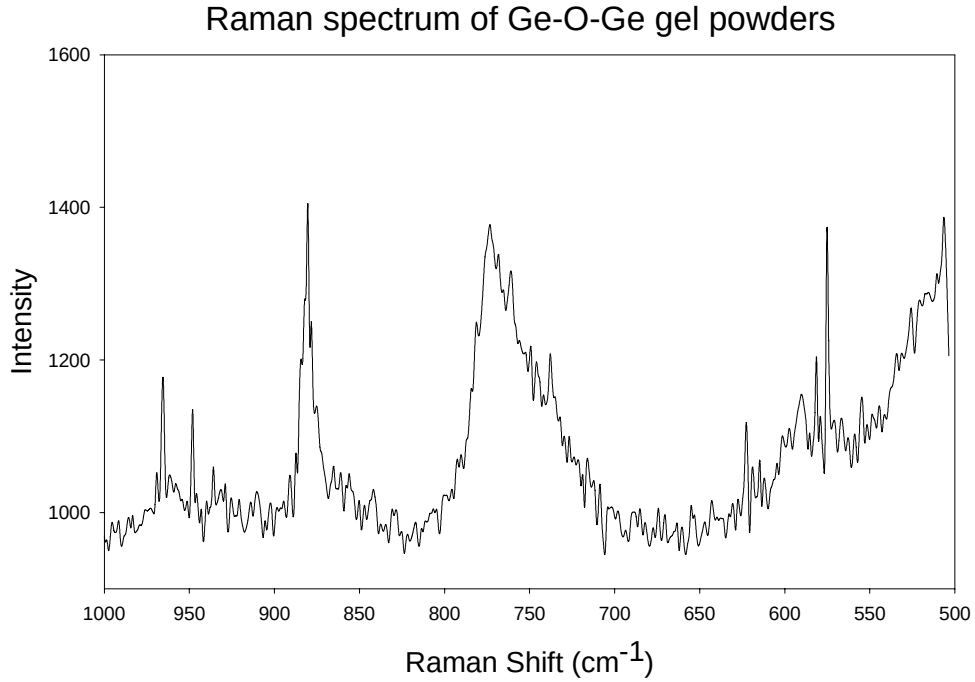

Fig. 3.3 Raman spectrum of Ge-O-Ge gel powders

3.5 Conclusion

The Ge-O-Ge gel powders and films on a substrate have been successfully fabricated by the sol-gel process, but the conversion from germanium oxide to germanium sulphide glass and further characterization of the films have not been done yet. Since a direct fabrication of the planar/slab germanium sulphide glass waveguides by chemical vapour deposition (CVD) has been developed, the future research work of this thesis will focus on the CVD process.

3.6 References

[1] H. Dislich, Glastech. Ber. **44** (1971) 1.

[2] C. J. Brinker, and G. W. Scherer, "The physics and chemistry of sol-gel processing", Academic Press, 1990.

[3] L.C. Klein, "Sol-Gel technology for thin film, fiber preforms, electronics, and specialty shaped", Noyes Publications, 1988.

[4] G. W. Scherer and J. C. Luong, "Glasses from colloids", Journal Non-Crystalline Solids **63** (1984) 163-172.

[5] R.R.A. Syms, V. Schneider, W. Huang, and M.M. Ahmad, "High-Δn silica-on-silicon channel waveguides based on sol-gel germano-phosphosilicate glass", Electronics Letters, **33** (1997) 1216.

[6] D. C. Bradley, R. C. Mehrotra and D. P. Gaur, "Metal Alkoxides", (Academic Press, London, 1978) p.42.

[7] J. Xu and R.M. Almeida, "Preparation and characterization of germanium sulphide based sol-gel planar waveguides", Journal of Sol-Gel Technology, **19** (2000) 243-248.

[8] J. Xu, R.M. Almeida, "Sol-gel derived germanium sulphide planar waveguides", Materials Science in Semiconductor Processing, **3** (2000) 339-344.

[9] O. M. Martins, J. Xu, and R. M. Almeida, "Sol-gel processing of germanium sulphide based films", Journal of Non-Crystalline Solids, **256&257** (1999) 25-30.

[10] V.N. Sigaev, I. Gregora, P. Pernice, B. Champagnon, E.N. Smelyanskaya, A. Aronne, P.D. Sarkisov, "Structure of lead germanate glass by Raman spectroscopy", Journal of Non-Crystalline Solids, **279** (2001) 136-144.

[11] A. K. Mairaj, "Optical waveguides and lasers in improved gallium lanthanum sulphide glass", PhD. Thesis, University of Southampton, 2003.

Chapter 4

CVD system and materials technology

4.1 Introduction

Chemical vapour deposition (CVD) is a versatile process suitable for the manufacturing of coatings, powders, fibres, and monolithic components. With CVD, it is possible to produce most metals, many non-metallic elements such as carbon and silicon as well as a large number of compounds including carbides, nitrides, oxides, intermetallics, chalcogenides and many others. This technology is now an essential factor in the manufacture of semiconductors and other electronic components, in the coating of tools, bearings, and other wear-resistant parts and in many optical, optoelectronics and electronic applications [1-5].

A schematic diagram showing the basics of CVD is shown in Figure 4.1. Gaseous reactants and precursors are introduced into a reactor in which the heated substrate is placed. On the surface of the substrate, or in the vicinity of the surface, chemical reactions will occur and as a result a solid material is deposited as a thin film. The gaseous reaction products are then pumped away from the reactor. Normally in a CVD process the precursors can be gases, liquids or even solids at room temperature. CVD is a chemical reaction which characteristically transforms gaseous molecules, called precursors, into a solid material, in the form of thin film or powder, on the surface of a substrate [4].

The materials and CVD reactor systems involved in the demonstration and application of chemical vapour deposition will be reviewed in this chapter.

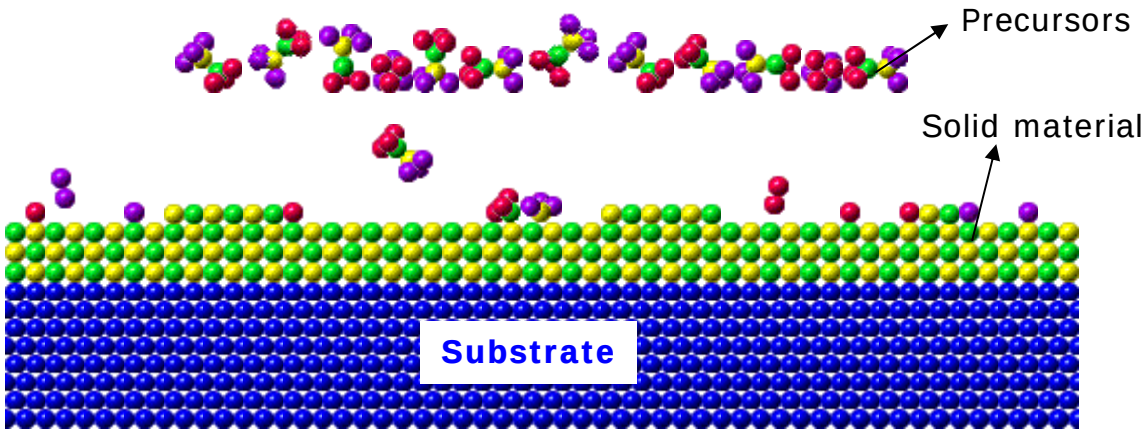

Fig. 4.1 Basic chemical vapour deposition (CVD) process

4.2 Fundamentals of CVD

Chemical vapour deposition is a synthesis process in which the chemical constituents react in the vapour phase near or on a heated substrate to form a solid deposit. The CVD technology combines several scientific and engineering disciplines including thermodynamics, plasma physics, kinetics, fluid dynamics, and of course chemistry. In this section, the fundamental aspects of these disciplines and their relationship will be examined as they relate to CVD [1-5].

4.2.1 Thermodynamics of CVD

A CVD reaction is governed by *thermodynamics,* that is the driving force which indicates the direction in which the reaction is going to

proceed (if at all), and by *kinetics*, which defines the transport process and determines the rate-control mechanism, in other words, how fast it is going [6-16].

Chemical thermodynamics is concerned with the interrelation of various forms of energy and the transfer of energy from one chemical system to another in accordance with the first and second laws of thermodynamics. In the case of CVD, this transfer occurs when the gaseous compounds, introduced in the deposition chamber, react to form the solid deposit and by-products gases.

4.2.1.1 ΔG Calculations and Reaction Feasibility

The first step of a theoretical analysis is to ensure that the desired CVD reaction will take place. This will happen if the thermodynamics is favourable, that is if the transfer of energy—the free energy change of the reaction known as ΔG_r is negative. To calculate ΔG_r it is necessary to know the thermodynamic properties of each component, specifically their free energies of formation (also known as Gibbs free energy), ΔG_f. The relationship is expressed by the following equation:

$$\Delta G_r = \Sigma \Delta G_{f,\,products} - \Sigma \Delta G_{f,\,reactants} \qquad \text{(Eq. 4.1)}$$

The free energy of formation is not a fixed value but varies as a function of several parameters which include the type of reactants, the molar ratio of these reactants, the process temperature, and the process pressure. This relationship is represented by the following equation:

$$\Delta G_r = \Delta G_f + RT \ln Q \qquad \text{(Eq. 4.2)}$$

where: $\Delta G_r = \Sigma_i z_i \Delta G_{f,i}$

z_i = stoichiometric coefficient of species "i" in the CVD reaction (negative for reactants, positive for products)

$\Delta G_{f,i}$ = standard free energy of formation of species "i" at temperature T and 1 atm.

R = gas constant

T = absolute temperature

$Q = \Pi_i a_i^{zi}$

a_i = activity of species "i" which is equal to 1 for pure solids and is $p_i = x_i P_T$ for gases

where p_i = partial pressure of species "i"

x_i = mole fraction of species "i"

P_T = total pressure

By definition, the free energy change for a reaction at equilibrium is zero, hence:

$$\Delta G = -RT \ln K \quad (K \text{ is the equilibrium constant}) \qquad \text{(Eq.4.3)}$$

It is the equilibrium conditions of composition and activities (partial pressure for gases) that are calculated to assess the yield of a desired reaction [6, 14-16].

A demonstration of the feasibility of the reaction between $GeCl_4$ and H_2S to form GeS_2, is the principal objective of this thesis, and will be discussed in chapter 5.

4.2.2 Kinetics and mass-transport mechanisms

4.2.2.1 Deposition sequence

As shown above, a thermodynamic analysis indicates what to expect from the reactants as they reach the deposition surface at a given temperature. The question now is, how do these reactants reach that deposition surface? In other words, what is the mass-transport mechanism? The answer to this question is important because the phenomena involved determine the reaction rate and the design and optimization of the CVD reactor [4, 5].

It should be first realized that any CVD process is subject to complicated fluid dynamics. The fluid, in this case a combination of gases, is forced through pipes, valves, and various chambers and, at the same time, is the object of large variations in temperature and to a lesser degree of pressure before it comes in contact with the substrate where the deposition reaction takes place. The reaction is heterogeneous which means that it involves a change of state, in this case from gaseous to solid [4, 5].

The sequence of events taking place during a CVD reaction is shown graphically in Figure 4.2 and can be summarized as follows [4]:

- Reactant gases enter the reactor by forced flow.
- Gases diffuse through the boundary layer.
- Gases come in contact with surface of substrate.
- Deposition reaction takes place on surface of substrate.
- Gaseous by-products of the reaction are diffused away from the surface, through the boundary layer.

These steps occur in the sequence shown and the slowest step determines the deposition rate. The rules of the boundary layer apply in most CVD depositions in the viscous flow range where pressure is relatively high. In cases where very low pressure is used (i.e., in the mTorr range), the rules are no longer applicable [4, 5].

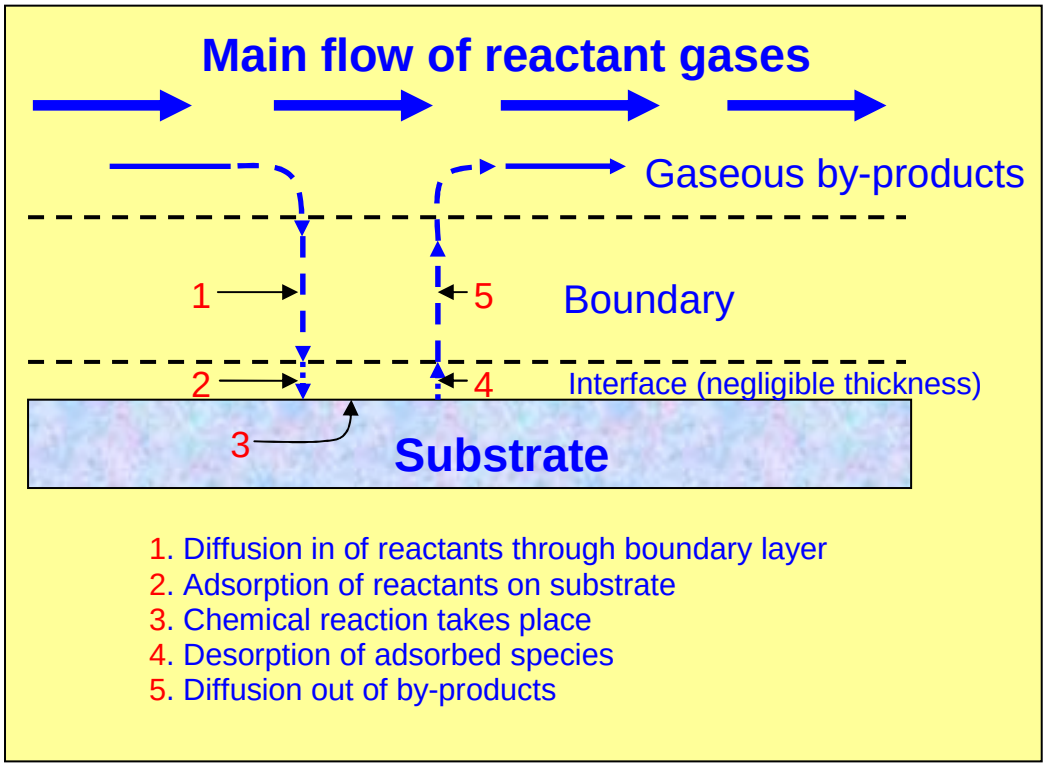

Fig. 4.2 Sequence of events during deposition

4.2.2.2 Boundary layer

The behaviour of the gas as it flows down the tube is controlled by fluid mechanics. It is enough to say that the Reynolds number, R_e, which is a dimensionless parameter that characterizes the flow of a fluid, is such that the gas flow is generally laminar, although in some instances the laminar flow may be disturbed by convective-gas motion and may become turbulent.

In the case of laminar flow, the velocity of the gas at the

deposition surface (the inner wall of the tube) is zero. The boundary is that region in which the flow velocity changes from zero at the wall to essentially that of the bulk gas away from the wall. This boundary layer starts at the inlet of the tube and increases in thickness until the flow becomes stabilized as shown in Figure 4.3. The reactant gases flowing above the boundary layer have to diffuse through this layer to reach the deposition surface as shown in Figure 4.2.

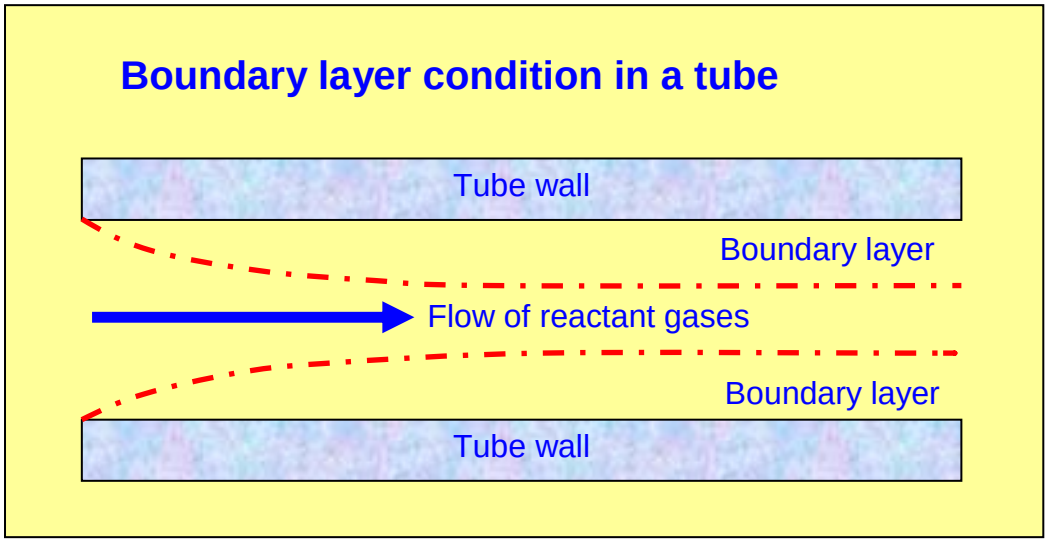

Fig. 4.3 Boundary layer conditions in a tube system

The thickness of the boundary layer, Δ, is inversely proportional to the square root of the Reynolds number as follows:

$$\Delta = \sqrt{\frac{x}{R_e}}$$

where $R_e = \frac{\rho \times u_x}{\mu}$

ρ = mass density

u = flow velocity

x = distance from inlet in flow direction

μ = viscosity

This means that the thickness of the boundary layer increases with lower gas-flow velocity and with increased distance from the tube inlet [1, 4-5].

4.2.2.3 Gas velocity

It is possible to obtain an approximate visualization of the gas-flow pattern by using TiO_2 smoke (generated when titanium chloride comes in contact with moist air), although thermal diffusion may keep the smoke particles away from the hot surface where a steep temperature gradient exists [17]. Figure 4.4 shows a typical velocity pattern in a horizontal tube. As mentioned above, a steep velocity gradient is noticeable going from maximum velocity at the centre of the tube to zero velocity at the surface of the wall. The gradient is also shallow at the entrance of the tube and increases gradually toward downstream [1, 4-5, 17-22].

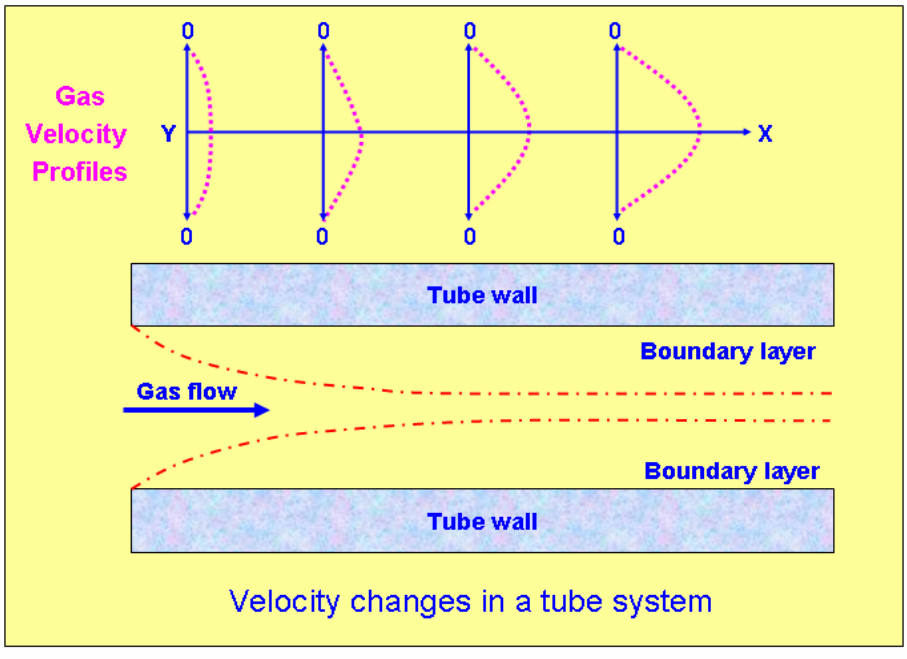

Fig. 4.4 Boundary layer and velocity changes in a tube system, showing the radial velocity recorded at different positions in the tube

4.2.2.4 Temperature

Figure 4.5 shows a typical temperature profile [4-5, 20-21]. The temperature boundary layer is similar to the velocity layer. The flowing gases heat rapidly as they come in contact with the hot surface of the tube, resulting in a steep temperature gradient. The average temperature increases towards the downstream end.

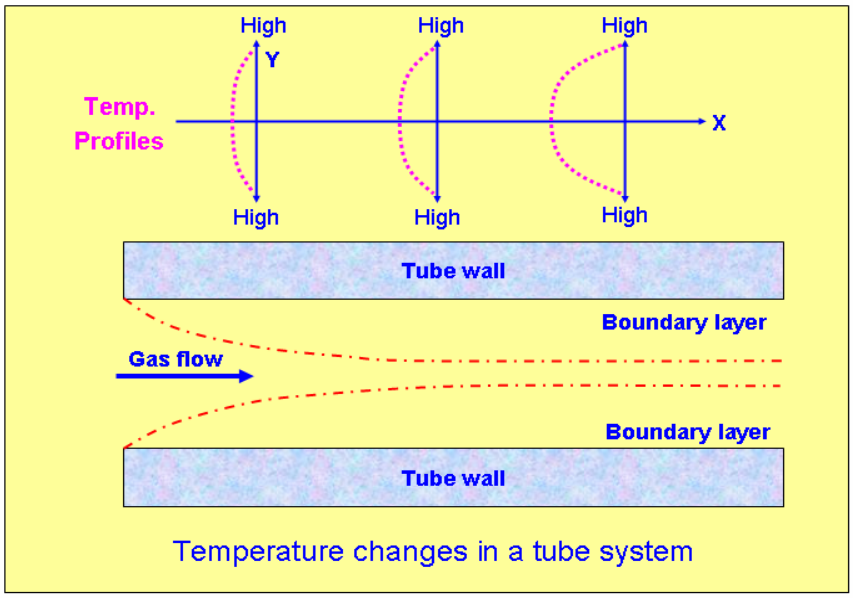

Fig. 4.5 Temperature boundary layer and temperature changes in a tube system, showing the temperature distribution at different positions in the tube

4.2.2.5 Reactant-gas concentration

As the gases flow down the tube, they become gradually depleted as the products are deposited and the amount of the by-product gases increase in the boundary layer. This means that, at some point downstream, deposition will cease altogether when the reactant is no longer present [1, 4-5, 21]. The reactant concentration is illustrated in Figure 4.6.

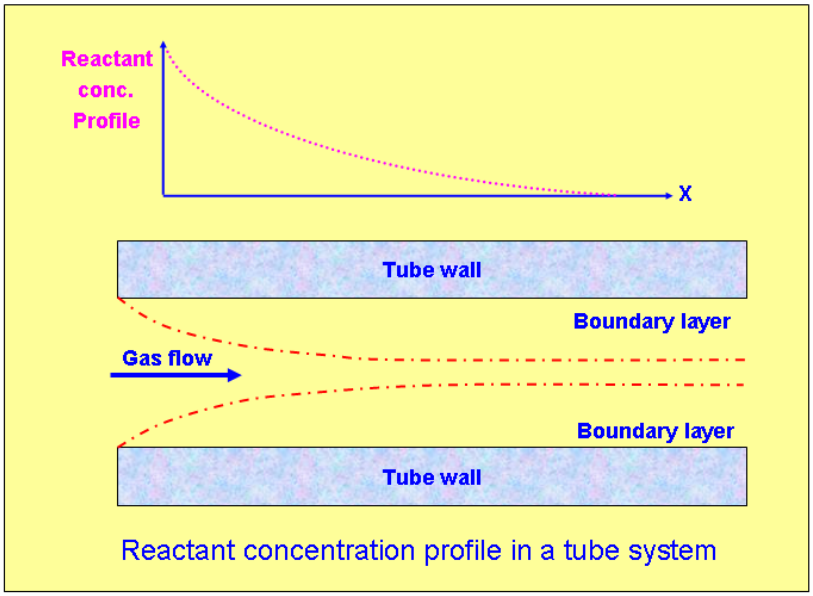

Fig. 4.6 Changes in reactant concentration in a tube system along the length of the tube

The boundary layers for these three variables (gas velocity, temperature, and concentration) may sometimes coincide, although in slow reactions, the profiles of velocity and temperature may be fully developed at an early stage while the deposition reaction is spread far downstream the tube.

4.2.2.6 Rate-limiting steps

What is the rate limiting step of a CVD reaction? In other words, what factor controls the growth rate of the deposit? The answer to this question is critical since it will help to optimize the deposition reaction, obtain the fastest growth rate and, to some degree, control the nature of the deposit.

The rate-limiting step is generally determined by either the surface reaction kinetics or by mass transport [4-5, 9-13].

4.2.2.7 Surface-reaction kinetics

In the case of control by surface reaction kinetics, the rate is dependent on the amount of reactant gases available. As an example, one can visualize a CVD system where the temperature and the pressure are low. This means that the reaction occurs slowly because of the low temperature and there is a surplus of reactants at the surface since, because of the low pressure, the boundary layer is thin, the diffusion coefficients are large, and the reactants reach the deposition surface with ease as shown in Figure 4.7(A).

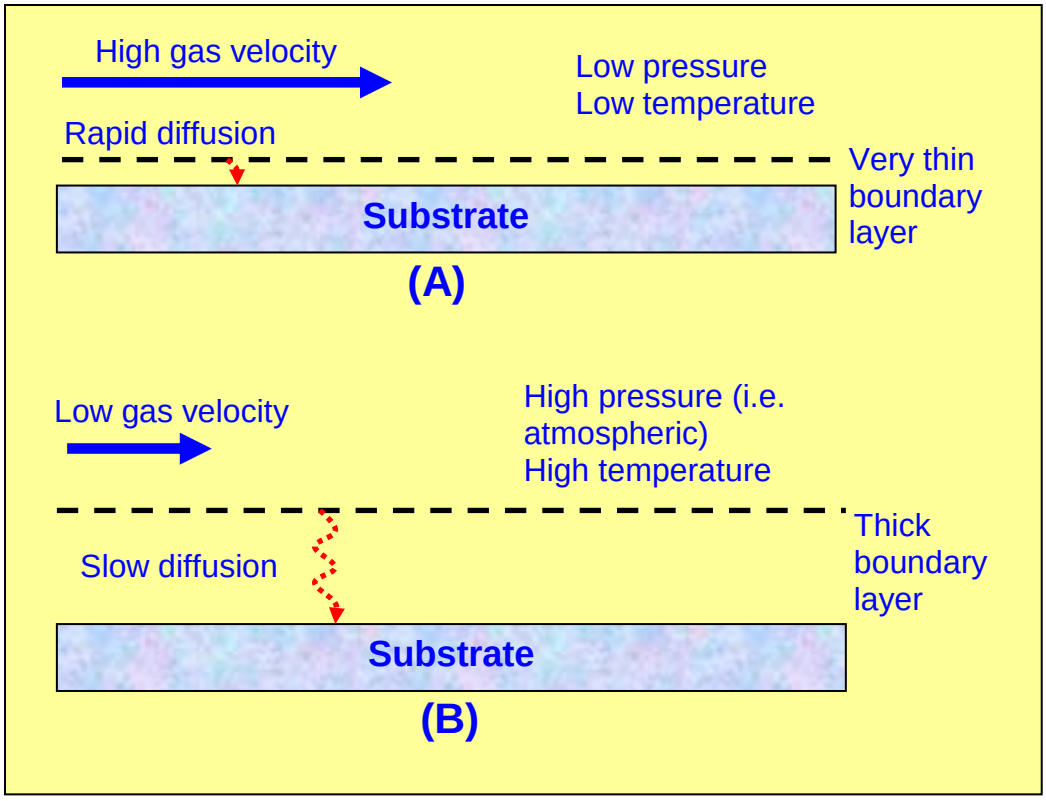

Fig. 4.7 Rate limiting steps in a CVD system (A) surface reaction kinetics control (B) diffusion control

4.2.2.8 Mass transport

When the process is limited by mass-transport phenomena, the controlling factors are the diffusion rate of the reactant through the boundary layer and the diffusion out through this layer of the gaseous by-products. This usually happens when pressure and temperature are high. As a result, the gas velocity is low (as was shown above) and the boundary layer is thicker making it more difficult for the reactants to reach the deposition surface. Furthermore, the decomposition reaction occurs more rapidly since the temperature is higher and any molecule that reaches the surface reacts instantly. The diffusion rate through the boundary layer then becomes the rate limiting step, as shown in Figure 4.7(B).

4.2.2.9 Pressure as rate-limiting factor

Pressure is similar to temperature as a rate limiting factor since the diffusibility of a gas is inversely related to its pressure. For instance, lowering the pressure 760 Torr (1 atm) to 1 Torr increases the gas-phase transfer of reactants to the deposition surface and the diffusion out of the by-products by more than 100 times. Clearly, at low pressure, the effect of mass-transfer variables is far less critical than at higher pressure.

However, the effect may not be as large if the overall pressure decrease is at the expense of the partial pressure of reactant gas, since the kinetic rate (for first-order reactions) is proportional to the partial pressure of the reactant. Reducing the pressure by reducing the flow of carrier gas (or eliminating it altogether) is a good alternative and is usually beneficial. At low pressure, surface reaction is the rate determining step and the mass-transfer variables are far less critical

than at atmospheric pressure.

It can be now seen that, by proper manipulation of the process parameters and reactor geometry, it is possible to control the reaction and the deposition to a great degree. The gas velocity is essentially constant and the boundary layer gradually increases in thickness toward downstream. This means that the thickness of the deposit will decrease as the distance from the tube inlet increases, as shown in Figure 4.8(A). This thickness decrease can be offset, and a more constant thickness obtained, simply by tilting the substrate, as shown in Figure 4.8(B). This increases the gas velocity due the flow constriction; the Reynolds number goes up; the boundary layer decreases and the deposition rate is more uniform [1, 4-5, 23].

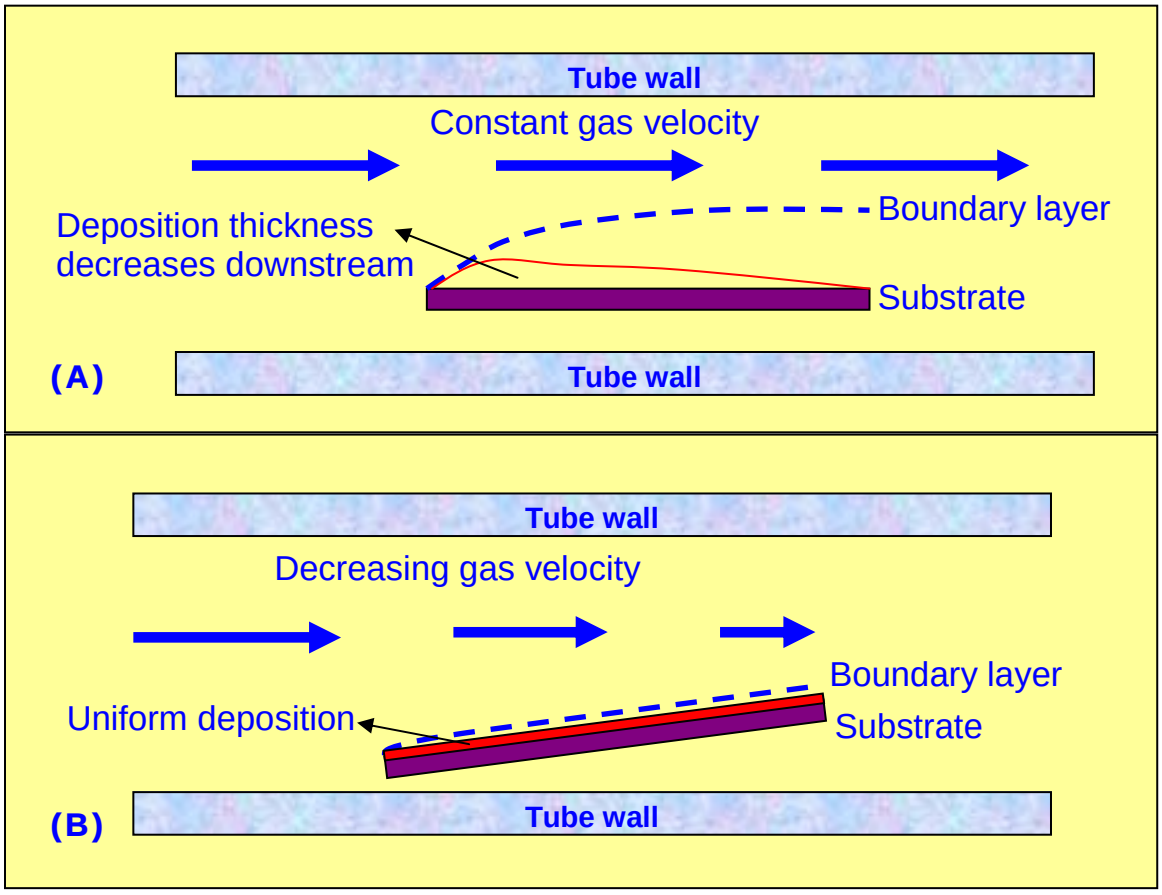

Fig. 4.8 Control of deposition uniformity in a tube system
(A) substrate parallel to gas flow (B) tilted substrate

4.3 CVD systems

In general, CVD systems can be divided into hot-wall and cold-wall reactors. In a cold-wall reactor only the substrate is heated and reactions take place on the substrate surface. The cold-wall reactor has the disadvantage of a narrow deposition zone and a low through-put (number of deposited films/time unit). In a hot-wall reactor the reactor tube is heated along with the substrate and film deposition takes place on both the substrate and reactor walls, this gives a wider deposition zone allowing many substrates to be deposited at the same time. The hot-wall system is described in following section [1, 4-5].

4.3.1 Hot-Wall CVD System

The hot-wall CVD apparatus that has been constructed for our integrated optical sulphide waveguides is shown in Figure 4.9. As described above, the CVD reactor is placed in a tube furnace. Therefore, the substrate and the wall of the reactor are both hot and the deposition will occur on the substrate and the inner wall of the reactor.

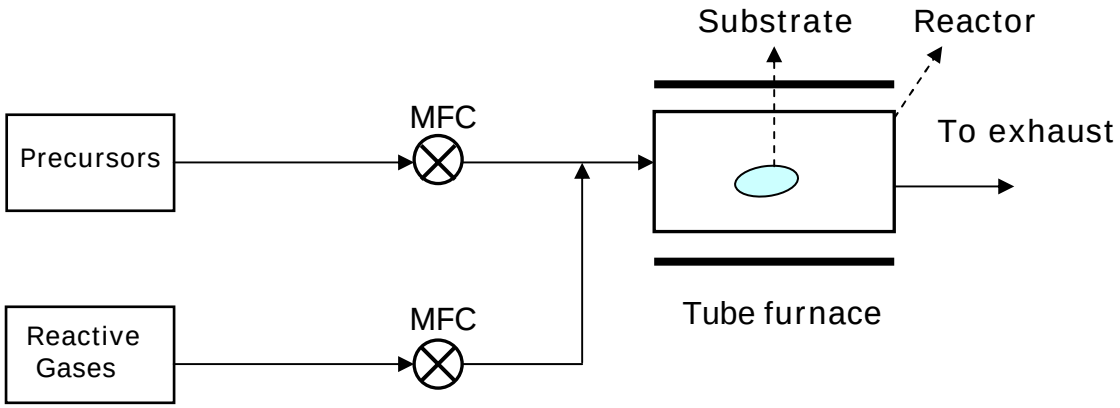

Fig. 4.9 Hot-wall CVD apparatus

4.3.2 Cold-Wall CVD System

A cold-wall CVD reactor, like a hot-wall CVD reactor, is a continuous flow system where the substrate is kept at the required high temperature, but all other surfaces bounding on the reacting gases and precursors are cold. The objective here is to cause the desired reaction only on the hot substrate and keep all other surfaces free of deposits.

Two different types of cold-wall CVD reactors will be considered, parallel flow and normal flow, to be discussed in the section. A normal-flow tube reactor configuration is shown in Figure 4.10. Here the reactant gas and precursors flow axially down a quartz tube over a heated susceptor aligned parallel to the flow. The substrate to be deposited is placed on this susceptor. The susceptor is heated inductively with a conducting coil placed around the tube. The coil is activated by an RF power supply.

In general, graphite is frequently used as a susceptor because it offers machinability, high resistivity (ideal for induction), and a temperature range up to 3000 ^{o}C. Susceptors can also be made from molybdenum, silicon carbide, stainless steel, niobium, aluminum, and other conductive materials. The susceptor can be made in the form of a crucible, disk, tube, a layer in the material, or whatever form best suits the application [24].

When heating a susceptor, solid state RF induction power supplies provide accuracy and speed. During heating, temperature ramping can be controlled by using pyrometers or thermocouples to form a closed loop system. Uniform surface temperature can be achieved with careful

coil design. Typical RF power supplies for susceptor heating range from 1 to 20 kW, depending on the parts and application requirements. There is a relationship between the frequencies of the alternating current; low frequencies of 5 to 30 kHz are effective for thicker materials requiring deep heat penetration, while higher frequencies of 100 to 400 kHz are effective for smaller parts or shallow penetration. The higher the frequency will have the higher the heat rate [24].

Under an inert atmosphere of nitrogen and hydrogen, the temperature of 1100 ^{o}C of the graphite susceptor can be achieved with the Ameritherm XP5 (5kW output solid state induction power supply) [24].

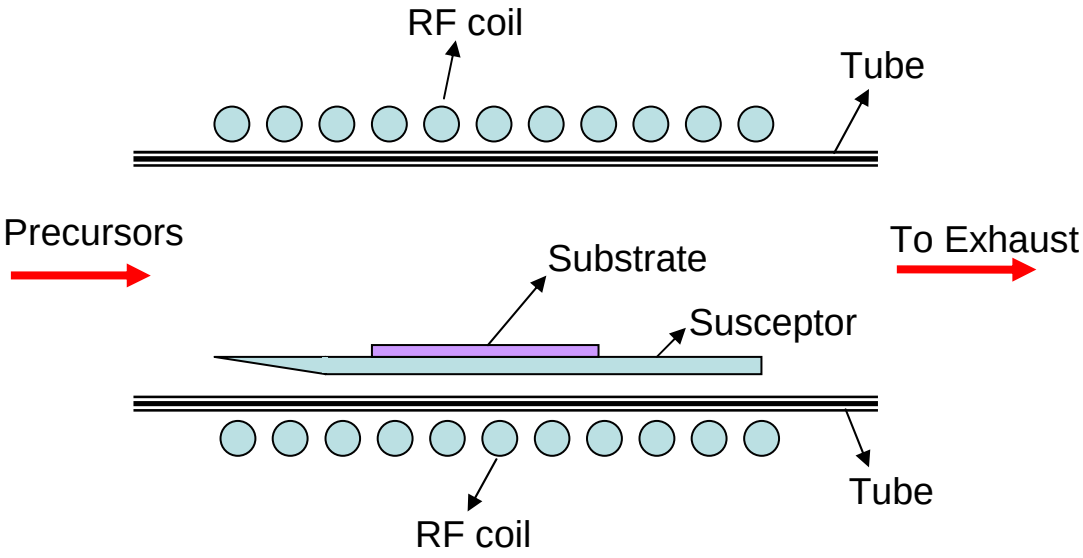

Fig. 4.10 Cold-Wall CVD Tube Reactor (parallel flow)

An alternative arrangement for such a reactor would be to align it vertically, and place the substrate on a pedestal normal to the flow direction. Such a system is shown in Figure 4.11.

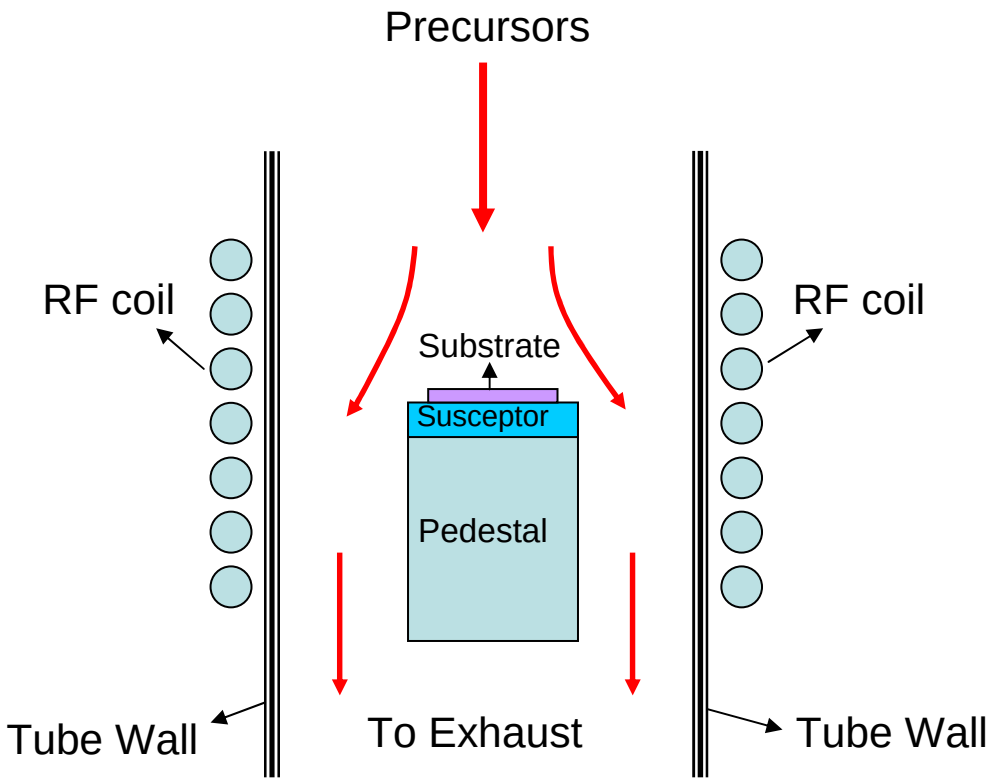

Fig. 4.11 Cold-Wall CVD Tube Reactor (normal flow)

The difference in these two configurations is in the flow pattern developed over the substrate. In Figure 4.11 the flow will develop as a classical boundary layer which will be thinner at the front and thicker towards the trailing edge. To whatever extent the deposition is diffusion controlled, it will be influenced by boundary layer thickness, so deposition rates may be higher near the front of the substrate than at the rear. However this problem can be improved by tilting up the susceptor.

For Figure 4.11 the flow pattern will be quite different and whatever non-uniformities occur will be axisymmetric which could be improved by delivering the precursors by a shower head [25].

4.4 Precursors

The main work in this thesis is to fabricate germanium sulphide based glass waveguides and bulk glass. Therefore, germanium tetrachloride was used as the main precursor in the experiment. Some other potential precursors, such as gallium trichloride, phosphorus trichloride, and antimony pentachloride, can be incorporated with germanium sulphide to form stable glasses. For active applications, rare-earth precursors are also under consideration.

Presursors	Melting point (^oC)	Boiling point (^oC)	Density (g/cm^3)
germanium tetrachloride, $GeCl_4$	-49.5	84.6	1.84
gallium trichloride, $GaCl_3$	77.9	201.3	2.47
phosphorus trichloride, PCl_3	-111.8	76	1.574
antimony pentachloride, $SbCl_5$	2.8	79	2.336
trimethyl Gallium, $Ga(Me)_3$	-15.8	55.7	1.151
tris(2,2,6,6-tetramethyl-3,5-heptandionato) dysprosium $Dy(TMHD)_3$	182-183	NA	NA
lanthanum hexafluoro-acethylacetonate, $La(hfac)_3$	NA	NA	NA

Table 4.1 Precursors for CVD experiment

The precursors summarized in Table 4.1 could be germanium tetrachloride ($GeCl_4$) which is 99.9999% pure from Eagle-Picher Technologies GmbH, gallium trichloride ($GaCl_3$) which is 99.999% pure from Alfa Aesar, phosphorus trichloride (PCl_3) which is 99.999% pure from Alfa Aesar, antimony pentachloride ($SbCl_5$) which is 99.999% pure from Alfa Aesar and some other metal-organic presursors.

4.5 Gas purification system

The gases used in the CVD experiment play very important roles either as the carrier gas or the reactive gas. However, the highest purity H_2S gas commercially available is only 99.5% pure and the inert carrier gas, argon, is only 99.95% pure. Therefore we need a purification system for all the gases involved in the CVD experiments.

The gas purification system is shown in Figure 4.12. Full details of the purification and synthesis apparatus can be found in Mairaj's PhD. thesis [26].

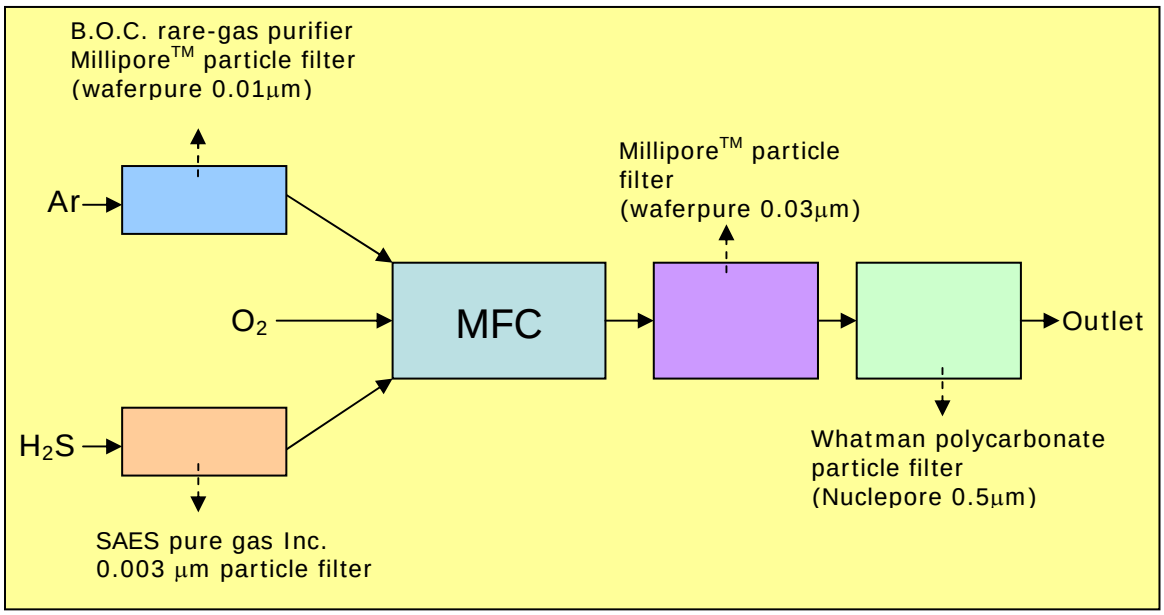

Fig. 4.12 Gases purification system

4.5.1 H_2S gas system

The liquid source of H_2S (99.5 % pure) was purchased from CK Gases, England. Manufacturer specified impurities were present in the form of carbon sulphides, carbon dioxide, nitrogen and moisture. Impurities present as carbon compounds are expected to be the leading contributor to contamination. Moisture is substantially reduced by the custom designed scrubber unit (SAES Pure Gas Inc), which has a 0.003 µm particle filter at the inlet and outlet, and the molecular sieve. The scrubber unit reduces moisture levels to better than < 1 ppm for H_2S with nominal flow rate 0 – 10 slpm (standard litre per minute) with guaranteed moisture levels < 1 ppb for argon with nominal flow rate 0 – 20 slpm.

4.5.2 Argon gas system

Cryogenic argon (99.95% pure), used in processing, was dried using a B.O.C. rare-gas purifier. The gas was supplied through stainless steel tubing attached with Swagelok™ fittings. Entry to the mass flow controller (MFC) was via an integral Millipore™ particle filter (Waferpure 0.01µm). The MFC has 3 inlet lines, for H_2S, argon and oxygen, all of which had a dedicated 5 µm particle filter. The outlet from the MFC was directed through a stainless steel Millipore™ particle filter (Wafergaurd 0.03µm). The outlet, carrying either argon or a mixture of H_2S and argon, was piped to the primary sleeving box which monitored the active line pressure. The primary sleeving box also contained a low-cost per process replaceable Whatman™ polycarbonate particle filter (Nuclepore 0.5 µm). This allowed a replacement of the filter per process and introduced a level of reliability in the materials processed. This particle filter is the last in filtration process.

4.5.3 Oxygen gas system

The integration of a Millipore™ filtered (0.5 µm) oxygen line for the processing of germanium oxide CVD process allowed extension of the system capabilities. Furthermore, the inclusion of a low-cost replaceable Whatman™ polycarbonate particle filter (Nuclepore 0.5 µm) to the mixed H_2S/argon gas lines provided a reliable level of purity during every process run.

4.5.4 Safety consideration

In addition, a number of safety features were built into the system design. All the high pressure lines were contained in an extracted gas cabinet. Should the gas operated relief valve fail, a mechanical and manual override was possible. In the event of failure of the H_2S release valve, the system could still be purged with argon through all of the high pressure and process lines via means of the bypass valves. All the system valves were labelled for clarity and their functions detailed. Meticulous processing steps were developed to ensure system and charge integrity both pre and post processing.

The gaseous fumes from the furnace generated during processing passed through a dry and wet bubbler which trapped particles and provided a seal against atmospheric leaching. Finally, the gaseous exhaust was burnt with a natural gas flame to remove any remaining H_2S and extracted to a sulphur dioxide scrubber. Full details of the purification and synthesis apparatus, including the electronic safety circuitry, can be found in an accompanying manual located on-site at the ORC fabrication Lab.

4.6 References

[1] A. Sherman, “Chemical vapor deposition for microelectronics principles, technology, and applications”, Noyes publications (USA), 1987.

[2] J. George, “Preparation of thin films”, Marcel Dekker, 1992.

[3] J. Mazumder, A. Kar, “Theory and application of laser chemical vapour deposition”, Plenum Press, 1995.

[4] D. M. Dobkin and M. K. Zuraw, “Principles of Chemical Vapor Deposition: What's Going on Inside the Reactor?”, Kluwer Academic Publishers, 2003.

[5] J. L. Vossen, W. Kern, “Thin Film Processes”, Academic Press, 1991.

[6] T. D. Eastop and D. Thomas, “Applied thermodynamics for engineering technologists”, Prentice Hall, 5th Edition, 1996.

[7] K.L Bjorklund, J. Lu, P. Heszler, and M. Boman, “Kinetics, thermodynamics and microstructure of tungsten rods grown by thermal laser CVD”, Thin solid films, **416** (2002) 41-48.

[8] S. de Persis, F. Teyssandier, ”Thermodynamic and kinetic criteria to select hydrocarbon precursor”, Journal de Physique IV, **11** (2001) 39-46.

[9] C. Bernard, “Thermodynamic, kinetic, and mass transport calculations, as the basis for materials processing by CVD”, Journal de Physique IV, **11** (2001) 3-15.

[10] M. Pons, C. Bernard, E. Blanquet, and R. Madar, “Combined thermodynamic and mass transport modelling for material processing from vapour phase”, Thin solid films, **365** (2000) 264-274.

[11] Z. J. Hu and K. J. Huttinger, “Determination of the kinetics of CVD in hat wall reactors”, Chemical Vapor Deposition, **6** (2000)

77-82.

[12] J. D. Chapple-Sokol, C. J. Giunta, and R. G. Gordon, “A kinetics study of the atmospheric pressure CVD reaction of Silane and Nitrous Oxide”, J. Electrochem. Soc., **136** (1989) 2993-3003.

[13] K.T. Raic, “Kinetics of film growth in CVD reactions”, Journal de Physique IV, **9** (1999) 229-236.

[14] H. Rouch, M. Pons, A. Benezech, C. Bernard, and R. Madar, “Thermodynamic equilibrium and mass transport coupled modelling of the chemical vapour deposition process”, Thin Solid Films, **281-282** (1996) 64-67.

[15] M. J. Hampden-Smith, T. T. Kodas, “Chemical vapour deposition of metals: part 1. an overview of CVD process”, Chemical Vapor Deposition, **1** (1995) 8-23.

[16] C. W. White, and W. D. Seider, ”Computation of phase and chemical equilibrium”, AIChE Journal, **27** (1981) 466-471.

[17] L. Stock, and W. Richter, “Vertical versus horizontal reactor: an optical study of gas phase in a MOCVD reactor”, Journal of Crystal Growth, **77** (1986)144-150.

[18] L.J. Giling, “Gas flow patterns in horizontal epitaxial reactor cells observed by interference holography”, J. Electrochem. Soc., **129** (1982) 634-644.

[19] R. Takahashi, Y. Koga, and K. Sugawara, “Gas flow pattern and mass transfer analysis in a horizontal flow reactor for chemical vapour deposition”, J. Electrochem. Soc., **119** (1972) 1406-1412.

[20] D. I. Fotiadis, M. Boekholt, K. F. Jensen, and W. Richter, “Flow and heat transfer in CVD reactors: comparison of Raman temperature measurements and finite element model predictions”, Journal of Crystal Growth, **100** (1990) 577-599.

[21] S. Rhee, J. Szekely, and O. J. Llegbusi, “On three-dimensional transport phenomena in CVD processes”, J. Electrochem. Soc.,

134 (1987) 2552-2559.

[22] H. K. Moffat and K. F. Jensen, “Three-dimensional flow effects in Silicon CVD in horizontal reactors”, J. Electrochem. Soc., **135** (1988) 459-471.

[23] W. K. Cho and D. H. Choi, “Optimization of a horizontal MOCVD reactor for uniform epitaxial layer growth”, International Journal of Heat and Mass Transfer, **43** (2000) 1851-1858.

[24] Ameritherm Inc., New York, USA. (http://www.ameritherm.com)

[25] Thomas Swan Scientific Equipment Ltd., UK. (http://thomasswan.co.uk)

[26] A. K. Mairaj, “Optical waveguides and lasers in improved gallium lanthanum sulphide glass”, PhD. Thesis, University of Southampton, 2003.

Chapter 5

Fabrication and characterization of germanium sulphide glass planar waveguides by CVD

5.1 Introduction

The conventional method of fabricating a chalcogenide glass is sealed ampoule melting. In this process the elements, as chunks or powders, are placed in a quartz tube, which is then evacuated to low pressures, typically 10^{-3} Torr or lower, and then sealed by melting and fusing the open end. The tube is placed in a furnace that typically rocks or oscillates the sealed ampoule in order to homogenize the melt. The ampoule is then cooled, broken open and the glass then further processed to form, for example, thin films, optical fibre and optoelectronic devices. Thin films of chalcogenide glass can also be deposited by a number of methods including evaporation [1-5], sputtering [6, 7], and ablation [8-11] of the bulk glass. These techniques can be adequate but in general suffer from impurity problems or difficulty in achieving the desired stoichiometry. The ability to fabricate thin films of chalcogenide is increasingly of interest, and the promise of practical planar integrated devices motivated this work [12].

Chemical vapor deposition (CVD) has proved to be highly advantageous for the fabrication of ultra high purity silica glass fiber preforms. It would be desirable to find an analogous approach for the fabrication of chalcogenide materials and there has been considerable work devoted to this objective [13], although no suitable process has been reported. Reaction between germanium tetrachloride ($GeCl_4$) and

hydrogen sulphide (H_2S) to form germanium disulphide (GeS_2), for example, was reported to be unsatisfactory for the fabrication of planar or preform structures because of a low reaction rate and a low yield of deposited product. Another approach to form germanium sulphide films by plasma-enhanced CVD [14] through the reaction between GeH_4 and H_2S was reported. However, the films were unstable and easily oxidized in air.

The synthesis of chalcogenide glass using CVD techniques has not been widely reported. Therefore, with a source of the high purity germanium tetrachloride (99.9999%) and the ability to melt in a reactive atmosphere of H_2S available in our laboratory, we began to review the reaction between $GeCl_4$ and H_2S to form GeS_2. This began with a thermodynamic analysis (section 5.2), which indicated that this reaction should be favoured, and therefore preliminary tests were undertaken.

The objective of this work is to fabricate germanium sulphide glass thin films on suitable substrates directly by means of chemical vapour deposition and to develop a reliable method for planar waveguide applications.

5.2 Thermodynamic calculation of germanium sulphide glass formation by CVD

In the germanium sulphide glass thin films CVD process, $GeCl_4$ was used as the precursor which reacts with H_2S and then forms the GeS_2 glass thin film on a substrate, as Eq. (5.1).

$$GeCl_{4(g)} + 2H_2S_{(g)} \longleftrightarrow GeS_{2(s)} + 4HCl_{(g)} \qquad (5.1)$$

The reason why we choose $GeCl_4$ as the precursor is because it can be commercially bought in very high purity (99.9999%) and, as it is also a crucial precursor in silica MCVD system, is readily available. Besides, as described in the previous Chapter, a H_2S high purity gas system is available in our lab, so the reactive gas is ready to use for a germanium sulphide glass CVD process.

In order to determine the feasibility of this reaction, as described in Chapter 4, we can calculate the Gibb's free energy of this reaction ($\Delta G_{reaction}$). If the $\Delta G_{reaction} \leq 0$, the reaction will occur spontaneously. Furthermore, we have to evaluate the efficiency of this reaction by the value of the equilibrium constant (K).

From thermodynamics, the Gibb's free energy of the reaction ($\Delta G_{reaction}$) is expressed as $\Delta G_{reaction} = \Sigma \Delta G_{products} - \Sigma \Delta G_{reactants}$, so the Gibb's free energy of the reaction can be calculated, and is presented in Table 5.1, where the data of ΔG of each compound at room temperature, 500K, and 800K are available from reference [15]. As the values of ΔG of the reaction at room temperature, 500K, and 800K are all less than zero, we can confirm that the reaction will occur spontaneously.

	Room Temp.	500K	800K
ΔG(kJ/mol),HCl	-95.293	-97.158	-99.452
ΔG(kJ/mol),$GeCl_4$	-154.588	-151.185	-141.381
ΔG(kJ/mol),H_2S	-33.329	-40.179	-45.694
ΔG(kJ/mol),$GeCl_4$	-461.547	-435.936	-398.51
ΔG(kJ/mol),Reaction	-7.555	-23.523	-49.291
K (equilibrium constant)	21.117	281.746	1616.049

Table 5.1 Gibb's free energy and equilibrium constant of germanium sulphide CVD reaction, equation (5.1)

We can also calculate the equilibrium constant (K) of the reaction from the following equation, $\Delta G_{reaction} = -RT \ln(K)$, where R is the gas constant and T is the temperature in Kelvin. Furthermore, the equilibrium constant can be expressed as Eq. (5.2).

$$K = \frac{a_{GeS_2} \times P_{HCl}^4}{P_{GeCl_4} \times P_{H_2S}^2} \tag{5.2}$$

where a_{GeS_2} is the activity of GeS_2 produced by Eq. (5.1)

P_{HCl} is the partial pressure of HCl produced by Eq. (5.1)

P_{GeCl_4} is the partial pressure of $GeCl_4$ participating in Eq. (5.1)

P_{H_2S} is the partial pressure of H_2S participating in Eq. (5.1)

From the calculation results presented in Table 5.1, the Gibb's free energy of this reaction at room temperature is only -7.555 kJ/mol and the equilibrium constant of the reaction is only about 21, but when the temperature goes up to 800K the Gibb's free energy changes to -49.291 kJ/mol and the equilibrium constant of the reaction increases to about 1616. Therefore, as the temperature is increased, the equilibrium constant becomes larger, favouring the formation of GeS_2. Non-stoichiometry is possible for germanium sulphide, which is not considered here. The Gibb's free energy and equilibrium constant (K) of the reaction at different temperatures are shown in Figure 5.1. Nonetheless, as the temperature is increased, this analysis suggested that the reaction should also be increasingly favoured for germanium sulphide with a stoichiometry that is close to 2.

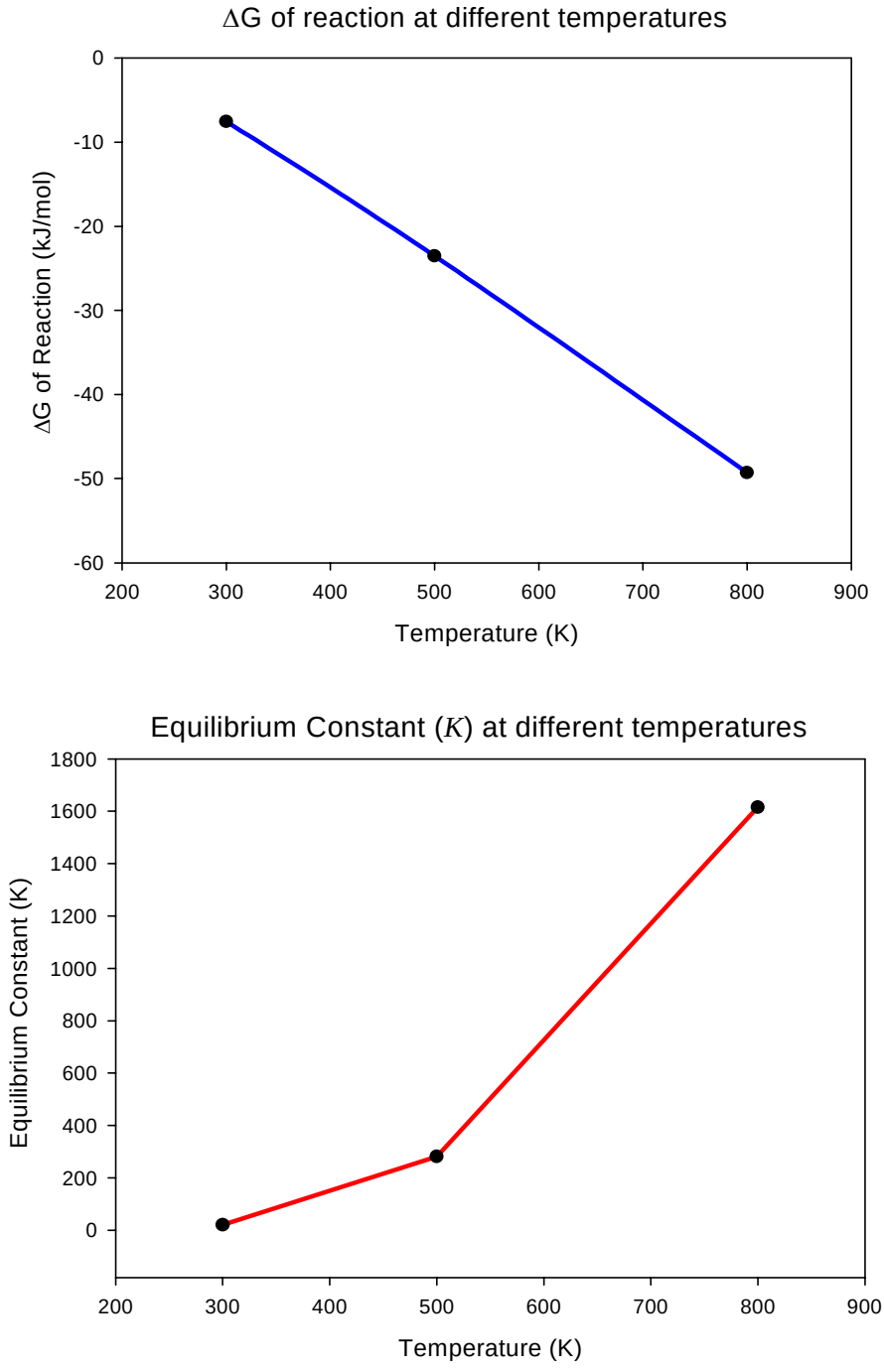

Fig. 5.1 Gibb's free energy and equilibrium constant (K) of the reaction at different temperatures

5.3 Optimization of CVD reaction parameters

The CVD apparatus we have developed for fabricating germanium sulphide planar waveguides is shown in Figure 5.2.

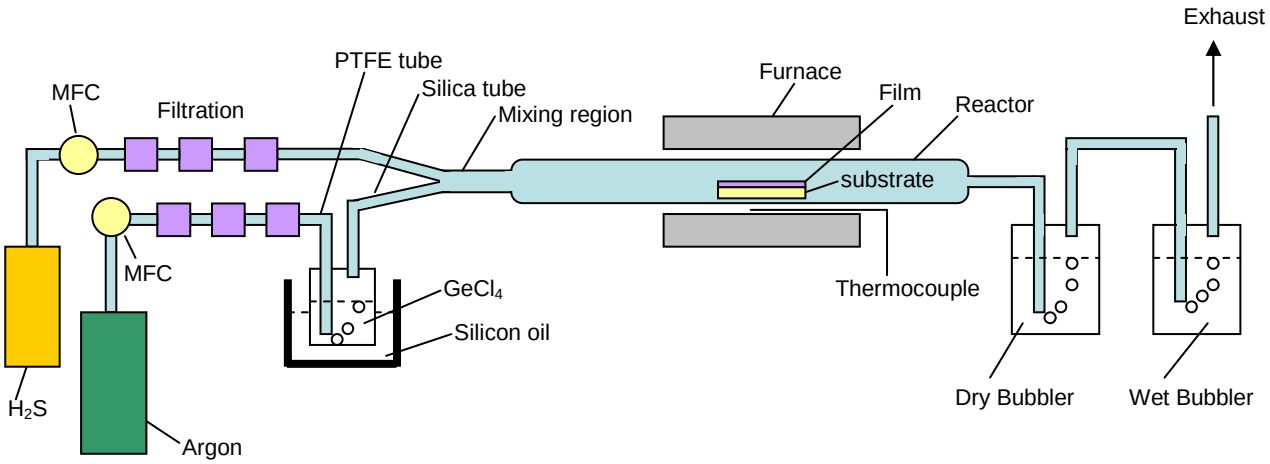

Fig. 5.2 Hot-wall CVD apparatus for Germanium sulphide based glass thin films

Thin films of germanium sulphide glass form on a substrate through reaction between $GeCl_4$, vaporized by means of a bubbler into argon carrier gas, and H_2S gas at temperatures in the range of 450°C-600°C. This is a hot-wall CVD process under atmospheric pressure, in which a horizontal quartz tube reactor (25mm O.D. x 500mm long) is heated in a tube furnace. The carrier gas for $GeCl_4$, argon, is typically delivered through the mass flow controllers (MFC) at the flow rate of 100 ml/min and the reactive gas, H_2S, with the diluting gas, argon, are typically delivered through the MFC at the flow rate ratio of H_2S/argon of 20/80 ml/min.

There are two main parameters in the fabrication of germanium sulphide glass by CVD processes, temperature and flow rate of the carrier gases. As described in the previous section, the temperature is the key to the Gibb's free energy of this reaction and also influences the formation of the glasses and efficiency. On the other hand, the flow rate of the carrier gases determines the reaction time of the CVD process.

5.3.1 Tube furnace calibration

The temperature profile of the furnace along the centre of the tube furnace from the left end to the right end is shown in the Figure 5.3. As the temperatures are calibrated without a gas flow, the actual temperatures will be slightly lower than the set temperatures.

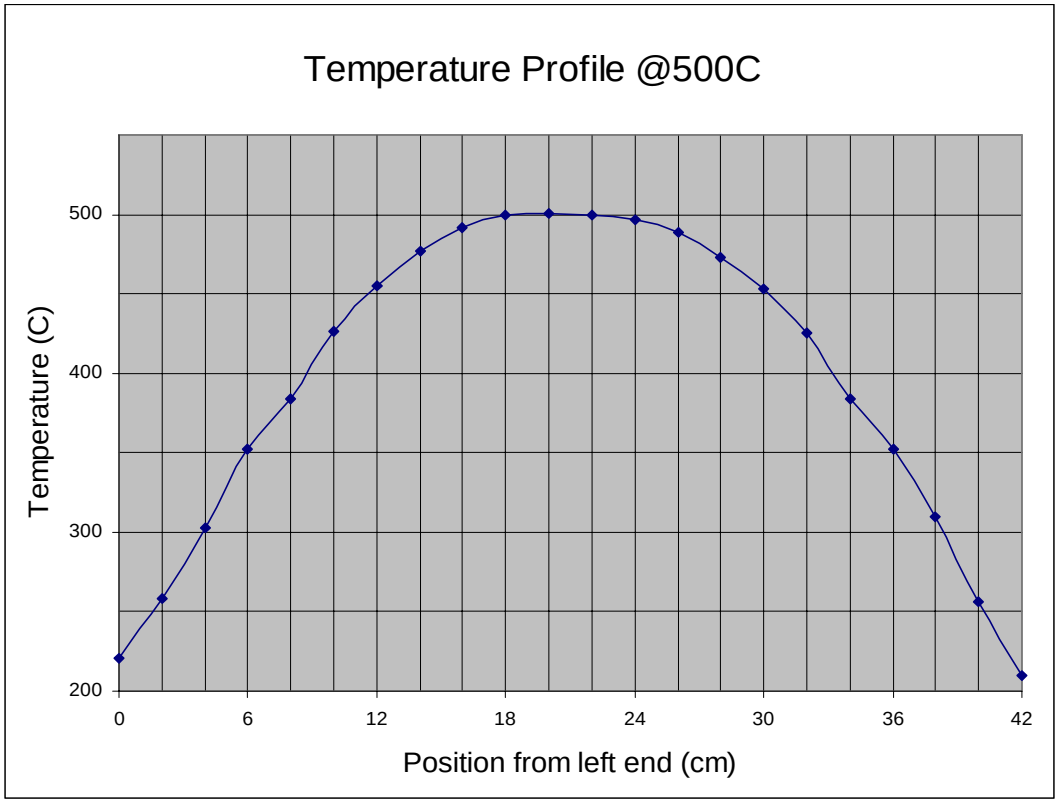

Fig. 5.3 Tube furnace temperature profile @ 500 ^{o}C

From Figure 5.3, the useful range of the tube furnace is only at the central (hot zone) and the hot zone is about 10-12 cm.

Furthermore, the calibration of hot zone temperature of the tube furnace from 500 to 1000 ^{o}C is shown in Figure 5.4. The temperature measured by a K-type (NiCr/Ni) thermocouple agrees quite well with the set temperature from 500 ^{o}C to 1000 ^{o}C, as given by the temperature controller of the furnace.

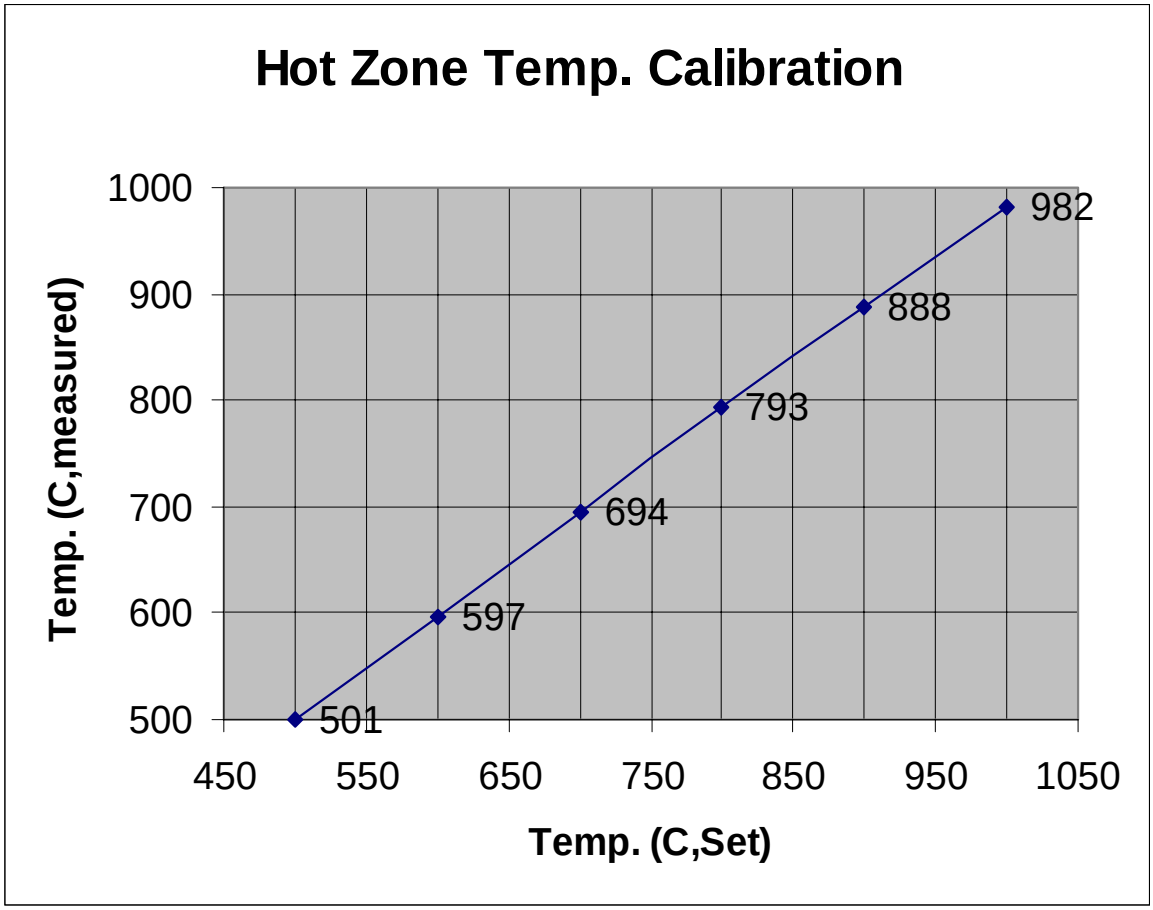

Fig. 5.4 Tube furnace hot zone temperature calibration

5.3.2 Early problems (from CVD run1 to run3)

From the calculation of Gibb's free energy and the equilibrium constant of the reaction, the CVD process for germanium sulphide glass formation from the reaction between $GeCl_4$ and H_2S is feasible. As the objective of this work is to form germanium sulphide glass films on suitable substrates, the initial aim is to optimize the conditions for directly fabricating germanium sulphide in the glass phase instead of crystalline phase.

From the preliminary investigation (run1 to run3), we were able to begin to optimize the parameters of the following CVD experiments. The parameters of CVD run1 to run 3 are summarized in Table 5.2.

	Precursors	Carrier Gas & Flow Rate	Reactive Gas & Flow Rate	Furnace Temp.(°C)	Deposition Rate(μm/hr)
CVD run1	$GeCl_4$	Ar (100ml/min)	Ar (100ml/min) H_2S (100ml/min)	450	0.7
CVD run2	$GeCl_4$	Ar (100ml/min)	Ar (100ml/min) H_2S(100ml/min)	500	7.5
CVD run3	$GeCl_4$	Ar (40ml/min) H_2S(20ml/min)		500	14.4

Table 5.2 Parameters of the germanium sulphide glass CVD experiments

In CVD run1 and run2, Ar was used as a carrier gas at 100 ml/min to transfer the vapour precursor, $GeCl_4$, from the bubbler into the reactor to mix with reactive gas (H_2S). However, in the CVD run3, in order to improve the mixing efficiency between the precursor and the reactive gas, an Ar and H_2S mixture was used as a carrier gas and also as a reactive gas.

5.3.2.1 Germanium sulphide thin film formation CVD run1

In the germanium sulphide CVD run1, a glassy film was fabricated on the inner wall of the quartz tube at 450 ^{o}C. The reactive gases are the 100ml/min H_2S mixed with 100ml/min argon. The glassy film, which was observed under a 50X objective microscope by CCD camera, is shown in Figure 5.5. Here, a lot of bubbles were observed to have been trapped on the surface of the germanium sulphide glassy film. Also, some cracks on this film have been found due to the thermal expansion coefficient mismatch between the germanium sulphide glassy film and the quartz tube substrate. Although we can make a germanium sulphide glassy film by this CVD experiment, most of the products are crystalline powders outside of the hot zone. The deposition rate was estimated to be 0.7μm/hr.

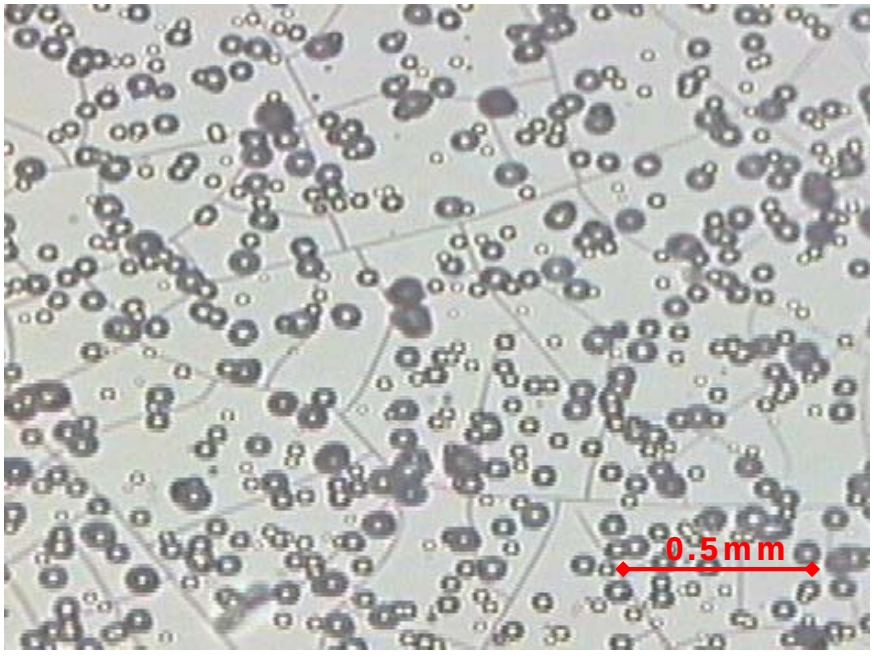

Fig. 5.5 Germanium sulphide glassy film by CVD run1

5.3.2.2 Germanium sulphide thin film formation CVD run2

In the germanium sulphide CVD run2, the glassy film has been fabricated on the inner wall of the quartz tube at 500 ^{o}C, a 50 ^{o}C increase over the previous run. As before, the carrier gas was argon at 100ml/min and the reactive gases were 100ml/min H_2S mixed with 100ml/min argon. The glassy film, which was observed under a 50X objective microscope by CCD camera, is shown in Figure 5.6.

From Figure 5.6, the decrease of the bubbles on this glassy film has been found to be due to the increase of the furnace temperature from 450 ^{o}C to 500 ^{o}C. Probably the bubbles have less chance to be trapped in the film at higher temperature. In addition, the thickness of the germanium sulphide glassy film also has been increased, due to the increased efficiency of the reaction, by a factor of about 10. The deposition rate was estimated to be 7.5μm/hr.

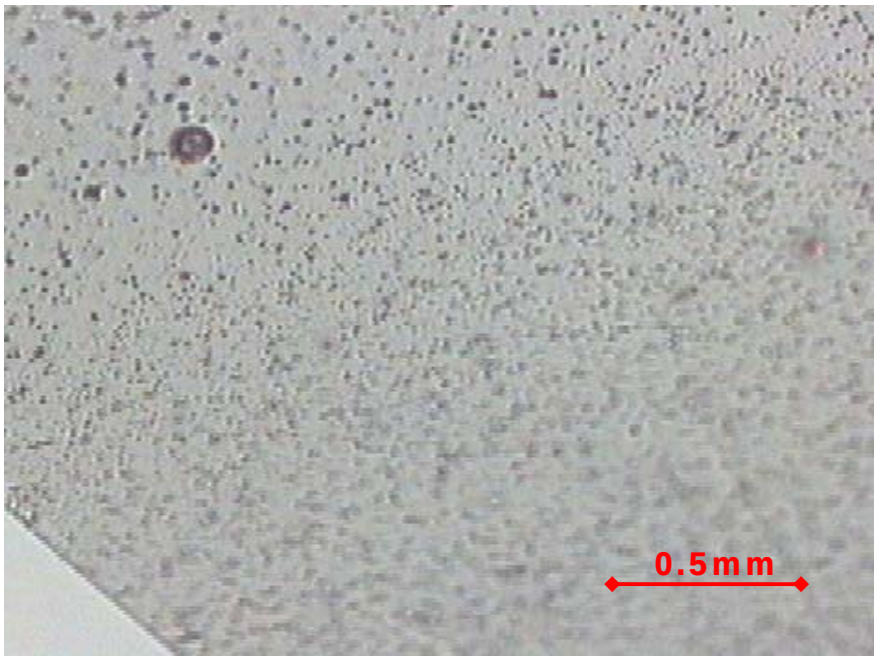

Fig. 5.6 Germanium sulphide glassy film by CVD run2

5.3.2.3 Germanium sulphide thin film formation CVD run3

In the germanium sulphide CVD run3, the glassy film has been fabricated on the inner wall of the quartz tube at 500 ^{o}C. The reactive gases, also acting as the carrier gases, are the 20ml/min H_2S mixed with 40ml/min argon. The glassy film, which was observed under a 50X objective microscope by CCD camera, is shown in Figure 5.7.

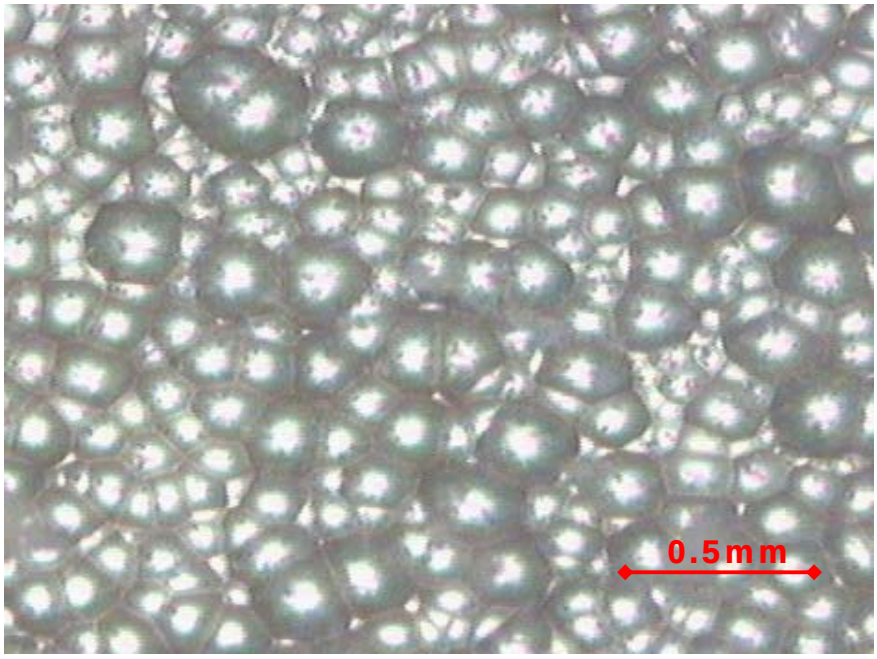

Fig. 5.7 Germanium sulphide thin film by CVD run3

A germanium sulphide glassy film was formed on a borosilicate glass slide substrate, with a thickness of about 68 μm, by CVD within 283 minutes. Therefore, the deposition rate of this CVD process is 14.4 μm/hr. However, the surface of the film was not homogeneous and lots of islands of germanium sulphide were formed, probably due to the higher deposition rate and the composition of the reactive gas.

Here, we find the yield in run3 was much better than that in run2 because we decreased the flow rate in run3 to increase the reaction time between the precursor and the reactive gas and we also improved the mixing effect of the precursor and reactive gas.

Further 19 experiments for the optimization of CVD condition are summarized in the Appendix II. From run 4 to run 13, 100% H_2S was used as the carrier gas to transfer $GeCl_4$ vapour from the bubbler to the reactor to obtain a better mix efficiency and the deposition temperature was also been increased to improve the deposition rate. However, higher $H_2S/GeCl_4$ molar ratio and higher temperature tend to form crystalline powders instead of glass. From run14 to run16, a higher H_2S /$GeCl_4$ molar ratio (up to ~31) was selected and the deposition temperature was increased to 800^oC. Unfortunately the same problem, crystalline products, has been produced. In particularly, germanium sulphide powders were collected in a vessel at room temperature in run 16. Therefore, from run 17 to run 22, the most critical parameters for germanium sulphide glass formation, molar ratio of $H_2S/GeCl_4$ (~2-3) and the deposition temperatures (below the crystalline temperature, 620^oC) have been verified.

Another key parameter is the substrate selection. It is very important to find a thermal expansion coefficient compatible substrate for the deposition of germanium sulphide glass by CVD process as described in the next section.

5.3.3 Summary

The objective is to achieve a germanium sulphide glass planar waveguide directly by chemical vapour deposition. From preliminary

results, we have successfully deposited a germanium sulphide glass film on substrates which has been analyzed by micro-Raman and EDX (details will be discussed in the section 5.6). The composition of the germanium sulphide glass film, determined by the Raman technique, was $GeS_{2\pm0.2}$, but that determined by the EDX technique was about $GeS_{1.66\text{-}1.75}$ this was probably due to the sulphur that escaped during the measurement. In addition, there are still some problems needing to be overcome, such as film cracks due to the thermal mismatch between the germanium sulphide glass film and the substrate, which can be overcome by using a thermally compatible substrate, and the inhomogeneous surface (overcome by optimum control of the molar ratio of $H_2S/GeCl_4$ at 2~3).

The typical hot-wall CVD parameters optimized for the planar/slab germanium sulphide glass waveguides are summarized in Table 5.3. The details of the influence of substrates will be discussed in the next Section.

Parameters	**Conditions**
Furnace type	Tube furnace
Temperature	500 ^{o}C
Precursor	Germanium tetrachloride ($GeCl_4$)
Substrates	Borosilicate glass slide Calcium fluoride (CaF_2) Schott N-PSK 58 Silica on silicon GeO_2/silica on silicon

	GeO_2/silicon
Reactive gas	Hydrogen sulphide (H_2S)
Carrier gas	Argon (Ar)
Flow rate of reactive gas	20 ml/min H_2S + 80 ml/min Ar
Flow rate of carrier gas	100 ml/min Ar
Molar ration of $H_2S/GeCl_4$	2-3 / 1 (typical 2.3/1)
Deposition rate	10-17 μm/hr
Composition by SEM-EDX	$GeS_{1.66-1.75}$
Composition by Raman spectrum	$GeS_{2\pm0.2}$

Table 5.3 Optimized parameters for germanium sulphide glass planar waveguide fabrication by Hot-wall CVD

5.4 Substrates selection for planar waveguides

As described in the previous section, the substrate is quite crucial in the direct deposition of germanium sulphide glass films by the CVD process. Therefore, the thermal properties of germanium sulphide glass need to be well investigated. As we use a hot-wall CVD reactor in the experiment, we can form glass film directly, however a high fraction of the precursors form crystalline powders.

The crystalline powders were collected and sealed in an evacuated quartz ampoule, then melted at 900°C and quenched in the air to form germanium sulphide glass. The thermal properties of this glass have been studied using a differential thermal analyzer (DTA) from which we can resolve the glass transition temperature (T_g), at 456°C, and the

onset of crystallization temperature (T_x), at 620°C, and a thermo-mechanical analyzer (TMA) from which we can find that the coefficient of thermal expansion is 12.9x10^{-6}/°C. (details will be discussed in chapter 6).

After understanding the thermal properties of germanium sulphide glass, some candidate substrates could be chosen, to match those of the film, including calcium fluoride (CaF_2), Schott glasses, and commercial wafers, these will be discussed in the following section.

5.4.1 Calcium fluoride (CaF_2)

Calcium fluoride (CaF_2) is one of the most popular optical materials. Calcium fluoride substrates (CaF_2), with two faces polished, with dimensions 10x20x1 mm, were obtained from Crystran Ltd., These had a thermal expansion coefficient of 18.85 x10^{-6} /K, a transmission range 0.13 to 10 μm, a refractive index about 1.43 at 1.5 μm, and a melting point 1360 °C. Thus CaF_2 would be a suitable substrate. In addition, these substrates were cleaned by acetone and IPA in an ultrasonic bath, rinsed by D.I water and then dried in the oven at 120 °C, before placed in the reactor for experiment.

We have successfully fabricated the planar/slab germanium sulphide glass waveguides by the hot-wall CVD system with the deposition parameters shown in Table 5.3. The SEM pictures from the top of the germanium sulphide glass on CaF_2 and the side profile of the germanium sulphide glass on CaF_2 are shown in Figure 5.8 and Figure 5.9 respectively.

From Figure 5.8, although there are still several tiny contamination spots on the surface of the germanium sulphide glass in an area of about 48 x 32 μm, we find that the surface is free of any inhomogeneity.

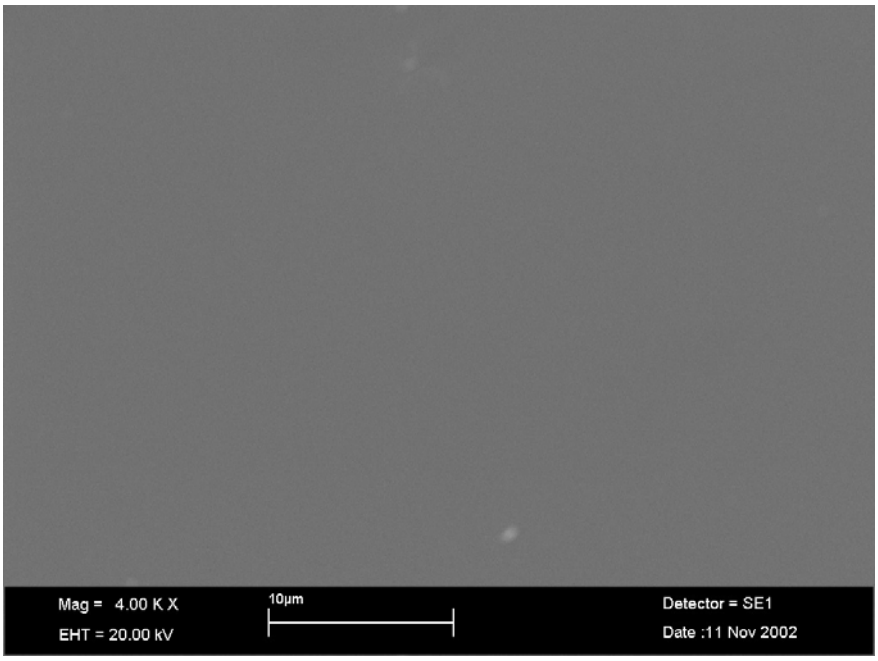

Fig. 5.8 SEM micrograph from a top view of the planar germanium sulphide glass waveguide on CaF_2 substrate by hot-wall CVD

Furthermore, a well defined germanium sulphide glassy film on a CaF_2 substrate was demonstrated, as shown in Figure 5.9 (cleaved simply by a diamond pen), and the thickness of the germanium sulphide glass film was estimated to be about 4.9 μm.

However, the difference in hardness between the germanium sulphide glass film and the calcium fluoride is so high that the germanium sulphide glass film cracked at the edges after end-face

polishing. Therefore, we need to find a softer substrate for the germanium sulphide glass film deposition by the hot-wall CVD process.

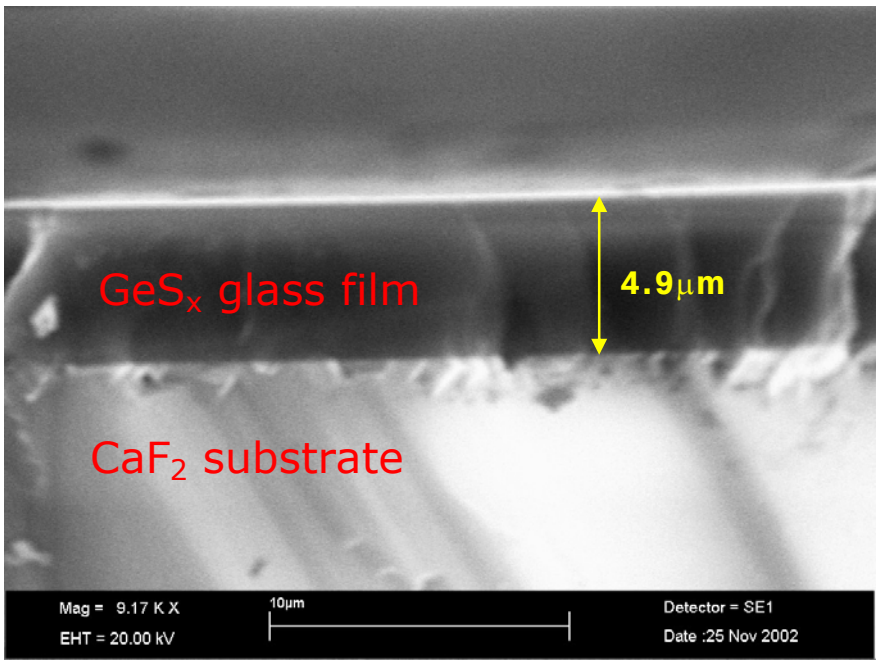

Fig. 5.9 SEM micrograph from a side view profile of the planar germanium sulphide glass waveguide on CaF_2 substrate by hot-wall CVD

5.4.2 Schott N-PSK 58 glass

Schott Corporation is one of the biggest commercial glass suppliers. From its data base, we found that N-PSK 58, N-PSK 57, and N-PK51 would be suitable for germanium sulphide glass film deposition and the properties of these three candidate glasses are summarized in Table 5.4. Considering the availability from the local Schott glasses supplier, the Schott N-PSK 58 glass was chosen for our first trial.

Table 5.4 Properties of substrate glasses vs. germanium sulphide

Properties	**GeS_2**	**CaF_2**	**Schott N-PSK58**	**Schott N-PSK57**	**Schott N-PK51**
R.I. @632.8nm	2.09	1.43	1.56739	1.59058	1.52711
T_g , (°C)	456	Nil	476	497	496
CTE, ($x10^{-6}$/°C)	12.9	18.85	15.1	14.8	14.4
Transmission Range (μm)	0.5-10.5	0.13-10	0.35-4 (this work)*	0.35-1.97 N.A. at >1.97μm	(0.35-2.5) N.A. at >2.5μm
Hardness (knoop)	N.A.	158.3	360	370	400

*measured by Perkin Elmer spectrum 2000 FT-IR shown in Figure 5.10

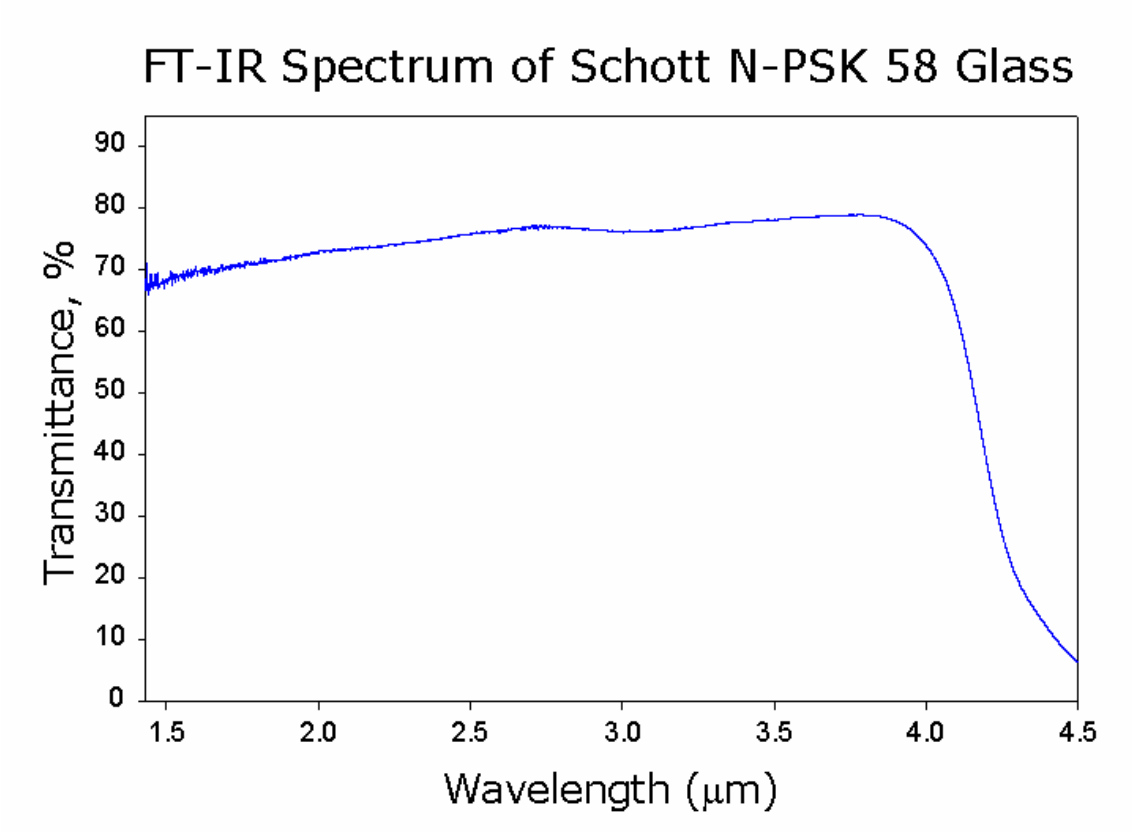

Fig. 5.10 FT-IR spectrum of Schott N-PSK 58 glass

Germanium sulphide glass film has been successfully deposited on the Schott N-PSK 58 glass, cleaned by acetone and IPA in an ultrasonic bath, rinsed by D.I. water and then dried in the oven at 120 ^{o}C. The deposition parameters were shown in Table 5.3, except the temperature changed to 480 ^{o}C to have the improved resistance to the crystallization of the film, and the deposition rate was estimated to be about 6 μm/hr. The germanium sulphide glass film was then annealed at 420 ^{o}C for 8 hours. The SEM micrograph from the side view profile is shown in Figure 5.11 which shows that the germanium sulphide glass film (~1.9μm) is well formed on the substrate (cleaved by a diamond pen).

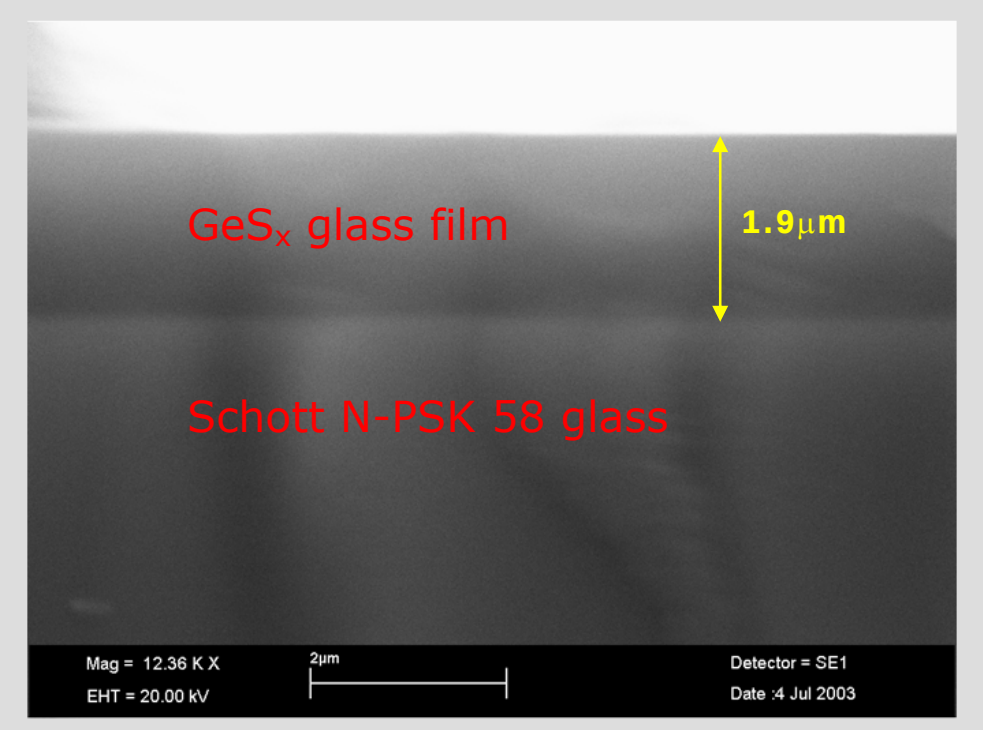

Fig. 5.11 SEM micrograph from a side view profile of the planar germanium sulphide glass waveguide on Schott N-PSK58 substrate by hot-wall CVD (run29)

Furthermore, germanium sulphide glass film can also be formed on the patterned Schott N-PSK58 substrate by an Ar-ion beam milling technique, the SEM micrograph of the side view profile is shown in Figure 5.12. Therefore, it is possible to form germanium sulphide glass film on pre-patterned substrates for desired structures.

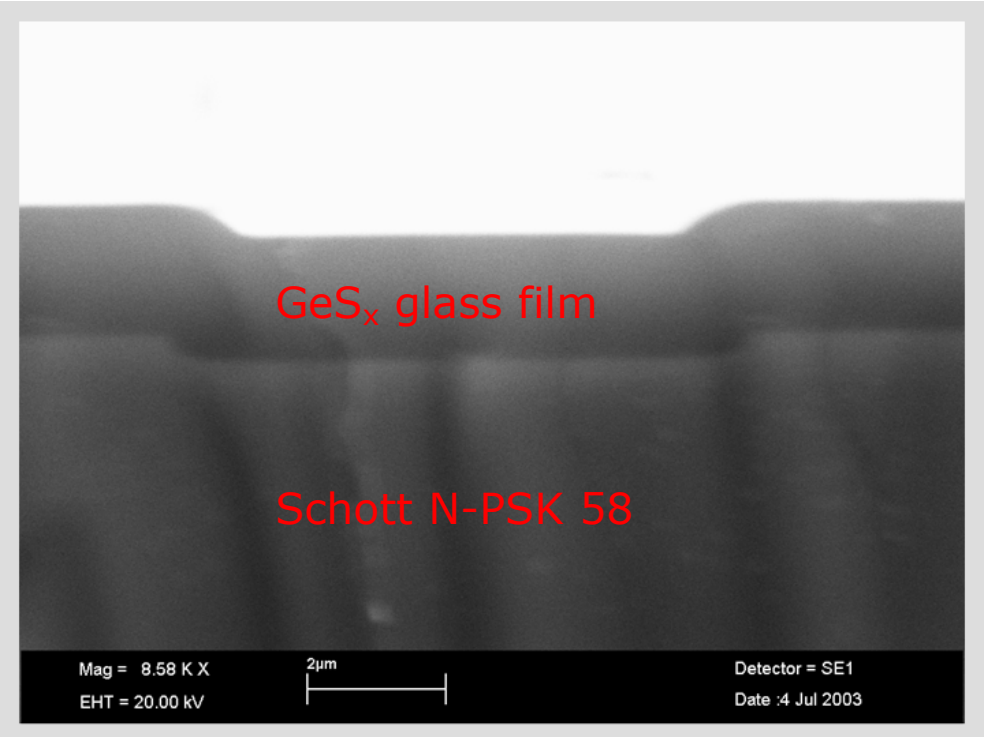

Fig. 5.12 SEM micrograph from a side view profile of the planar germanium sulphide glass waveguide on Ar-ion beam milling patterned Schott N-PSK58 substrate by hot-wall CVD

5.4.3 Silica on silicon

The idea here is to form germanium sulphide glass film on a commercial wafer directly by a hot-wall CVD process, thus the fabrication cost can be reduced and it will be more convenient to combine the process with current semiconductor fabrication techniques. In our previous experience, germanium sulphide glass film can be directly formed on a silica (SiO_2) glass substrate but the germanium sulphide glass film will have cracks due to the mismatch in the coefficient of thermal expansion (CTE) between this glass film and the substrate (the value of CTE of SiO_2 glass is only about $0.55x10^{-6}/^oC$). However, if the thickness of silica could be reduced to less than the critical thickness, the cracking problem of germanium sulphide glass film on silica substrate can probably be solved.

Therefore, some commercial thermal oxide wafers (silica on silicon) from Dr. Graham Ensell (ECS, University of Southampton) and Professor James Wilkinson (ORC, University of Southampton) have been studied for this purpose. The thickness of thermal oxide layers on silicon wafers are available ranging from 40nm, 200nm, 580nm to 2000nm.

We have successfully formed homogeneous crack-free germanium sulphide glass films on 40nm SiO_2 on Si wafer and 200nm SiO_2 on Si wafer by the hot-wall CVD system. For the 580nm SiO_2 on Si wafer, we can form the crack-free germanium sulphide glass film on this substrate, but this glass film is very sensitive to the temperature control. For the 2000nm SiO_2 on Si wafer, we cannot form a crack-free germanium sulphide glass film on this substrate.

The SEM micrographs from the top of the germanium sulphide glass on 580nm silica on silicon and the side profile of the germanium sulphide glass on 580nm silica on silicon are shown in Figure 5.13 and Figure 5.14 respectively. From Figure 5.13, in an area of about 400 x 560 μm, we can find the surface is free of any inhomogeneity. From Figure 14, we can confirm that the germanium sulphide glass film (about 3μm) is well formed on the 580nm SiO_2 on Si wafer. However, in order to form a homogeneous crack-free germanium sulphide glass film on a silica on silicon substrate by the hot-wall CVD process, it would be suggested to choose a thermal oxide wafer with the thickness of oxide layer less than 500nm.

However, if the objective is to fabricate the germanium sulphide glass waveguide for telecommunication (1.31 or 1.55μm) applications, it would be better to have a thermal oxide buffer layer thicker than 2 μm to isolate the field from silicon substrate.

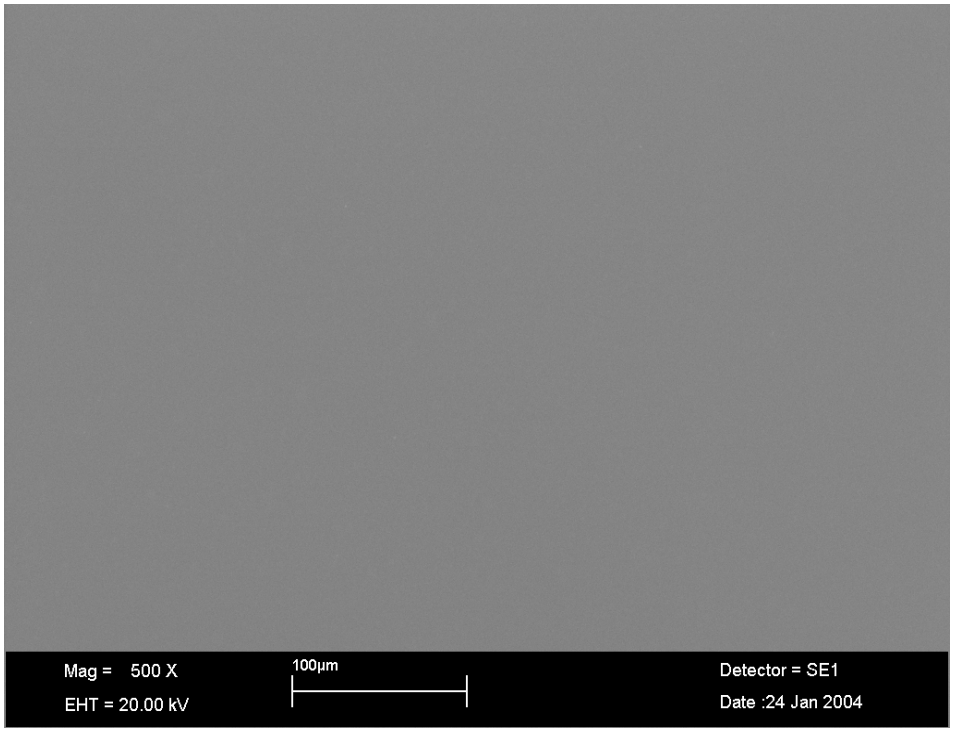

Fig. 5.13 SEM micrograph from the top view of the planar germanium sulphide glass waveguide on silica on silicon wafer by hot-wall CVD

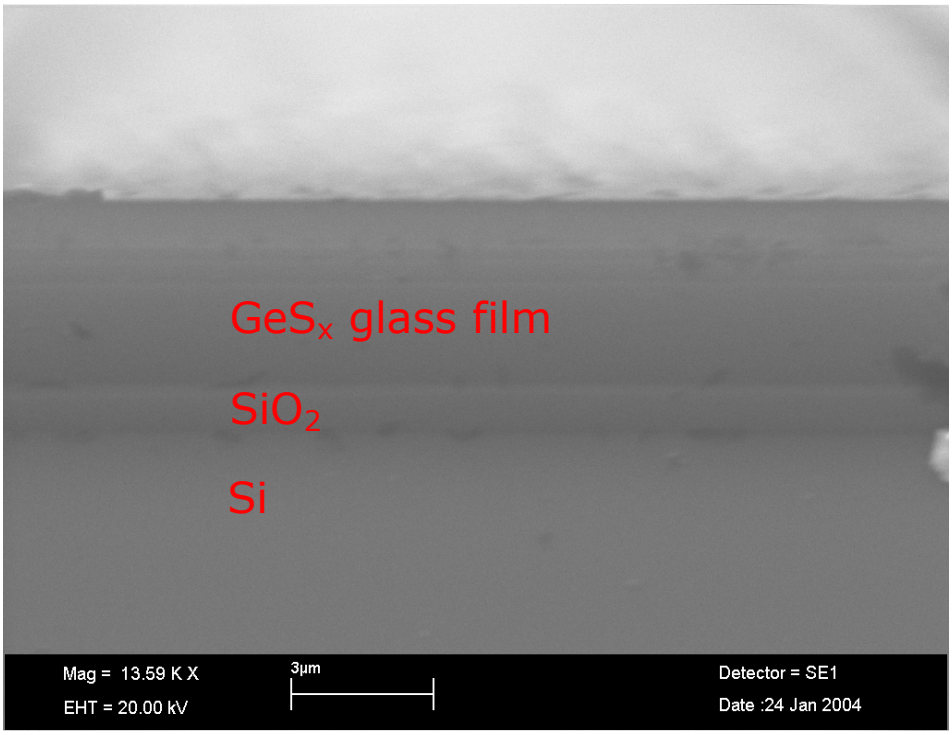

Fig. 5.14 SEM micrograph from the side view profile of the planar germanium sulphide glass waveguide on silica on silicon wafer by hot-wall CVD

5.4.4 GeO_2 on silica on silicon

From the previous section, we have successfully fabricated germanium sulphide glass films on the thermal oxide wafer (SiO_2 on Si) when the thickness of the oxide layer is less than 500nm. However, we still have a problem if we want to fabricate a waveguide on the thermal oxide wafer for telecommunication applications because a buffer layer thicker than 2μm is needed to isolate the field from the silicon substrate.

In order to solve this problem, we need to add another buffer layer on the thermal oxide wafer as a thicker layer is not feasible. We found that probably germanium oxide would be the best candidate for this idea because it can form germanate glass with silica at any molar ratio and it has a coefficient of thermal expansion (CTE) of about $7.5 \times 10^{-6}/^{o}C$, a melting temperature of $1086^{o}C$, and a refractive index of about 1.62 [16].

To fabricate the germanium oxide (GeO_2) buffer layer on a thermal oxide wafer, we use germanium tetrachloride ($GeCl_4$) to react with oxygen gas (O_2) in the same hot-wall CVD system, described in section 5.3, at about $1000^{o}C$ as Eq. (5.3).

$$GeCl_{4(g)} + O_{2(g)} \longleftrightarrow GeO_{2(s)} + 2Cl_{2(g)} \qquad (5.3)$$

We found that the homogeneous germanium oxide films can be formed on all 40nm, 200nm, 580nm, and 2000nm SiO_2 on Si wafers. The deposition rate of germanium oxide on a thermal oxide wafer with conditions is about 4μm/hr. These substrates were then used in the deposition of germanium sulphide glass films by CVD. From Figure

5.15, we can see that the germanium sulphide glass film (~3μm) has been formed on a ~1.9μm GeO_2 on 200nm SiO_2 on Si wafer. However, these germanium sulphide glass films are difficult to make crack free.

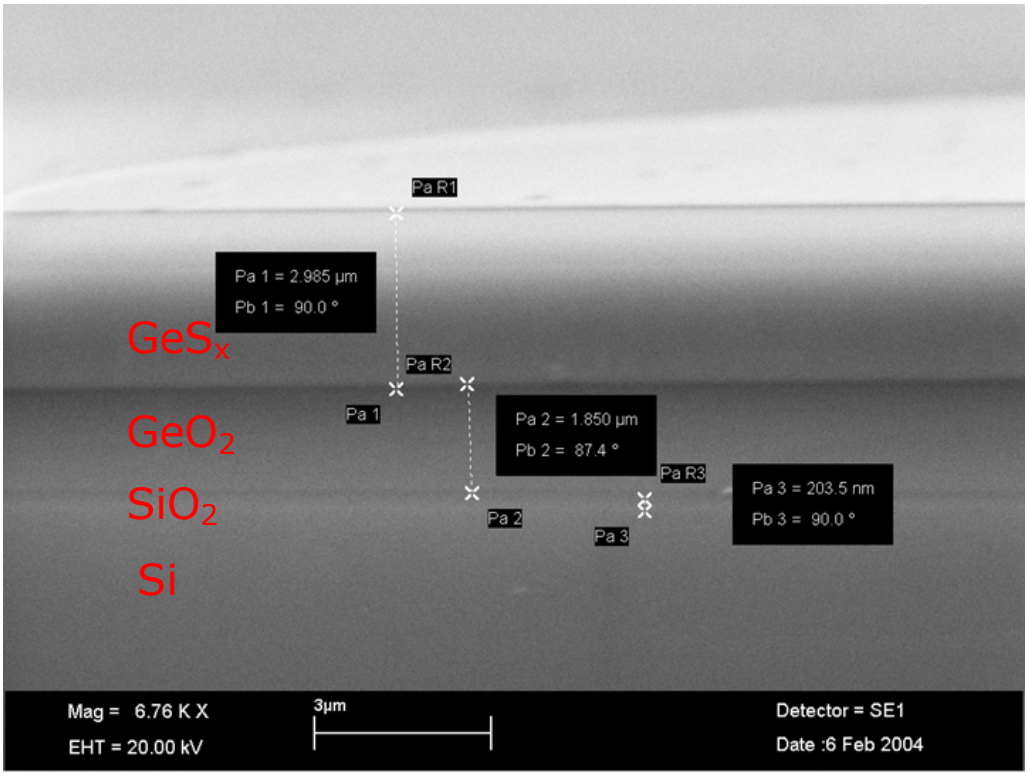

Fig. 5.15 SEM micrograph from a side view profile of the planar germanium sulphide glass waveguide on GeO_2 on silica on silicon wafer by hot-wall CVD

5.4.5 GeO_2 on silicon

In order to form a crack free germanium sulphide glass film on a suitable GeO_2 buffer layer on commercial wafers, germanium sulphide film formed on the silicon wafer (100) with GeO_2 buffer prepared by the same process as described in the previous section has been successfully demonstrated.

The SEM micrograph shown in Figure 5.16, demonstrates that a homogenous and crack free germanium sulphide glass film has been successfully formed on the commercial silicon wafer (100) with a 4.5μm GeO_2 buffer layer.

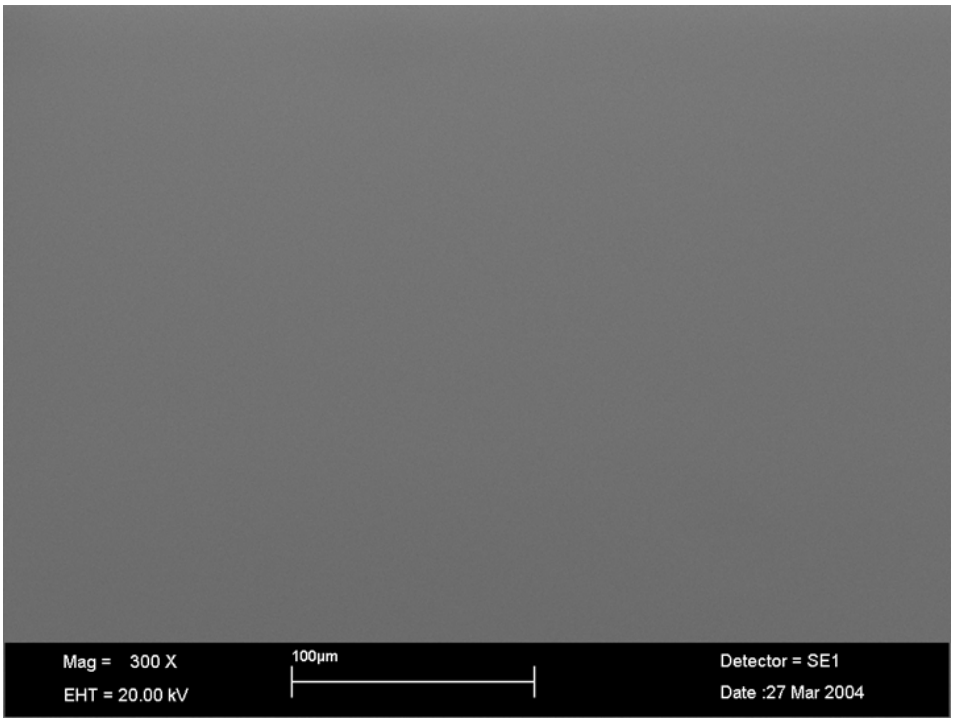

Fig. 5.16 SEM micrograph from the top view of the planar germanium sulphide glass waveguide GeO_2 on silicon wafer by hot-wall CVD

Moreover, from the side profile of the germanium sulphide glass film on GeO_2 on silicon wafer (Figure 5.17), a 2.4μm thick germanium

sulphide glass film has been well formed on the silicon wafer (100) with a 4.5μm thick GeO_2 buffer layer.

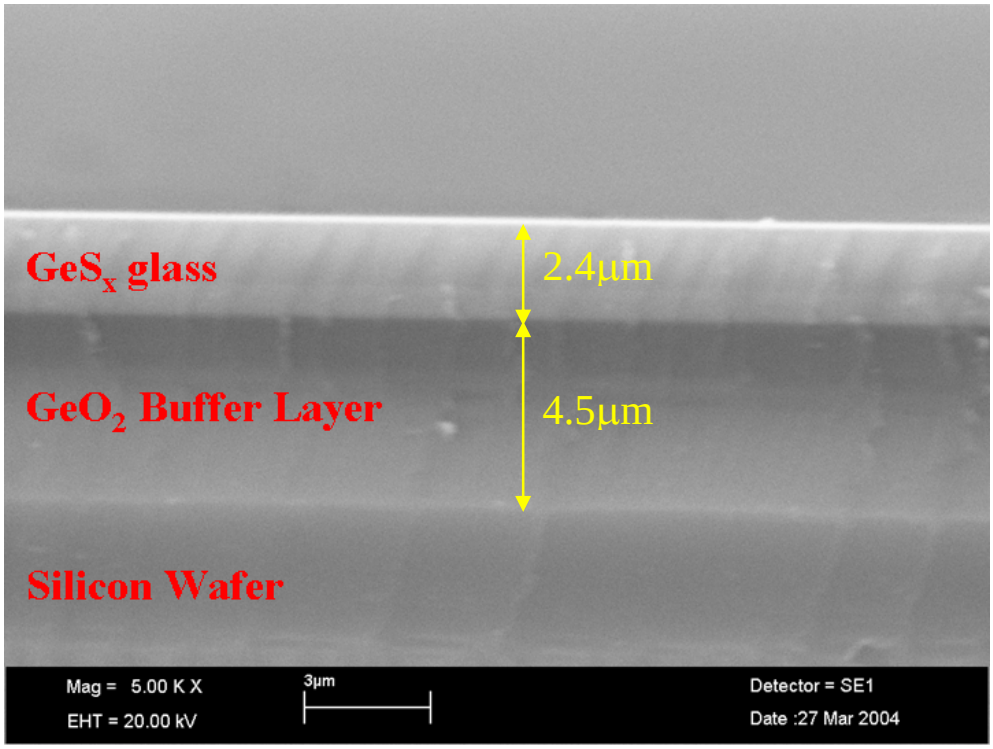

Fig. 5.17 SEM micrograph from a side view profile of the planar germanium sulphide glass waveguide on GeO_2 on silicon wafer by hot-wall CVD

To summarize, germanium sulphide glass films can be deposited on commercial wafers under some conditions, as shown in Table 5.5, by the hot-wall CVD.

Wafers	**SiO_2 / Si**	**GeO_2 / SiO_2 / Si**	**GeO_2 / Si**
Buffer layer	SiO_2	GeO_2/SiO_2	GeO_2
CTE of substrate ($x10^{-6}/^oC$)	4.15	4.15	4.15
CTE of buffer layer ($x10^{-6}/^oC$)	0.55	~7.5/0.55	~7.5
CTE of GeS_2 ($x10^{-6}/^oC$)	12.9	12.9	12.9
Quality of GeS_2 film	Stable if SiO_2 < 500nm	unstable	stable

Table 5.5 parameters of germanium sulphide glass deposited on commercial wafers

5.5 Channel waveguides by Ar-ion beam milling

Germanium sulphide glass planar waveguides with rib structures have been fabricated by using photolithography and argon ion-beam milling processes. The substrate used for the deposition was Schott N-PSK58, two faces were polished by Crystran Ltd, with a dimension of 50x13x1.5 mm.

Shipley S1813 photoresist and Puddle MF319 developer have been used in the photolithography process. The details are summarized in Table 5.6.

Step1	One drop of Shipley S1813 on the target sample
Step2	Spin coating at 6000rpm for 60 secs
Step3	Baking at 90 ^{o}C for 30mins
Step4	Put the sample under Karl Suss UV mask aligner
Step5	UV exposure for 9.5 secs
Step6	Developed by Puddle MF319 for 45secs

Table 5.6 Photolithography process for germanium sulphide glass rib waveguides

After the photolithography process, an Ar ion-beam milling instrument, which is a combination of OXFORD and EDWARD, was used to etch the slab germanium sulphide glass waveguide. The Ar ion-beam is non-selective and etched the photoresist and germanium sulphide glass at about the same rate of 30nm/min. The thickness of the photoresist patterned on the germanium sulphide glass was about 1μm, therefore a run time of 30mins was used. The residual

photoresist on the surface was removed with acetone, followed by a rinse in D.I. water.

An alpha-step technique was used to measure the surface structures shown in Figure 5.18. From which, some rib structures with the heights of about 880 nm and the widths of about 28 μm have been demonstrated.

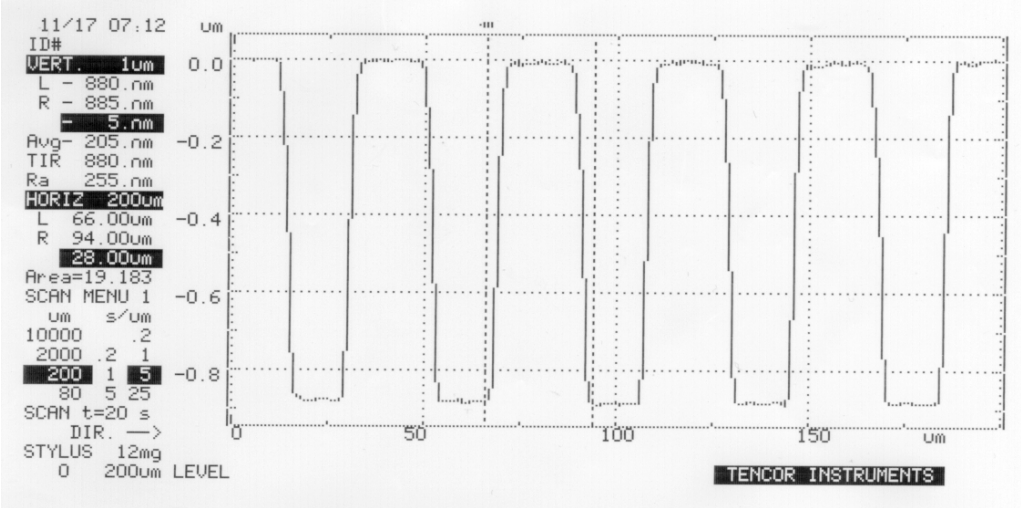

Fig. 5.18 Alpha-step profile of ribs structures of germanium sulphide glass waveguide by photolithography and Ar ion-beam milling

In Figure 5.19, a SEM micrograph shows well defined rib structures, with a width of about 5μm, which have been achieved by photolithography and ion-beam milling. Thus, we have proved that this CVD process is promising for producing integrated optical circuits on a single substrate.

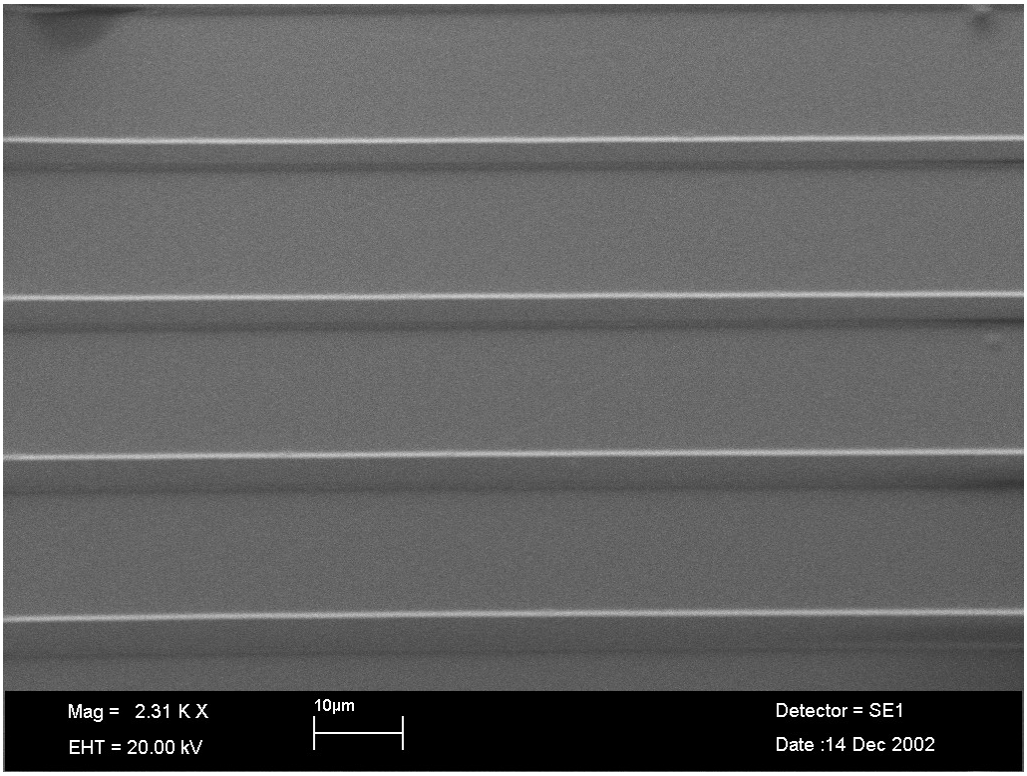

Fig. 5.19 SEM micrograph of rib structures of germanium sulphide glass waveguide by photolithography and Ar ion-beam milling

5.6 Characterization

As described in the previous sections, the germanium sulphide films have been successfully deposited on a variety of substrates. These films are now analyzed by a series of methods. First of all, the composition and bonding structures of germanium sulphide films can be determined by micro-Raman spectroscopy. The surface morphology can be studied by scanning electron microscopy (SEM) and the energy dispersion X-ray analysis (EDX) technique can also be applied to determine the composition of the germanium sulphide films. The structure of germanium sulphide films can be further studied by the X-ray diffraction technique. The refractive index of the germanium sulphide films can be measured by both prism coupling and single transmission techniques. The thickness of the films can be determined by the SEM technique and calculated from the fringe patterns of the UV-VIS-NIR or FT-IR transmission spectra. Furthermore, the attenuation of the germanium sulphide glass planar waveguides can be determined by a fibre coupling technique [17, 18].

5.6.1 Micro-Raman spectroscopy

In this work, we use micro-Raman to characterize the composition of germanium sulphide glass. Raman spectroscopy, like infrared absorption spectroscopy, is used to determine the vibrational energy of a material, which will help us to understand the binding structures of the materials. For IR absorption spectroscopy associated with molecular vibrational energy levels, it is the change in dipole moment during the vibration that is measured (IR-active). For Raman spectroscopy, the mechanism has its origins in the general phenomenon of light scattering, in which the electromagnetic radiation

interacts with a pulsating, deformable (polarizable) electron cloud. In the specific case of vibrational Raman scattering, this interaction is modulated by the molecular vibrations. The Raman spectrometer used is a RENISHAW Ramascope which is equipped with a CCD camera. A 633nm He-Ne laser was used to excite the sample and the Raman shift spectrum was measured, from 800cm^{-1} to 100cm^{-1}, with a resolution of 1cm^{-1}. The Raman spectrum is shown in Figure 5.20, from which we can verify the main GeS_4 tetrahedra band at 342cm^{-1} and 374cm^{-1}, the band at 434cm^{-1} due to short S-S (S_8) chains between GeS_4 tetrahedra, and the weak band at about 180cm^{-1} due to the GeS_4 tetrahedra bending vibration [19-21].

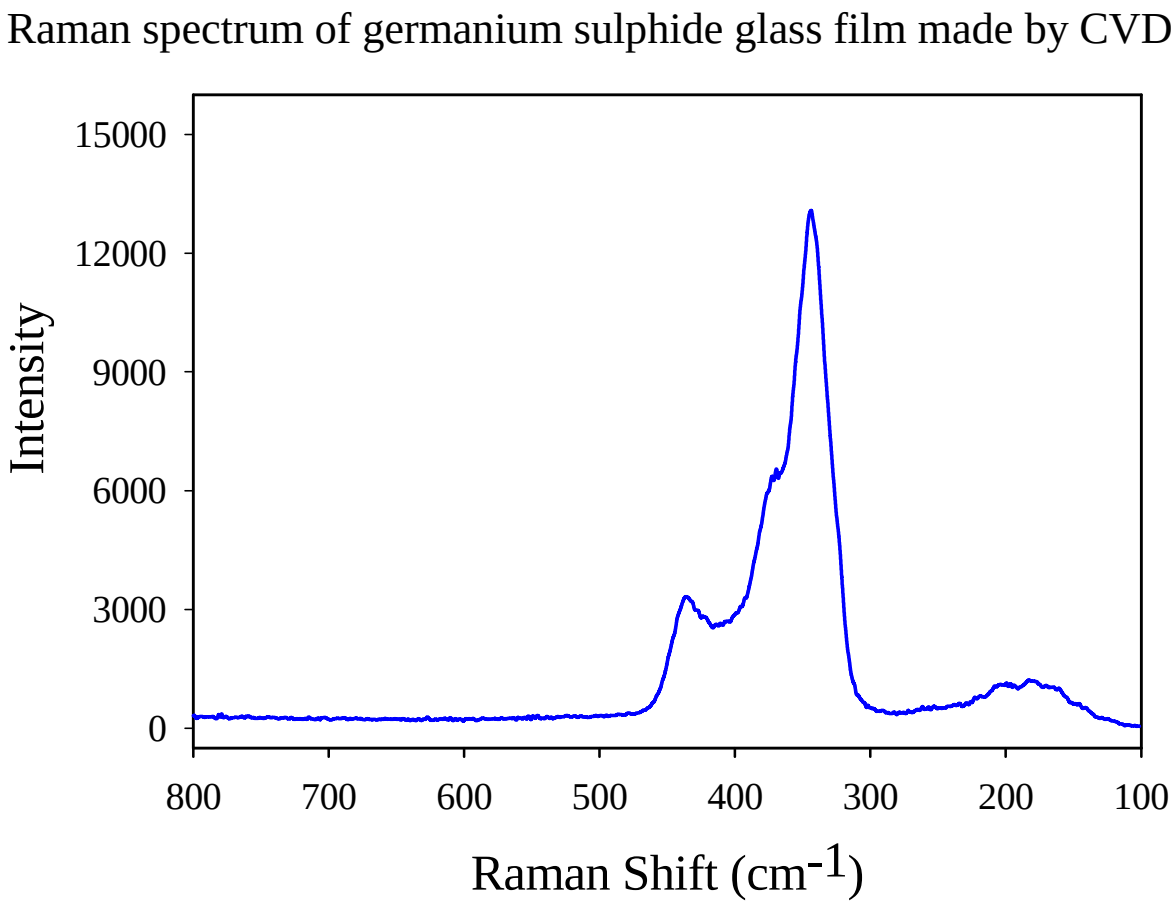

Fig. 5.20 Typical Raman spectrum of germanium sulphide glass film made by CVD

Comparison of the measured spectrum with that (Figure 5.21) in reference [19] allows us to estimate the germanium sulphide glass to have a sulphur to germanium ratio of 2±0.2.

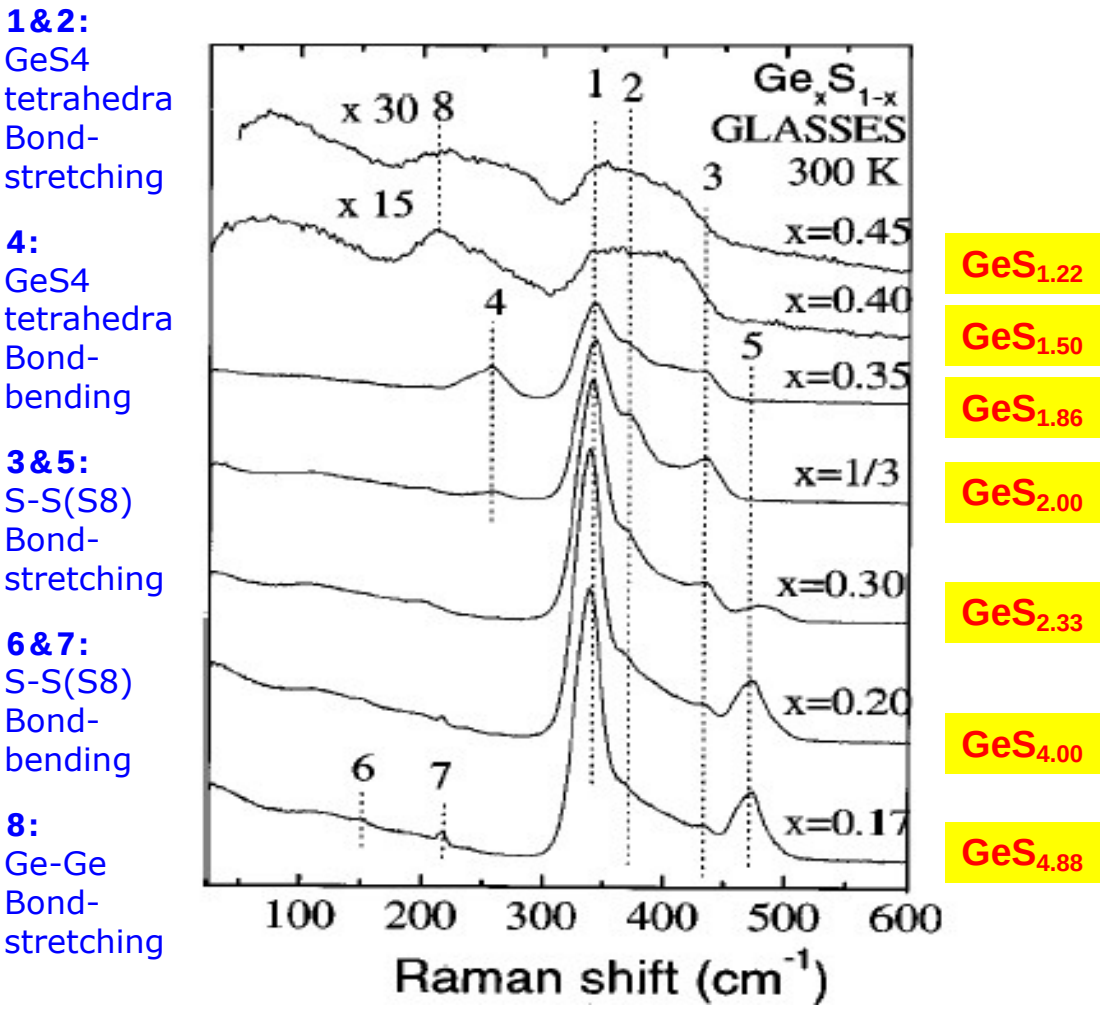

Fig 5.21 Raman spectra of Ge_xS_{1-x} glass [19]

Furthermore, if we compare the Raman spectrum of germanium sulphide crystalline material, shown in Figure 5.22, the peaks of the crystalline material are much sharper than those of germanium sulphide glass, shown in Figure 5.20. This is because the arrangements

of atoms in the crystalline structure are more rigid than those in an amorphous structure. Also, we can find that the crystalline material has two phases, α-GeS_2 and β-GeS_2, which also agrees with reference [21]. Therefore, from this Raman spectrum, an amorphous phase of the germanium sulphide has been demonstrated.

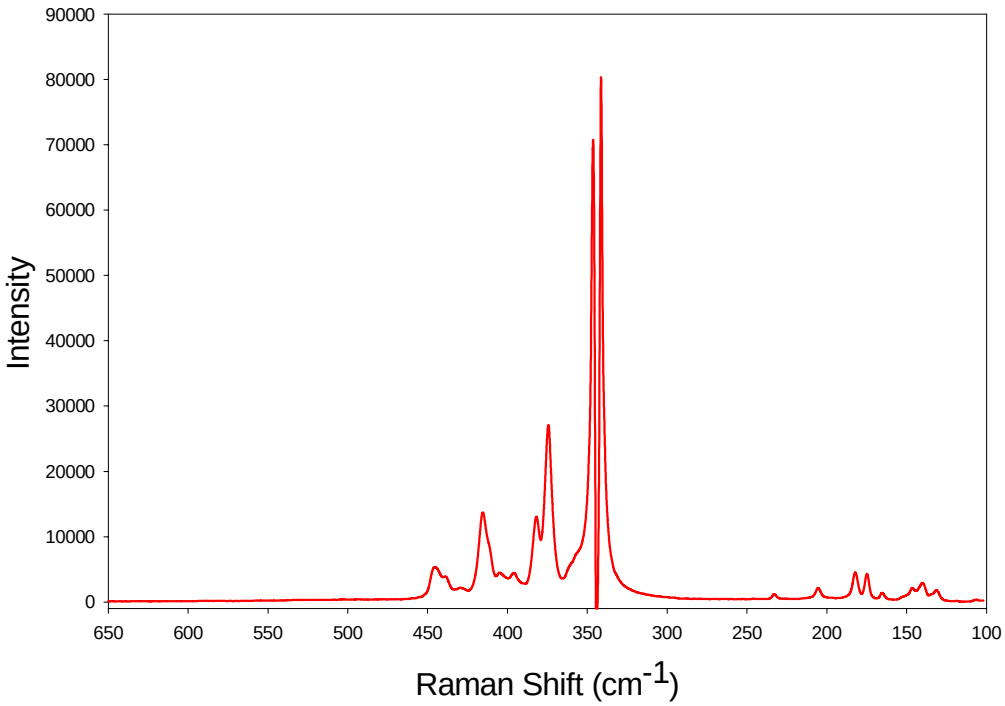

Fig. 5.22 Raman spectrum of germanium sulphide crystalline material by CVD run7

5.6.2 Scanning electron microscopy (SEM) and energy dispersion X-ray analysis (EDX) techniques

The scanning electron microscope as shown in Figure 5.23 has many advantages over traditional microscopes. The SEM has a large depth of field, which allows more of a specimen to be in focus at one time. The SEM also has a much higher resolution, so closely spaced specimens can be magnified at much higher levels. Because the SEM

uses electromagnets rather than lenses, the researcher has much more control in the degree of magnification. All of these advantages, as well as the clear images, make the scanning electron microscope one of the most useful instruments in research today [22, 23].

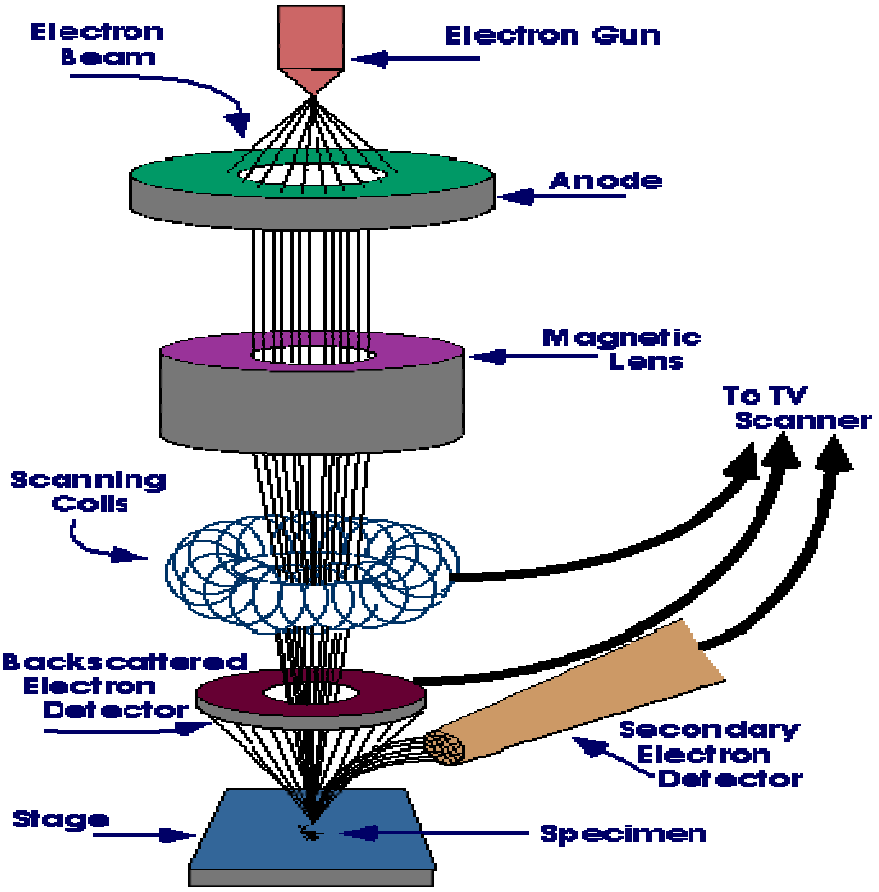

Fig. 5.23 Typical scanning electron microscope (SEM) system [23]

Furthermore, the SEM is an instrument that produces a largely magnified image by using electrons instead of light to form an image. A beam of electrons is produced at the top of the microscope by an electron gun. The electron beam follows a vertical path through the microscope, which is held within a vacuum. The beam travels through electromagnetic fields and lenses, which focus the beam down

toward the sample. Once the beam hits the sample, electrons and X-rays are ejected from the sample. Detectors collect these X-rays, backscattered electrons, and secondary electrons and convert them into a signal that is sent to a screen similar to a television screen. This produces the final image.

A LEO 430 SEM, equipped with an energy dispersive X-ray analyzer (EDX), was used to determine the morphology and composition of the germanium sulphide glass films coated by graphite. The SEM micrographs of the germanium sulphide glass films have been shown in the previous section. Nevertheless, the typical SEM-EDX spectrum of the germanium sulphide glass film shown in Figure 5.24 indicated that sulphur may have escaped during the analysis. Therefore, the composition of the germanium sulphide glass film, measured by EDX technique, would suffer from an error in the molar ratio between Ge and S. The results summarized in Table 5.3 indicate that the molar ratio of S/Ge is between 1.66 and 1.75. Unfortunately, it is difficult to estimate how much sulphur has been lost during the EDX measurement. Therefore, the values from the EDX technique are less than that estimated from Raman spectrum.

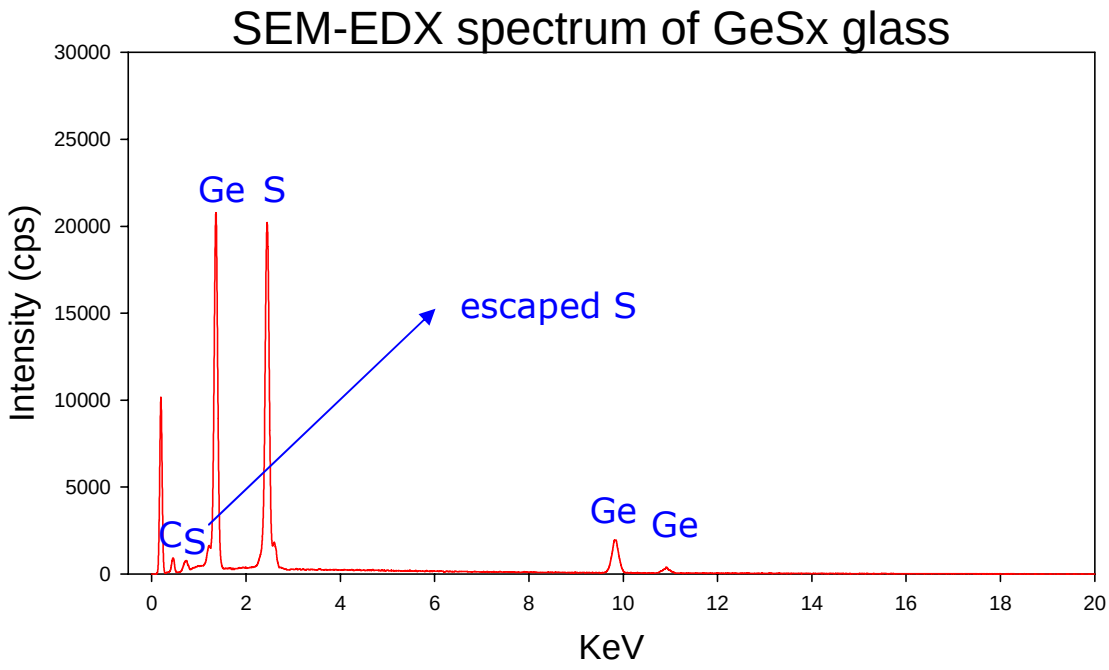

Fig. 5.24 SEM-EDX spectrum of germanium sulphide glass film by CVD

5.6.3 X-ray diffraction (XRD)

The X-ray diffraction (XRD) measurement was made by the EPSRC National Crystallography Service at the Department of Chemistry in the University of Southampton.

The X-ray diffraction (XRD) technique (using Bragg's law) is used to investigate the structure of the germanium sulphide glass film. The result, shown in Figure 5.25, indicates that no significant crystalline peak, in comparison to the structure of the crystalline GeS_2 below for reference. The arrangements of atoms in the crystalline structure are more rigid than those in amorphous structure. Therefore, 2θ values were much sharper in the crystalline phase due to the rigid and long range order structures. On the other hand, 2θ values were much

broader in the amorphous phase due to the irregular arrangements of atoms and short range ordered structures. From this pattern, we can confirm that the glass film is amorphous and is of a glassy phase [21]. In addition, the XRD pattern of the germanium sulphide glass film also agrees with the micro-Raman analysis.

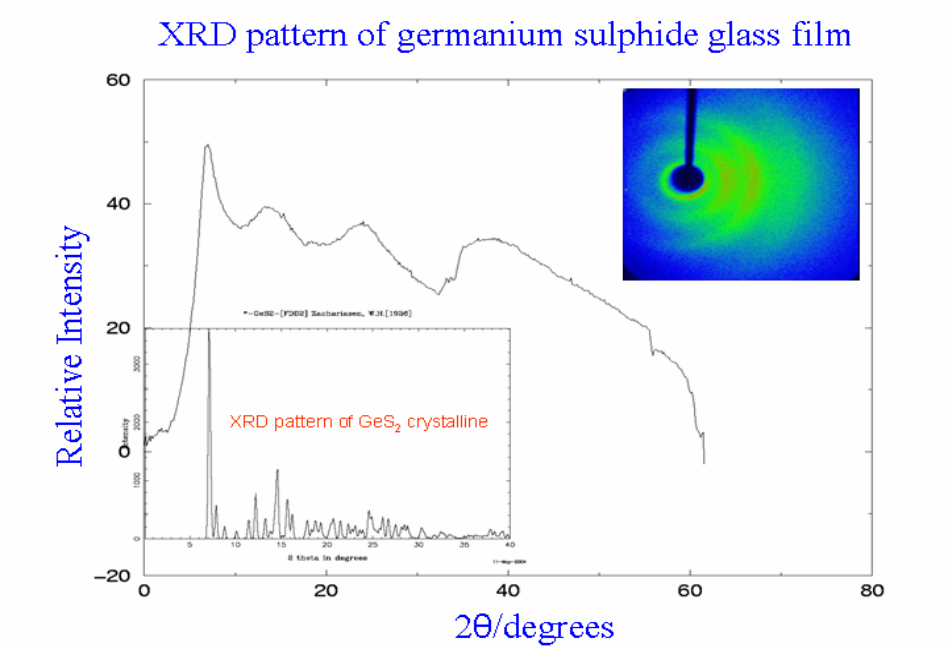

Fig. 5.25 XRD pattern of germanium sulphide glass film by CVD

5.6.4 Refractive index measurement

The main parameters of thin dielectric films such as refractive index (n) and the film thickness (d) are very crucial in the planar waveguide applications. One method that is particularly well adapted is the prism coupling technique because it can give accurate results simply and quickly [11, 24-31]. Another single transmission method, suggested by Swanepoel [32], has also been widely used to determine the above optical constants.

These two methods will be applied to determine the optical constants of germanium sulphide glass planar waveguides formed by CVD. Besides, the refractive index is a very crucial optical constant for waveguide applications and the value of the refractive index is strongly related to the composition of the materials. Therefore, the value of the refractive index will help us to estimate the composition of the germanium sulphide glass film [33].

5.6.4.1 Prism coupling technique

The refractive index of germanium sulphide glass film has been characterized by the prism coupling technique, shown in Figure 5.26. The prism used in the measurement was rutile with a refractive index (n_p) of 2.584 for light polarized to excite the TM mode.

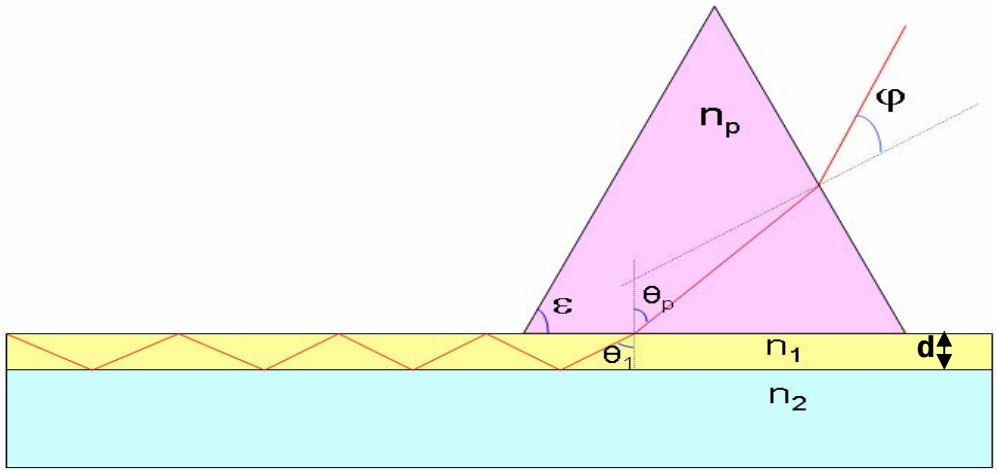

Fig. 5.26 Prism coupling technique for refractive index measurement, where n_p is the refractive index of the rutile prism, n_1 is the refractive index of the germanium sulphide glass film, n_2 is the refractive index of the substrate, φ is the incidence angle of

the He-Ne laser on the first surface, ε is the refracting angle of the rutile prism, θ_p is the incidence angle of He-Ne laser on the second surface, θ_1 is the refractive angle in the germanium sulphide glass film, d is the thickness of the film.

The waveguides fabricated are multi-mode, thus light guidance was observed for five guided modes (CVD run29). The effective index (N) shown in Table 5.7 is calculated using Eq.5.4.

Effective index (N) = β/k_0

$= n_1 \sin\theta_1$

$= \sin\varphi\cos\varepsilon + (n_p^2 - \sin^2\varphi)^{1/2}\sin\varepsilon$ (Eq.5.4)

	ε (degree)	φ (degree)	N (effective index)
1 (N_0)	60	-19.8	2.0491
2 (N_1)	60	-21.7	2.0299
3 (N_2)	60	-24.8	1.9984
4 (N_3)	60	-29.3	1.9526
5 (N_4)	60	-35.2	1.8932

Table 5.7 Effective Index of germanium sulphide glass film by the prism coupling technique

The propagation constants for the modes in waveguide N_m are determined by the following equation [34],

$$k_0 d(n_1^2 - N_m^2)^{1/2} = m\pi + \tan^{-1}[(\frac{n_1}{n_2})^2(\frac{N_m^2 - n_2^2}{n_1^2 - N_m^2})]^{1/2} + \tan^{-1}[(\frac{n_1}{1})^2(\frac{N_m^2 - 1^2}{n_1^2 - N_m^2})]^{1/2}$$

(Eq.5.5)

where k_0 is the magnitude of wave vector in free space

m is the mode number

d is the thickness of the film

n_1 is the refractive index of the film

Since five guided modes were observed in the measurement and by using the Mathcad software every two modes can be fitted into Eq. 5.5 to calculate the refractive index (n_1) and thickness of the thin film (d), this data was then used to calculate these optical constants and full details are shown in Table 5.8. The refractive index and film thickness of germanium sulphide glass films were 2.093±0.008 and 1.83±0.08μm respectively. The results also agree with that in reference [33].

Modes	Refractive Index (n_1)	Film thickness (d, μm)
N_0-N_1	2.091	1.96
N_0-N_2	2.093	1.86
N_0-N_3	2.095	1.80
N_0-N_4	2.096	1.78
N_1-N_2	2.098	1.79
N_1-N_3	2.099	1.76
N_1-N_4	2.100	1.75
N_2-N_3	2.074	1.99
N_2-N_4	2.084	1.84
N_3-N_4	2.101	1.75
Average	**2.093±0.008**	**1.83±0.08**

Table 5.8 Optical constants of germanium sulphide glass film measured by the prism coupling technique

5.6.4.2 Single transmission technique

The refractive index (n) of germanium sulphide glass waveguides was measured by using only the transmission spectra, as was suggested by Swanepoel [32]. According to Swanepoel's method of creating the upper and lower envelopes of the transmission spectrum with interference fringes, the refractive index was calculated by the following equation (Eq. 5.6).

$$n = \sqrt{N + \sqrt{N^2 - s^2}} \qquad \text{(Eq. 5.6)}$$

where $N = 2s\frac{T_M - T_m}{T_M T_m} + \frac{s^2 + 1}{2}$

s (the refractive index of the substrate)$= \frac{1}{T_s} + \sqrt{\frac{1}{T_s^2} - 1}$

T_s = transmission of substrate at the wavelengths

T_M = value of transmission maximum at the wavelengths of the upper envelopes

T_m = value of transmission minimum at the wavelengths of the lower envelopes

The accuracy to which the wavelength can be measured is ±1nm. The maximum absolute accuracy of T_M and T_m is ±0.001.

Also, if n_1 and n_2 are the refractive indices at two adjacent maxima (or minima) at wavelengths λ_1 and λ_2, using the basic equation for interference fringes (Eq. 5.7):

$$2nd = m\lambda \qquad \text{(Eq. 5.7)}$$

where m is an integer for maxima and half integer for minima, the thickness (d) is given by Eq. 5.8.

$$d = \frac{\lambda_1 \lambda_2}{2(\lambda_1 n_2 - \lambda_2 n_1)} \qquad \text{(Eq.5.8)}$$

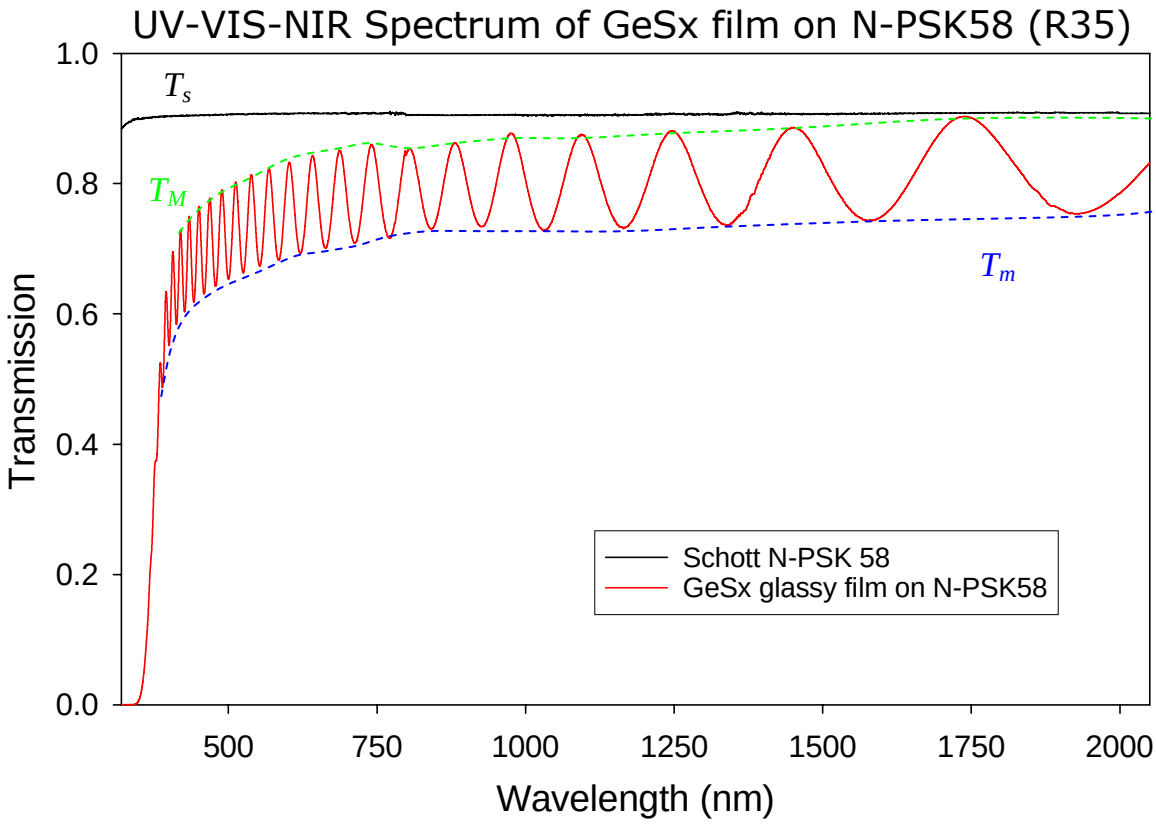

Fig. 5.27 UV-VIS-NIR spectrum of germanium sulphide glass planar waveguide

The transmission spectrum of the germanium sulphide glass planar waveguide was measured by a Varian Cary 500 Scan UV-VIS-NIR Spectrophotometer at the resolution of 1nm (shown in Figure 5.27). By using the Swanepoel's method, we can calculate the refractive index and the thickness of the germanium sulphide glass

planar waveguides at some wavelengths and the results are summarized in Table 5.9. The refractive index of the germanium sulphide glass film measured by the single transmission method agrees with the previous measurement made by a prism coupling technique.

λ *(nm)* (±1nm)	T_M (±0.001)	T_m (±0.001)	T_s (± 0.001)	S (± 0.001)	*n*	*d* (μm)
770	0.857	0.716	0.908	1.563	2.075 ± 0.004	
741	0.860	0.712	0.909	1.559	2.093 ± 0.003	2.12
713	0.856	0.708	0.907	1.568	2.105 ± 0.004	2.24
687	0.851	0.705	0.908	1.563	2.102 ± 0.005	2.26
663	0.847	0.701	0.908	1.563	2.105 ± 0.005	2.25
642	0.843	0.697	0.908	1.563	2.107 ± 0.003	2.18
621	0.838	0.693	0.908	1.563	2.109 ± 0.005	2.10
603	0.832	0.688	0.908	1.565	2.117 ± 0.003	2.17
585	0.828	0.683	0.907	1.568	2.126 ± 0.003	2.17
569	0.823	0.678	0.908	1.563	2.129 ± 0.004	2.16
553	0.818	0.674	0.907	1.568	2.137 ± 0.005	2.20
539	0.813	0.668	0.907	1.568	2.141 ± 0.003	2.17
525	0.807	0.663	0.907	1.568	2.148 ± 0.005	2.27
512	0.802	0.659	0.907	1.568	2.152 ± 0.005	
500	0.796	0.654	0.907	1.568	2.156 ± 0.005	

***Film thickness from calculation:* 2.19±0.05μm**

Table 5.9 Values of λ, T_M, T_m, T_s, and s for the calculation of refractive index and film thickness of germanium sulphide glass planar waveguides.

5.6.5 Waveguide attenuation

The attenuation of germanium sulphide planar waveguides has been measured by the fibre coupling technique with the He-Ne laser at the wavelength of 632.8nm. The image taken by a CCD camera was converted to the pixel intensity along the length and the attenuation was fitted by the linear regression. As the results show, in Figure 5.28, the attenuation of germanium sulphide glass planar waveguide was 2.1±0.3 dB/cm.

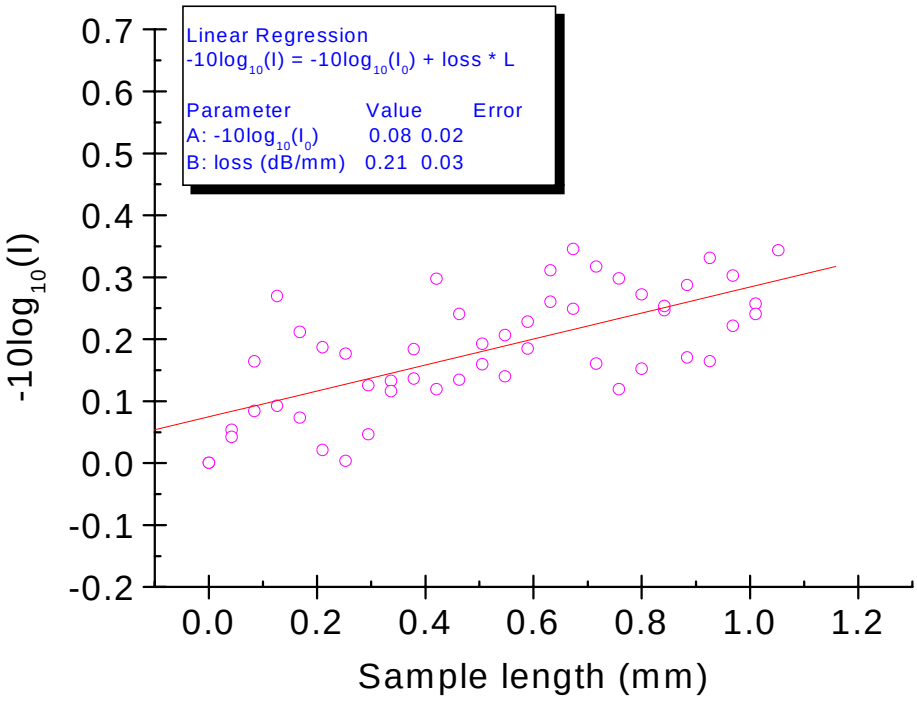

Fig. 5.28 Attenuation of germanium sulphide glass planar waveguides

5.7 Summary

From a thermodynamic analysis, we have shown that germanium sulphide glass formation from germanium tetrachloride and hydrogen sulphide is spontaneous and that the yield will be improved at higher temperatures. Germanium sulphide glass films were successfully fabricated on a variety of substrates, including CaF_2, Schott-N-PSK58, silica on silicon, GeO_2/silica on silicon, and GeO_2/silicon, at the temperature range from 450 to 600 ^oC and the deposition rate is estimated to be about 12μm/hr at 500 ^oC by the CVD processes.

These films have been characterized by micro-Raman spectroscopy, scanning electron microscopy (SEM) and energy dispersive X-ray spectroscopy (EDX) technique, and X-ray diffraction (XRD). Their transmission range extends from 0.5μm to 10.5μm as measured by UV-VIS-NIR and FT-IR spectroscopy. The refractive index of germanium sulphide glass films, measured by the prism coupling technique, was 2.093±0.008, and measured by the single transmission technique, was 2.107±0.003 at 642nm. The Raman spectrum and the refractive index of the germanium sulphide glass film both suggested that the germanium sulphide glass formed by CVD has a stoichiometry that is close to 2; although the SEM-EDX results of the germanium sulphide glassy films show the composition of the films as (~ $GeS_{1.7}$). The waveguide loss measured at 632.8nm by He-Ne laser was 2.1±0.3 dB/cm.

Furthermore, the properties of the waveguides have been studied and the light guidance of the waveguide has been demonstrated. These results show that this fabrication technique has a great potential in optoelectronics, particularly to make waveguides for optical

integrated circuits applications. We are currently extending this work to deposition on other semiconductor substrates.

5.8 References

[1] M.M. El-Nahass, A.A.M. Farag, E.M. Ibrahim, and S. Abd-El-Rahman, "Structural, optical and electrical properties of thermally evaporated Ag_2S thin films", Vacuum, **72**(2004)453-460.

[2] V. Lyubin, M. Klebanov, B. Sfez, and B. Ashkinadze, "Photo-luminescence and photodarkening effect in erbium-doped chalcogenide glassy films", Materials Letters, **58**(2004)1706-1708.

[3] L. Jiang, A. G. Fitzgerald, M. J. Rose, K. Christtova, V. Pamukchieva, "X-ray photoelectron spectroscopy studied of thin $Ge_xSb_{40-x}S_{60}$ chalcogenide thin films", Journal of Non-Crystalline Solids, **297**(2002)13-17.

[4] E. Marquez, T. Wagner, J. M. Gonzalex-Leal, A. M. Bernal-Oliva, R. Prieto-Alcon, R. Jimenez-Garay, and P.J.S Ewen, "Controlling the optical constants of thermally-evaporated $Ge_{10}Sb_{30}S_{60}$ chalcogenide glass films by photodoping with silver", Journal of Non-Crystalline Solids, **274**(2000)62-68.

[5] J. Fick, E. J. Knystautas, A. Villeneuve, F. Schiettekatte, S. Roorda, and K.A. Richardson, "High photoluminescence in erbium-doped chalcogenide thin film", Journal of Non-Crystalline Solids, **272**(2000)200-208.

[6] A. Jdanov, J. Pelleg, Z. Dashevsky, and R. Shneck, "Growth and characterization of PbTe films by magnetron sputtering", Materials Science and Engineering, **B106**(2004)89-94.

[7] S. Ramachandran and S.G. Bishop, "Excitation of Er^{3+} emission by host glass absorption in sputtered films of Er-doped $Ge_{10}As_{40}Se_{25}S_{25}$ glass", Applied Physics Letters, **73**(1998)3196.

[8] A.P. Caricato, M. De Sario, M. Fernandez, M. Ferrari, G. Leggieri, A. Luches, M. Martino, M. Montagna, F. Prudenzano, and A. Jha, ”Chalcogenide glass thin film waveguides deposited by excimer laser ablation”, Applied Surface Science, **208-209**(2003)632-637.

[9] P. Nemec, M. Frumar, J. Jedelsky, M. Jelinek, J. Lancok, and I. Gregora, “Thin amorphous chalcogenide films prepared by pulsed laser deposition”, Journal of Non-Crystalline Solids, **299-302** (2002)1013-1017.

[10] Yu. Mourzina, M.J. Schoning, J. Schubert, W. Zander, A.V. Legin, Yu.G. Vlasov, P.Kordos, and H. Luth, “A new thin-film Pb microsensor based on chalcogenide glasses”, Sensors and Actuators, **B71**(2000)13-18.

[11] D.S. Gill, R.W. Eason, C. Zaldo, H.N. Rutt, and N.A. Vainos, “Characterisation of Ga-La-S chalcogenide glass thin film optical waveguides, fabricated by pulsed laser deposition”, Journal of Non-Crystalline Solids, **191**(1995)321-326.

[12] A.V. Kolobov, "Photo-induced Metastability in Amorphous Semiconductors", Wiley-VCH, 2003.

[13] P.J. Melling, "Alternative Methods of Preparing Chalcogenide Glasses", Ceramic Bulletin, **63** (1984) 1427-1429.

[14] E. Sleeckx, P. Nagels, R. Callaerts and M. Vanroy, "Plasma-enhanced CVD of amorphous GexS1-x and GexSe1-x films", J. de Physique IV, **3** (1993) 419-426.

[15] Ihsan Barin, "Thermochemical Data of Pure Substances", 3rd edition, VCH Publishers, 1995.

[16] A. Margaryan, and M.A. Piliavin, “Germanate Glasses: Structure, Spectroscopy, and Properties”, Artech House, 1993.

[17] Chao-Yi Tai, PhD thesis, “Tantalum pentoxide waveguides for photonic crystal circuits”, 2004, University of Southampton.

[18] A. Ashida, H. Ohta, T. Nagata, Y. Nakano, N. Fujimura and T. Ito, "Optical propagation loss of ZnO films grown on sapphire", Journal of Applied Physics, **95** (2004) 1673-1676.

[19] I. P. Kotsalas and C. Raptis, "High-temperature structural phase transitions of GexS1-x alloy studied by Raman spectroscopy", Phys. Rev. B, **64**(2001)125210.

[20] K. Jackson, A. Briley, and S. Grossman, "Raman-active modes of α-$GeSe_2$ and α-GeS_2: A first principles study", Phys. Rev. B, **60**(1999)14985.

[21] Z. Cernosek, E. Cernoskova, and L. Benes, "Raman scattering in GeS_2 glass and its crystalline polymorphs compared", Journal of Molecular Structure, **435**(1997)193-198.

[22] J. Goldstein, D. Newbury, P. Kchlin, D.C. Joy, C.E. Lyman, E. Lifshin, L. Sawyer, J.R. Michael, "Scanning Electron Microscopy and X-Ray Microanalysis", Kluwer Academic Publishers, 2003.

[23] http://mse.iastate.edu/microscopy/home.html

[24] P.K. Tien, R. Ulrich, and R.J. Martin, "Modes of propagating light waves in thin deposited semiconductor films", Applied Physics Letters, **14** (1969) 291-294.

[25] J.H. Harris, R. Shubert, and J.N. Polky, "Beam coupling to films", Journal of the Optical Society of America, **60** (1970) 1007-1016.

[26] P.K. Tien and R. Ulrich, "Theory of prism-film coupler and thin-film light guides", Journal of the Optical Society of America, **60** (1970) 1325-11337.

[27] R. Ulrich and R. Torge, "Measurement of thin film parameters with a prism coupler", Applied Optics, **12** (1973) 2901-2908.

[28] J. Hurtado-Ramos, H. Wang, "Analysis of accuracy in prism coupling methods and a proposal of two simple ways for coupling to guided waves and/or for exciting surface plasmon resonance", Optical Materials, **7** (1997) 153-164.

[29] D. Chen, B.C. Potter, J.H. Simmons, "GeO_2-SiO_2 thin films for planar waveguide applications", Journal of Non-Crystalline Solids, **178** (1994) 135-147.

[30] M.J. Bergmann, U. Ozgur, H.C. Casey, H.O. Everitt, J.F. Muth, "Ordinary and extraordinary refractive indices for $Al_xGa_{1-x}N$ epitaxial layers", Applied Physics Letters, **75** (1999) 67-69.

[31] T. Sharda, T.Soga and T. Jimbo, "Optical properties of nano-crystalline diamond films by prism coupling technique", Journal of Applied Physics, **93** (2003) 101-105.

[32] R. Swanepoel, "Determination of the thickness and optical constants of amorphous silicon", J. Phys. E: Sci. Instrum., **16**(1983)1214-1222.

[33] R. Todorov, Tz. Iliev, and K. Petkov, "Light-induced changes in the optical properties of thin films of Ge-S-Bi(Ti,In) chalcogenides", Journal of Non-Crystalline Solids, **326&327**(2003)263-267.

[34] M.J. Bergmann, U. Ozgur, H.C. Casey, H.O. Everitt, J.F. Muth, "Ordinary and extraordinary refractive indices for $Al_xGa_{1-x}N$ epitaxial layers", Applied Physics Letters, **75** (1999) 67-69.

Chapter 6

Fabrication and characterization of germanium sulphide bulk glass by CVD

6.1 Introduction

Chalcogenide glasses, as described in Chapter 2, are defined as glasses containing at least one of the elements S, Se, and Te. They are available in a stable vitreous state and with a wide optical transmission range. Of the chalcogenide glasses, sulphide glasses exhibit relatively low toxicity compared to other chalcogenide glasses such as selenide and telluride glasses. In addition, sulphide glasses have a relatively high softening temperature, which results in a more stable vitreous state [1, 2].

Sulphide glasses for binary systems are, in principle, divided into two groups: arsenic sulphide and germanium sulphide glasses [1, 2]. In addition, another famous composition, Ga-La-S glass, which has shown a great potential, has been intensively studied by D.W. Hewak *et al.* at the ORC, University of Southampton [3-23]. Details of Ga-La-S glasses will not be discussed in this chapter.

Arsenic sulphide glass is one of the most practical choices of chalcogenide glasses for infrared fibre optics. The first As-S infrared optical fibre with an optical loss of 20 dB/m at 5.5μm was reported by Kapany and Simms in 1965 [24]. However, the fabrication of arsenic compounds is forbidden, due to the toxicity consideration, at the ORC.

Germanium sulphide glass systems, on the other hand, have a relatively high softening temperature, a large glass forming area, and low toxicity. These systems have been studied extensively by Shibata *et al.* [25-27]. It was reported that the appropriate glass compositions for GeS_x range from x=2 to 4. It was also reported that the addition of phosphorous to the germanium sulphide glass increases glass forming ability and optical homogeneity if the amount of phosphorous is less than 10 mol.% [27]. In addition, some other precursors such as As, Sb, and Ga, have also been added into germanium sulphide glass systems to form ternary Ge-As-S [28], Ge-Sb-S [29, 30], and Ge-Ga-S [31-44] respectively, and to improve the properties of germanium sulphide glasses. Using the good rare-earth solubility, rare-earth doped germanium sulphide based optical fibres have been demonstrated [43, 44].

The conventional method of fabricating a chalcogenide glass involves melting the precursors or raw materials in a sealed silica ampoule. The raw elements, in the form of pieces or powders, are placed in the silica ampoule and sealed under a vacuum lower than 1.3 Pa (~10^{-2} Torr). This procedure will prevent the raw materials reacting with oxygen. The ampoule is heated in a rocking furnace for longer than 10 hours between 700 and 900 ^{o}C [1, 2].

In addition, chemical vapour deposition (CVD) has proved to be highly advantageous for the fabrication of ultra high purity silica glass fiber preforms. It would be desirable to find an analogous approach for the fabrication of high purity chalcogenide materials by the CVD method. So far, there has not been much work devoted to this objective [45, 46]. The first CVD process for Ge-Se binary glass

(fabricated from the reaction between $GeCl_4$ and $SeCl_2$) was reported by Katsuyama *et al.* in 1986 [45].

As described in the previous chapter, the germanium sulphide glass planar waveguides have been successfully fabricated by the CVD process (from the reaction between $GeCl_4$ and H_2S). It would be more desirable if this CVD technique could be applied to fabricate bulk glass such as infrared transmission windows and fibre preforms.

In this chapter, the fabrication process of germanium sulphide bulk glass by CVD will be discussed. The optical properties of germanium sulphide glass will be studied by UV-VIS-NIR (0.2μm to 2.5μm) and FT-IR spectroscopy (1μm to 25μm). The purity of germanium sulphide glass will be studied by glow-discharge mass spectrometry (GD-MS). Also, the thermal properties of germanium sulphide glass will be studied by differential thermal analyzer (DTA) and thermo-mechanical analyzer (TMA) techniques.

The objective in this chapter is to provide a novel CVD method for fabricating germanium sulphide bulk glass, or fibre performs, with a capability to incorporate into the glass modifying or active precursors.

6.2 Fabrication of germanium sulphide bulk glass by CVD

The germanium sulphide raw materials (powders and glass) were prepared by the CVD process. During the process, a quartz ampoule reactor (Figure 6.1) was situated inside the tube furnace at a temperature of 650^{o}C. The process was a continuous flow system maintained at the atmospheric pressure. The precursor, $GeCl_4$, was

delivered by argon gas through a mass flow controller (MFC) at a flow rate of 100 ml/min to react with H_2S and form germanium sulphide glass and crystalline powders inside the reactor. The H_2S active gas was delivered together with argon gas with a H_2S/Ar ratio of 20ml/80ml to control the molar ratio between Ge and S close to 1:2. The deposition process was finished when the pressure inside the reactor was over 15mbar and the deposition efficiency was estimated to be about 50%. The deposition efficiency is defined by the following equations.

Deposition efficiency

= (mole of $GeS_{2,\ collected\ in\ the\ reactor}$) / (mole of $GeS_{2,\ expected}$)

= (mole of $GeS_{2,\ collected\ in\ the\ reactor}$) / (mole of $GeCl_{4,\ consumed}$)

Although about 50% of the GeS_2 escaped from the reactor, the deposition efficiency is still be acceptable.

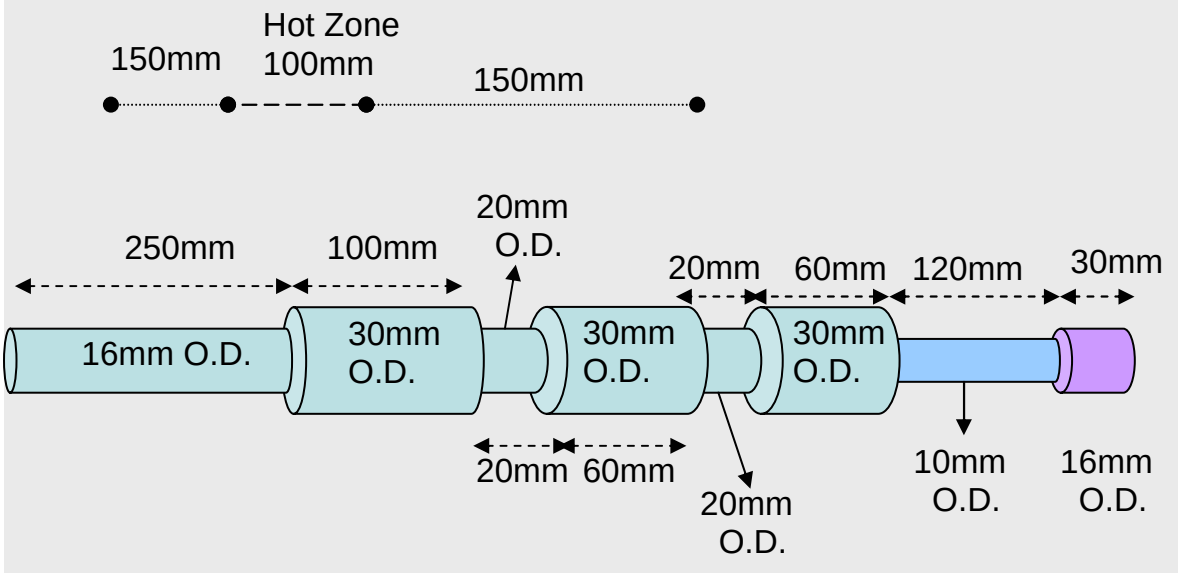

Fig. 6.1 Quartz ampoule reactor for germanium sulphide bulk glass fabrication by CVD

With reference to Figure 6.1, the left end of the quartz ampoule reactor was sealed by an oxy-hydrogen hand torch and the ampoule was evacuated to $1x10^{-6}$ mbar and then the right end of the ampoule was sealed again by the oxy-hydrogen hand torch. The conventional melt-quenching technique was applied to prepare the germanium sulphide bulk glass [1, 2]. The quartz ampoule was put in a tube furnace, with a capability of heating up to 1500 ^{o}C, and heated up from room temperature to 1050 ^{o}C at a ramping rate of 1 ^{o}C/min, kept at 1050 ^{o}C for 2hours, and pushed out to a water jacketed silica tube for a quicker quenching step. The germanium sulphide glass was then annealed at 420 ^{o}C for 8 hours.

The germanium sulphide bulk glass shown in Figure 6.2 was polished into slides with a dimension 20x12x1mm by Crystran Ltd [47].

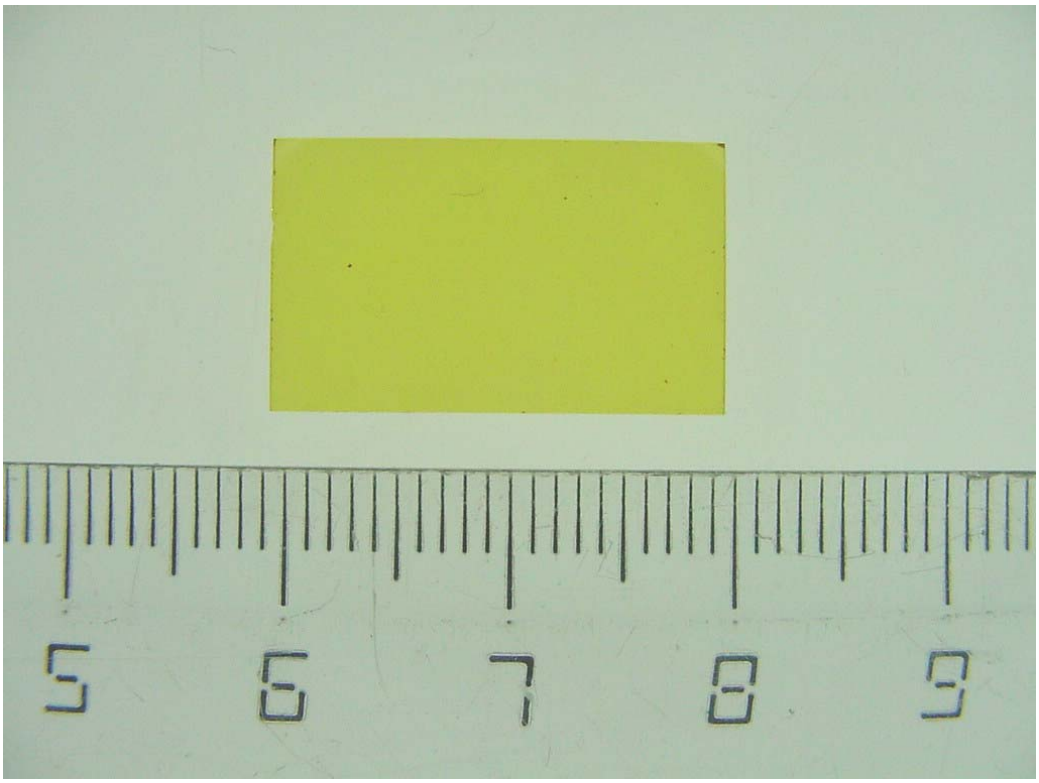

Fig. 6.2 Germanium sulphide glass slide with a dimension of 20x12x1 mm

6.3 UV-VIS-NIR and FT-IR spectroscopy

The optical transmission range of germanium sulphide glass has been studied by UV-VIS-NIR and FT-IR spectroscopy. A Varian Cary 500 scan UV-VIS-NIR Spectrophotometer was used to study the optical transmission range of germanium sulphide glass from 0.2μm to 2.5μm. Furthermore, a Perkin Elmer spectrum 2000 FT-IR was used to study the optical transmission range of germanium sulphide glass from 1μm to 25μm. The combination UV-VIS-NIR and FT-IR spectra of germanium sulphide bulk glass, fabricated in a standard silica ampoule, are shown in Figure 6.3. This 2.7mm thick germanium sulphide glass sample was remelted from the germanium sulphide bulk glass, formed by the CVD process, and polished by Crystran Ltd [47].

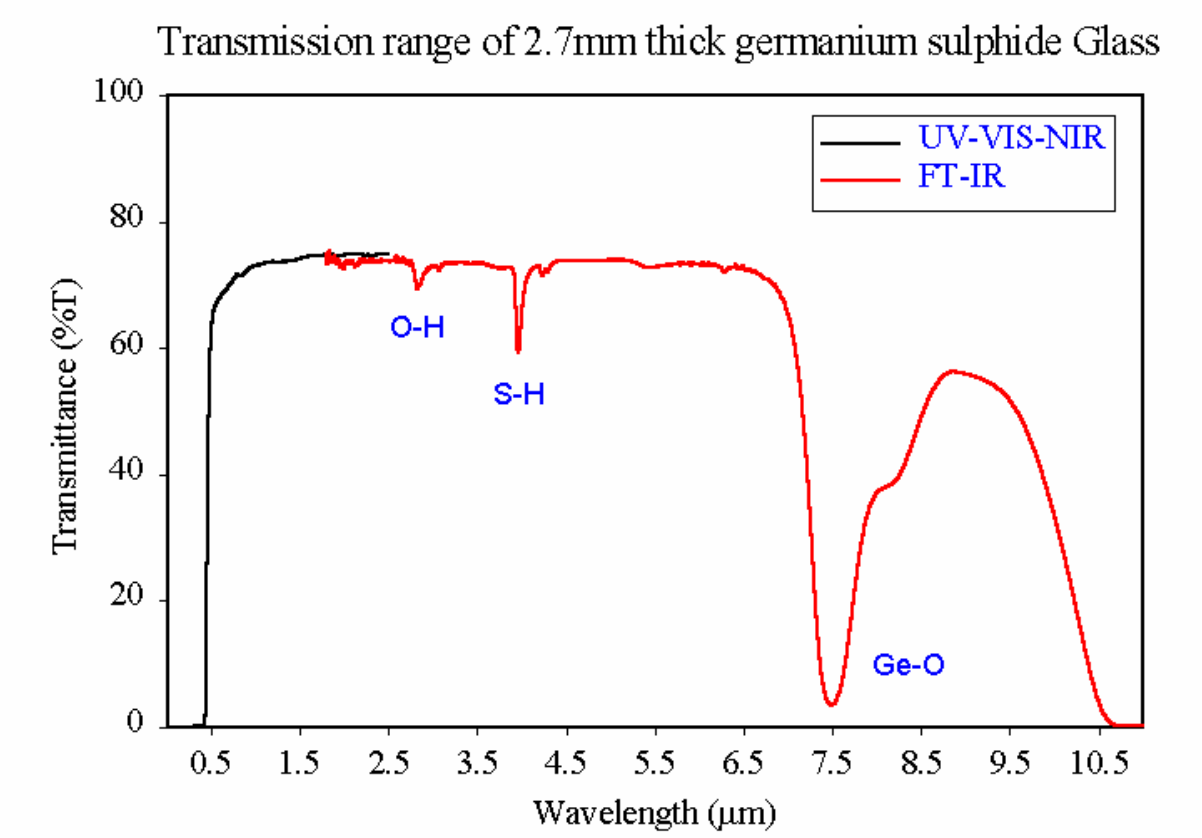

Fig. 6.3 Optical transmission range of germanium sulphide glass, 2.7mm thick sample, by CVD (standard silica ampoule reactor)

In Figure 6.3, there absorption bands at about 4μm due to S-H, at about 2.8μm due to O-H, and at about 7.5μm due to Ge-O which are typical of many chalcogenide glasses. With knowledge of the extinction ratios for these impurities [48], we can estimate their concentration to be ~3ppm, ~37ppm, and ~800ppm respectively.

Moreover, as shown in Figure 6.3, a strong absorption peak at about 7.5μm, due to the Ge-O bonding probably resulted from the reaction between the germanium sulphide glass and water present in the standard silica ampoule reactor. However, the useful transmission range of germanium sulphide glass (fabricated within a standard silica ampoule reactor) is from 0.5μm to 7μm.

However, if we use the high purity silica ampoule (made from Heraeus F300 quartz tube with an extremely low OH level, < 1ppm) reactor, the Ge-O impurity can be improved significantly as shown in Figure 6.4. Again, three impurity peaks can be found at about 2.8μm, 4μm, and 7.5μm due to O-H, S-H, and Ge-O absorptions respectively. Moreover, from the extinction coefficients of the impurities [48], these three impurity concentrations were estimated to be ~3ppm, ~185ppm, and ~58ppm respectively. Also the improved transmission range now extends from 0.5μm to 10.5μm.

From the visible and infrared spectroscopy study of the germanium sulphide bulk glass, we found that the quality of the quartz ampoule will strongly influence the purity of germanium sulphide glass, particularly regarding the Ge-O impurity. In addition, it should be noticed that there is still a considerable amount of S-H trapped or bonded in the germanium sulphide glass.

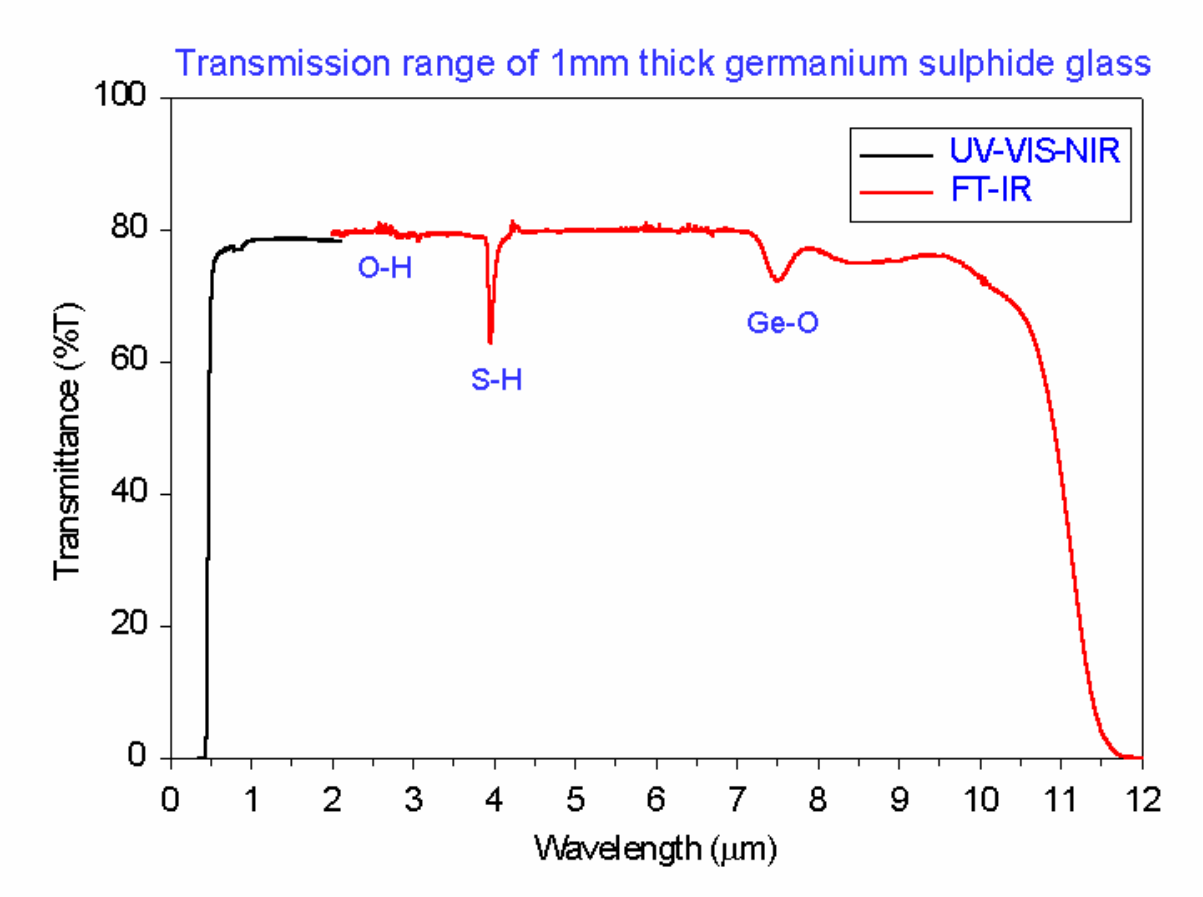

Fig. 6.4 Optical transmission range of a 1mm thick sample of germanium sulphide glass made by CVD (high purity/ low OH silica ampoule reactor)

Besides, the transmission loss of germanium sulphide fabricated by CVD process can be estimated by the following method [2, 49-50].

The intensity of transmitted light gradually decreases with the distance because of absorption and scattering loss. The intensity I_t of the light transmitted in the material of thickness t is given by the Lambert-Beer law:

$$I_t = I_0 \exp(-\alpha t) \qquad (6.1)$$

where I_0 is the intensity of input light

α is the "absorption coefficient"

If the reflections at the input and output surfaces are taken into account, the equation (6.1) can be rewritten as:

$$I_t = I_0(1-R)^2 \exp(-\alpha t) \qquad (6.2)$$

where R is the reflectivity with air at normal incidence, and is approximately given by:

$$R \approx (\frac{n-1}{n+1})^2 \qquad (6.3)$$

here n is the refractive index of the material. The insertion of equation (6.3) into equation (6.2) gives:

$$\frac{I_t}{I_0} \approx [1-(\frac{n-1}{n+1})^2]^2 \exp(-\alpha t) \qquad (6.4)$$

The absorption coefficient α is normally expressed in cm^{-1}. Therefore, the relation between the absorption coefficient α (in cm^{-1}) and the "transmission loss" L is expressed as:

$$L \text{ (dB/m)} = 434\alpha \text{ (cm}^{-1}\text{)} \qquad (6.5)$$

Based on the above equations, the transmission loss of germanium sulphide glass fabricated by the CVD process can be re-plotted and shown in Figure 6.5A and Figure 6.5B. It should be noticed

that the background transmission loss in a 2.7mm thick germanium sulphide glass sample is about 200dB/m, but that in the 1mm thick germanium sulphide sample is about 430dB/m. This is probably because the relative error in the approximation of reflectivity is larger in the thinner sample. Therefore, we need to prepare a thicker sample for this measurement in the future.

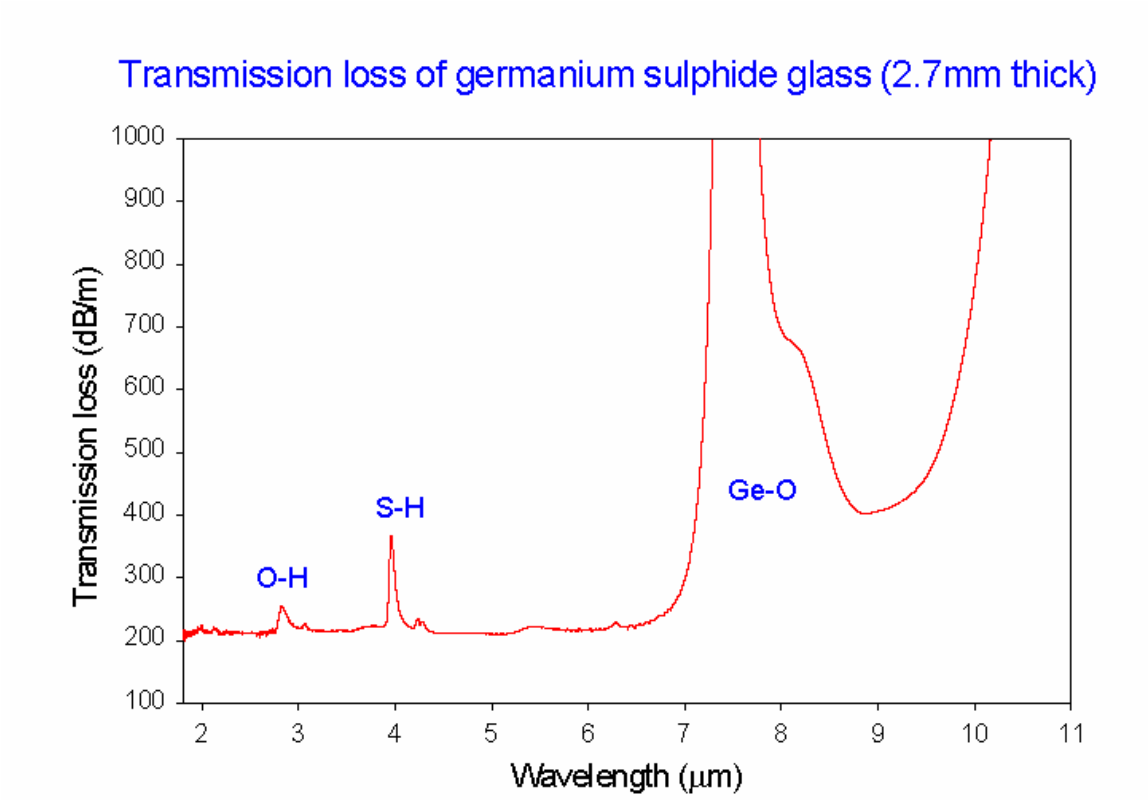

Fig. 6.5A Transmission loss of germanium sulphide glass (2.7mm thick)

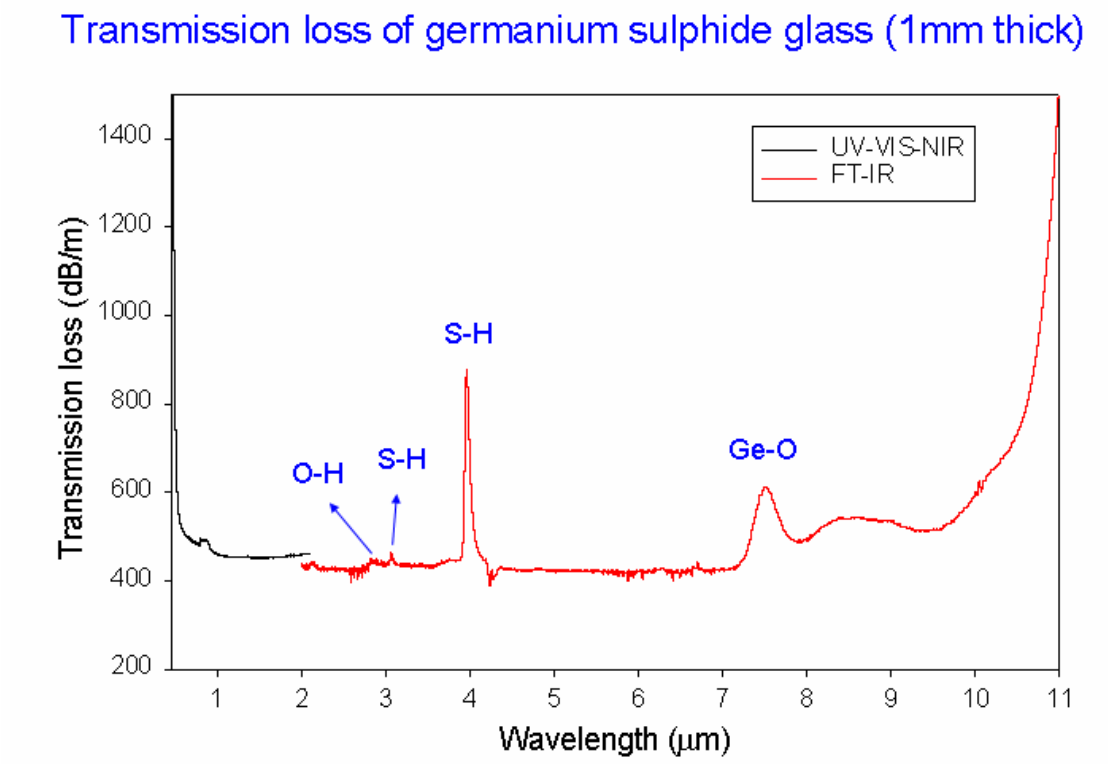

Fig. 6.5B Transmission loss of germanium sulphide glass (1mm thick)

6.4 Purity measurement by GDMS

To determine the purity of germanium sulphide glass, compositional analysis was undertaken by glow-discharge mass spectrometry (GDMS) performed off-site by Dr. Cuq-Bramhall at Shiva Technologies in Ramonville, France. High resolution GDMS is a well suited analytical technique for the direct measurement of bulk concentrations in solid materials down to the ppb range. A sample, typically between 6 – 20 mm in diameter, is inserted into a vacuum chamber where a gas discharge is struck using the sample as the cathode. The glow discharge sputtering process removes material layer by layer with each layer measuring ~ 2 µm in thickness. Sputtering rates of the glow discharge for metals and alloys is in the range of 0.05 – 0.5 µm/min. The compounds under investigation are non-conductive and hence, indium of known impurity level was used as a binder. The ions produced in the discharge are then extracted and directed into a high resolution mass spectrometer. The detection limit of the transition metal species is 0.005 ppm. Impurity levels measured with the GDMS technique stated in this work have an absolute accuracy of better than 50%. The results presented in Table 6.1 show exceptionally low levels of transition metal impurities, significantly better than the impurity levels achieved in chalcogenide glass prepared by conventional methods [1, 2]. However, in this GDMS analysis, the germanium sulphide glass was prepared within the standard silica ampoule reactor. Therefore, the oxygen level in the glass sample used in this measurement is still quite high (~460ppm) and this impurity also exists as the Ge-O absorption, in the FT-IR measurement at about 7.5µm. However, by using the high purity/low OH silica ampoule reactor, the oxygen level in the germanium sulphide glass was reduced from ~800ppm (Figure 6.3) to ~58ppm (Figure 6.4).

It should be noted that the Ge-O concentration in Figure 6.3 is about 800ppm, but the oxygen concentration from GDMS is about 460ppm. That is probably because the germanium sulphide bulk glass only had one melting step with sealed standard silica ampoule technique, however, the 2.7mm thick germanium sulphide disk sample experienced two melting steps.

Element	Concentration (ppm wt)	Element	Concentration (ppm wt)
C	≤ 0.6	V	< 0.005
O	≤ 460	Cr	< 0.005
Na	< 0.005	Mn	< 0.01
Mg	0.02	Fe	< 0.05
Al	0.17	Co	< 0.005
Si	4.0	Ni	< 0.05
S	Matrix	Cu	< 0.05
Cl	65	Zn	< 0.05
K	< 0.05	Ga	< 0.05
Ca	< 0.05	Ge	Matrix
Ti	< 0.005	Ce	< 0.005

Table 6.1 Compositional analysis of germanium sulphide glass formed by CVD

6.5 Thermal analysis

In order to understand the thermal properties of germanium sulphide glass made by the CVD process, the differential thermal analyzer (DTA) and Thermo-mechanical analyzer (TMA) have been applied to study the glass transition temperature (T_g), crystallization temperature (T_x), melting temperature (T_m), and coefficient of thermal expansion (CTE) of this glass. The understanding of T_g and T_x of germanium sulphide glass, will be helpful in the selection of the deposition temperature for CVD process. In addition, with the understanding of CTE of germanium sulphide glass, it will be useful to choose a CTE compatible substrate.

6.5.1 DTA

A differential thermal analyzer (DTA), Perkin-Elmer DTA7 has been used to scan a temperature range by heating or cooling at a linear rate for the study of endothermal and exothermal reactions. From which we can understand the glass transition temperature (T_g), crystallization temperature (T_x), the peak of crystallization temperature (T_p), and melting temperature (T_m).

In the DTA experiment, we use N_2 as the purging gas at a flow rate of 20ml/min, and the temperature programs are: holding the sample at 50 ^oC for 1min, heating up to 300^oC at a rate of 40^oC/min, holding at 300^oC for 20mins, and then heating up to 900^oC at a rate of 10^oC/min. The measurement principle is based on the difference in temperature between two alumina cups, both of which are seated in individual platinum pans and are at the centre of a uniform temperature furnace. One cup (reference) holds an inert material

(alumina powder), and the other holds a small piece of the glassy sample (of known mass), contained in alumina powder to provide good thermal contact. As the furnace is ramped up, evaluation of characteristic thermal events that require (endothermic) or release (exothermic) heat is recorded as a function of temperature.

In thermal analysis measurements a single glass sample, so as to allow homogeneous heating, measuring 1.5 – 2 mm with mass ~ 10 – 15 mg is required. Heating takes place at a constant rate of 10 ºC/min under nitrogen. The apparatus was calibrated with metal standards (indium and zinc) before any thermal measurements were carried out. Background subtraction was performed for each measurement to eliminate any equipment induced thermal variations. Each data point was extracted over an average of 3 runs on different pieces from the same sample. The results obtained were reproducible with an error margin of ±3 ºC. The DTA thermograms showed distinct events, starting with glass transition (T_g) where glass solid and glass liquid phases intersect, followed by the onset (T_x) of a crystallization peak (T_p) and ending with the onset of a melting event (T_m) (the position of these events depend on the heating rate). Glass transition temperature also has a dependence on the heating rate [51].

The DTA result of germanium sulphide glass by our CVD experiment is shown in the Figure 6.6. The glass transition temperature (T_g), which is the temperature for transition from glass solid phase to glass liquid phase (endothermal reaction), is estimated to be about 456^{o}C. The onset of crystallization temperature (T_x), which is the temperature for transition from glass phase to the most stable crystalline phase (exothermal reaction) is estimated to be about 620^{o}C and the peak of crystallization temperature (T_p) is estimated to be

about 650°C. The melting temperature (T_m), which is the temperature for transition from solid phase to liquid phase (endothermal reaction) is estimated to be about 715°C.

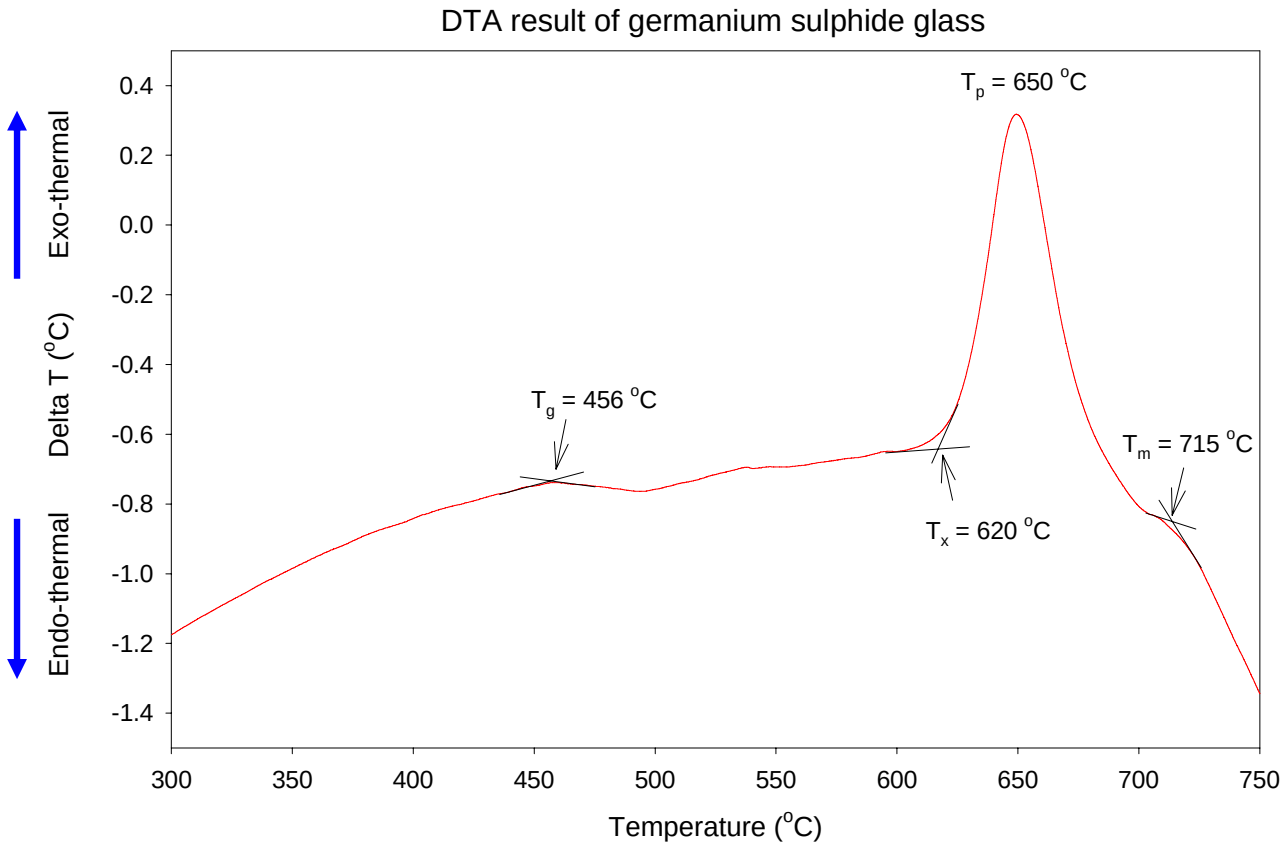

Fig. 6.6 DTA result of germanium sulphide glass

Furthermore, the simple criterion for a good glass for fibre drawing is that the separation of the drawing temperature (T_η) and the crystallization temperature (T_x) should be large (>100°C). However, for two similar glasses a slightly larger T_x-T_η in one does not necessarily mean that the glass will draw to a fibre with less crystallization than the other. The suitability of a glass for fibre drawing is enhanced by a large separation of T_g and T_x , a broad and weak crystallization peak (the half width of the peak is given by T_p-T_x),

and a small separation of T_m and T_p. The reasoning behind this can be readily understood in terms of what is happening to the glass [52]:

The glass transition temperature (T_g) approximates to the intersection of the glass solid and glass liquid phases, so fibre drawing must be carried out at temperatures above T_g. If T_x-T_g is small, the drawing temperature will be close to the temperature for the onset of crystallization, which will probably result in more crystallization in the fibre compared to a glass where this separation is large. If the half width of the crystallization peak (T_p-T_x) is small, then there is a very sharp crystallization event, which implies that only a small structural re-arrangement is required to give crystallization. This makes the glass very unstable with respect to crystallization as the thermodynamic driving force for crystallization is large, and any nucleation sites will immediately grow and propagate rapidly through the glass releasing heat and generating more crystallization. A wide crystallization peak can be thought of as being the superposition of many very sharp crystallization events. Because they all occur at different temperatures, each of these events will occur in a slightly different phase or composition. While the overall thermodynamic driving force for crystallization may be as large as in the case of the narrow crystallization peak, the driving force for each event is smaller resulting in a much slower growth of nuclei. There may also be a kinetic barrier to crystal growth as each phase or crystal growing may compete with neighbouring crystallites for the limited supply of elements available, again resulting in slower growth [52].

The separation of the onset of crystallization (T_x) and the fibre drawing temperature (T_η) gives a strong indication as to how a glass will draw to fibre, with a large value of T_x-T_η generally offering an

easier draw. However, if the half width of the crystallization peak (T_p-T_x) is small, but the separation of the drawing temperature and the onset of crystallization (T_x- T_η) is large, that material may not necessarily draw into fibre more easily than a material with relatively small T_x- T_η but larger T_p-T_x [52].

For fibre drawing, the glass must have a significant viscosity (~10^6 poise). At the melting point T_m, the viscosity of the glass/melt is low (~1 poise). Hence if T_m-T_p is small the viscosity of the glass immediately before crystallization is also low, resulting in fibre drawing temperatures significantly lower than the onset of crystallization. A comparison of the thermal properties of various significant chalcogenide glasses is summarized in Table 6.2 [52]

Glass	T_g (^oC)	T_x-T_g (^oC)	T_p-T_x (^oC)	T_m-T_p (^oC)	T_x-T_η (^oC)
GLS ($65GaS_x$:$2La_2O_3$:$33La_2S_3$)	559	136	20	102	58
GLSO (77.5:22.5)	567	192	62	155	80
GNS (66:34)	490	98	17	104	63
As_2S_3	197	290	60	63	NA
GeAsSeTe	50-200	134-317	NA	NA	>130
GeS_2 (this work)	456	164	30	65	NA

Table 6.2 A comparison of the thermal properties of various chalcogenide glasses

The thermal properties of germanium sulphide glass fabricated by the CVD process in this work are also presented in Table 6.2. Although the T_η of germanium sulphide has not been measured yet, the

separation of T_g and T_x is 164 ^oC, which is a good indication for fibre drawing. In addition germanium sulphide based glasses, GeS_3 [25, 26], Ge-P-S [27], and Ge-Ga-S [43, 44], have been drawn into fibres.

6.5.2 TMA

The coefficient of thermal expansion of germanium sulphide glass was determined using the parallel plate technique [53, 54]. A commercial thermo-mechanical analyser, Perkin-Elmer TMA 7, with high displacement sensitivity (up to 50 nm) and temperature range up to 1000 ºC was used for thermo-mechanical analysis (TMA). A cylindrical sample prepared by the melt-quenching method, as mentioned in the previous section, 5 mm in diameter and 3.38mm in height, is held between two parallel plates of Inconel (0.1 mm thick and 8 mm in diameter). The sample chamber is purged with helium to ensure rapid temperature equilibrium. The coefficient of thermal expansion (CTE) is measured between 50 – 300 ºC (increased at a rate of 5 ºC/min) with a 10 mN load. Heating is from room temperature to the point where the sample begins to deform and the deflection is measured as a function of temperature. The coefficient of thermal expansion (CTE) is derived directly from the gradient of the line as shown in Figure 6.7 and the value of CTE is estimated to be about $12.9x10^{-6}/^oC$.

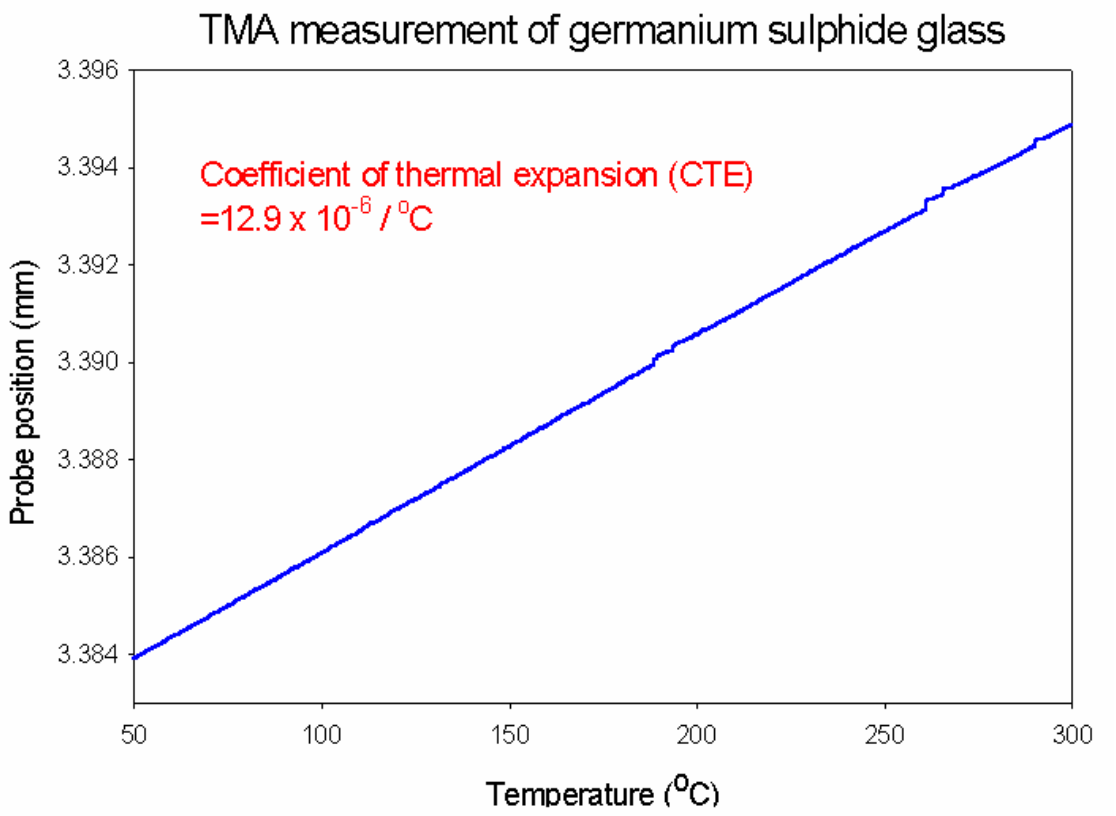

Fig. 6.7 TMA Measurement of germanium sulphide glass

6.6 Summary

Germanium sulphide bulk glass, fabricated by means of CVD at an efficiency of about 50%, has been developed in this chapter. The properties of germanium sulphide bulk glass are summarized in Table 6.3. The optical properties of this glass, studied by UV-VIS-NIR and FT-IR spectroscopy, indicate that the glass has a transmission range from 0.5 to 10.5μm. The results for the purity of germanium sulphide glass measured by GD-MS show exceptionally low levels of transition metal impurities, significantly better than the impurity levels achieved by a conventional fabrication method. Furthermore, the thermal properties of germanium sulphide glass studied, by DTA and TMA,

confirm that this stable glass has a glass transition temperature (T_g) of 456 ^oC, a crystalline temperature (T_x) of 620 ^oC, a melting temperature (T_m) of 715 ^oC, and a coefficient of thermal expansion (CTE) of $12.9x10^{-6}$ /^oC.

Optical properties			
Composition	Transmission Range	R. I. (n)	References
GeS_2	0.5-10.5 μm	2.09 @0.633μm	This work
GeS_2	0.5-10 μm	2.0 @3μm	[57]
GeS_3	0.5-11 μm	2.113	[26, 55]
GeS_4	0.8-5 μm		[56]

Thermal properties				
Composition	T_g (^oC)	T_x (^oC)	CTE ($x10^{-6}/^oC$)	References
GeS_2	456	620	12.9	This work
GeS_2	490	620		[59]
GeS_2			13	[57]
$Ge_{30}S_{70}$	368		14.7	[58]
GeS_3	260	500	25	[26,55,59]
GeS_3	270	520		[60]
GeS_4	170	450		[59]

Table 6.3 Some properties of germanium sulphide glasses

6.7 References

[1] Jas S. Sanghera and Ishwar D. Aggarwal, “Infrared Fiber Optics”, CRC Press, USA, 1998.

[2] Toshio Katsuyama and Hiroyoshi Matsumura, “Infrared Optical Fibers”, IOP publishing Ltd, 1989.

[3] A. K. Mairaj, P. Hua, H. N. Rutt, D. W. Hewak, “Fabrication and characterization of continuous wave direct UV (λ=244 nm) written channel waveguides in chalcogenide (Ga:La:S) glass”, Journal of Lightwave Technology, **20** (2002) 1578-1584.

[4] M.N. Petrovich, A. Favre, D.W. Hewak, H.N. Rutt, A.C. Grippo, J.F. Gubeli I, K.C. Jordan, G.R. Neil, M.D. Shinn, ”Near-IR absorption of Ga:La:S and Ga:La:S:O glasses by FEL-based laser calorimetry”, Journal of Non-Crystalline Solids, **326&327** (2003) 93-97.

[5] J. Requejo-Isidro, A. K. Mairaj, V. Pruneri, D. W. Hewak, M. C. Netti, J.J. Baumberg, “Self refractive nonlinearities in chalcogenide based glasses”, Journal of Non Crystalline Solids, **317** (2003) 241-246.

[6] S. Smolorz, X. Liu, L. Qian, F. Wise, J. Wang, D. Brady, D.W. Hewak, D.N. Payne, “Reduction of optical nonlinearities of Ga-La-S glasses for active fibre applications through addition of CsCl”, Electronics Letters, **34** (1998) 2268-2269.

[7] T. Schweizer, F. Goutaland, E. Martins, D.W. Hewak, W.S. Brocklesby, “Site-selective spectroscopy in dysprosium-doped chalcogenide glasses for 1.3 μm optical fiber amplifiers”, Journal of the Optical Society of America B, **18** (2001) 1436-1442.

[8] T.M. Monro, Y.D. West, D.W. Hewak, N.G.R. Broderick, D.J. Richardson, “Chalcogenide holey fibres”, Electronics Letters, **36** (2000) 1998-2000.

[9] H. Yayama, S. Fujino, H. Takebe, K. Morinaga, D.W. Hewak, “Refractive index dispersion of gallium lanthanum sulfide and oxysulfide glasses”, Journal of Non-Crystalline Solids, **239** (1998) 187-191.

[10] Y.D. West, T. Schweizer, D.J. Brady, D.W. Hewak, “Gallium lanthanum sulphide fibres for infrared transmission”, Fiber and Integrated Optics, **19** (2000) 229-250.

[11] H. Takebe, D.J. Brady, D.W. Hewak, K. Morinaga, “Thermal properties of Ga_2S_3-based glass and their consideration during fiber drawing”, Journal of Non-Crystalline Solids, **258** (1999) 239-243.

[12] D.J. Brady, T. Schweizer, J. Wang, D.W. Hewak, “Minimum loss predictions and measurements in gallium lanthanum sulphide based glasses and fibre”, Journal of Non-Crystalline Solids, **242** (1998) 92-98.

[13] J.R. Hector, J. Wang, D. Brady, M. Kluth, D.W. Hewak, W.S. Brocklesby, D.N. Payne, “Spectroscopy and quantum efficiency of halide-modified gallium-lanthanum sulfide glasses doped with praseodymium”, Journal of Non-Crystalline Solids, **239** (1998) 176-180.

[14] T. Schweizer, B.N. Samson, J.R. Hector, W.S. Brocklesby, D.W. Hewak, D.N. Payne, “Infrared emission from holmium doped gallium lanthanum sulphide glass”, Infrared Physics and Technology, **40** (1999) 329-335.

[15] T. Schweizer, B.N. Samson, J.R. Hector, W.S. Brocklesby, D.W. Hewak, D.N. Payne, “Infrared emission and ion-ion interactions

in thulium and terbium doped gallium lanthanum sulphide glass", Journal of the Optical Society of America B, **16** (1999) 308-315.

[16] T. Schweizer, D.J. Brady, D.W. Hewak, "Fabrication and spectroscopy of erbium doped gallium lanthanum sulphide glass fibres for mid-infrared laser applications", Optics Express, **1** (1997) 102-107.

[17] J. Wang, J.R. Hector, D. Brady, D.W. Hewak, W.S. Brocklesby, M. Kluth, R. Moore, D.N. Payne, "Halide-modified Ga-La sulfide glasses with improved fibre-drawing and optical properties for Pr^{3+}-doped fibre amplifiers at 1.3µm", Applied Physics Letters, **71** (1997) 1753-1755.

[18] T. Schweizer, B.N. Samson, R.C. Moore, D.W. Hewak, D.N. Payne, "Rare-earth doped chalcogenide glass fibre laser", Electronics Letters, **33** (1997) 414-416.

[19] T. Schweizer, D.W. Hewak, B.N. Samson, D.N. Payne, "Spectroscopy of potential mid-infrared laser transitions in gallium lanthanum sulphide glass", Journal of Luminescence, **72** (1997) 419-421.

[20] V. Pruneri, P.G. Kazansky, D.W. Hewak, J. Wang, H. Takebe, D.N. Payne, "Frequency doubling in Ga:La:S optical glass with microcrystals", Applied Physics Letters, **70** (1997) 155-157.

[21] D.W. Hewak, R.C. Moore, T. Schweizer, J. Wang, B.N. Samson, W.S. Brocklesby, D.N. Payne, E.J. Tarbox, "Gallium lanthanum sulphide optical fibre for active and passive applications", Electronics Letters, **32** (1996) 384-385.

[22] D.W. Hewak, J.A. Madeiros-Neto, B.N. Samson, R.S. Brown, K.P. Jedrzejewski, J. Wang, E.R. Taylor, R.I. Laming, G. Wylangowski, D.N. Payne, "Quantum efficiency of praseodymium-doped Ga:La:S glass for 1.3µm optical fibre amplifiers", IEEE Photonics Technology Letters, **6** (1994) 609-612.

[23] A.K. Mairaj, A.M. Chardon, D.P. Shepherd, D.W. Hewak, "Laser performance and spectroscopic analysis of optically written channel waveguides in neodymium-doped gallium lanthanum sulphide glass", IEEE Journal of Selected Topics in Quantum Electronics, **8** (2002) 1381-1388.

[24] N. S. Kapany and R. J. Simms, "Recent developments of infrared fiber optics", Infrared Physics, **5** (1965) 69-75.

[25] S. Shibata, T. Manabe, and M. Horiguchi, "Preparation of Ge-S glass fibers with reduced OH, SH content", Japanese Journal of Applied Physics, **20** (1981) L13-L16.

[26] S. Shibata, Y. Terunuma, and T. Manabe, "Sulfide glass fibers for infrared transmission", Materials Research Bulletin, **16** (1981) 703-714.

[27] S. Shibata, Y. Terunuma, and T. Manabe, "Ge-P-S chalcogenide glass fibers", Japanese Journal of Applied Physics, **19** (1980) L603-L605.

[28] R. Ston, Mir. Vlcek, H. Jain, "Structure and photoinduced changes in bulk and films of As-Ge-S system", Journal of Non-Crystalline Solids, **326&327** (2003) 220-225.

[29] T.S. Kavetskyy, A.P. Kovalskiy, V.D. Pamukchieva, O.I. Shpotyuk, "IR impurity absorption in Sb_2S_3-GeS_2(Ge_2S_3) chalcogenide glasses", Infrared Physics & Technology **41** (2000) 41-45.

[30] B. Zhong, I. Watanabe, and T. Shimizu, "Effect of Sb incorporation in Ge-S glasses", Japanese Journal of Applied Physics, **22** (1983) 780-784.

[31] Z.G. Ivanova, V.S. Vassilev, E. Cernoskova, Z. Cernosek, "Physicochemical, structural and fluorescence properties of Er-doped Ge-S-Ga glasses", Journal of Physics and Chemistry of Solids, **64** (2003) 107-110.

[32] X. Liu, B.B. Kale, V.K. Tikhomirov, A. Jha, "Reduction of OH^--related photoluminescence quenching in Pr^{3+}-doped GeS_2-based glasses by means of purification", Journal of Non-Crystalline Solids, **256&257** (1999) 294-298.

[33] D. Marchese, A. Jha, "The structural aspects of the solubility of Pr^{3+} ions in GeS_2-based glasses", Journal of Non-Crystalline Solids, **213&214 (**1997) 381-387.

[34] B. Frumarova, J. Oswald, P. Krecmer, M. Frumer, V. Cerny, V. Smrcka, "Synthesis and physical properties of the system $(GeS_2)_{80-x}(Ga_2S_3)_{20}$:xPr glasses", Optical Materials, **6** (1996) 217-223.

[35] S.H. Park, J. Heo H.S. Kim, "Compositional dependence of the 1.3μm emission and energy transfer mechanism in Ge-Ga-S glasses doped with Pr^{3+}", Journal of Non-Crystalline Solids, **259** (1999) 31-38.

[36] K. Abe, H. Takebe, K. Morinaga, "Preparation and properties of Ge-Ga-S glasses for laser hosts", Journal of Non-Crystalline Solids, **212** (1997) 143-150.

[37] T. Yu. Ivanova, A. A. Man'shina, A. V. Kurochkin, Yu. S. Tver'yanovich, V.B. Smirnov, "Er^{3+} to glass matrix energy transfer in Ga-Ge-S: Er^{3+} system", Journal of Non-Crystalline Solids, **298** (2002) 7-14.

[38] Yu.S. Tver'yanovich, S.V. Degtyarev, S.S. Pivovarov, V.B. Smirnov, A.V. Kurochkin, "The environment of Nd^{3+}, Sm^{3+}, Yb^{3+} in chalcogenide glasses containing gallium and germanium", Journal of Non-Crystalline Solids, **256&257** (1999) 95-99.

[39] B. Frumarova, M. Frumar, J. Oswald, "Synthesis and properties of GeS_2-Ga_2S_3: $NdCl_3$ and GeS_2-Ga_2S_3: Nd_2O_3 glasses", Journal of Non-Crystalline Solids, **213&214** (1997) 58-62.

[40] J. Heo, Y. B. Shin, "Absorption and mid-infrared emission spectroscopy of Dy^{3+} in Ge-As(or Ga)-S glasses", Journal of Non-Crystalline Solids, **196** (1996) 162-167.

[41] Y.B. Shin, W.Y. Cho, J. Heo, "Multiphonon and cross relaxation phenomena in Ge-As(or Ga)-S glasses doped with Tm^{3+}", Journal of Non-Crystalline Solids, **208** (1996) 29-35.

[42] W.J. Chung, J. Heo, A. Jha, "Effect of alkali halides on the persistent spectral hole burning in Ge-Ga-S glasses doped with Eu^{3+}", Journal of Non-Crystalline Solids, **326&327** (2003) 292-295.

[43] D.R. Simons, A.J. Faber, H. de Waal, "GeS_x glass for Pr^{3+}-doped fiber amplifiers at 1.3 μm", Journal of Non-Crystalline Solids, **185** (1995) 283-288.

[44] K. Wei, D.P. Machewirth, J. Wenzel, E. Snitzer, G.H. Sigel Jr., "Pr^{3+}-doped Ge-Ga-S glasses for 1.3 μm optical fiber amplifiers", Journal of Non-Crystalline Solids, **182** (1995) 257-261.

[45] T. Katsuyama, S. Satoh, and H. Matsumura, "Fabrication of high-purity chalcogenide glasses by chemical vapour deposition", Journal of Applied Physics, **59** (1986) 1446-1449.

[46] E. Sleeckx, P. Nagels, R. Callaerts, and M. Vanroy, "Plasma-enhanced CVD of amorphous Ge_xS_{1-x} and Ge_xSe_{1-x} films", Journal de Physique IV, **3** (1993) 419-426.

[47] Crystran Ltd. UK. (http://www.crystran.co.uk)

[48] J. S. Sanghera and I. D. Aggarwal, "Active and passive chalcogenide glass optical fibers for IR applications: a review", J. Non-Cryst. Solids, **256&257**(1999)6-16.

[49] J. Nishii, T. Yamashita, and T. Yamagishi, "Oxide impurity absorptions in Ge-Se-Te glass fibres", Journal of Materials Science, **24** (1989) 4293-4297.

[50] M. Vlcek, L. Tichy, J. Klikorka, and A. Triska, "Influence of oxygen traces on physical properties of glassy $GeSe_2$", Journal of Materials Science, **22** (1987) 2119-2123.

[51] S.R. Joshi, A. Pratap, N. S. Saxena, M. P. Saksena, and A. Kumar, "Heating rate and composition dependence of the glass transition temperature of a ternary chalcogenide glass", Journal of Materials Science Letters, **13** (1994) 77-79.

[52] D.J. Brady, PhD thesis, "Gallium lanthanum sulphide based glasses for mid-infrared optical fibres", 1999, University of Southampton.

[53] J. Wang, "Glass viscosity and structural relaxation by parallel plate rheometry using a thermal-mechanical analyzer", Materials Letters, **31**(1997)99-103.

[54] A.K. Mairaj, PhD thesis, "Optical waveguides and lasers in improved gallium lanthanum sulphide glass", 2003, University of Southampton.

[55] T. Miyashita, and T. Manabe, "Infrared optical fibers", IEEE Journal of Quantum Electronics, **10** (1982), 1432-1450.

[56] T. Kanamori, Y. Terunuma, S. Takahashi, and T. Miyashita, "Chalcogenide glass fibers for mid-infrared transmission", Journal of Lightwave Technology, **5** (1984) 607-613.

[57] P. N. Kumta and S.H. Risbud, "Novel glasses in rare-earth sulphide systems", Ceramic Bulletin, **69** (1990) 1977-1984.

[58] A. B. Seddon, "Chalcogenide glasses: a review of their preparation, properties, and application", J. Non-Cryst. Solids, **184** (1995) 44-50.

[59] Y. Kawamoto, and S. Tsuchihashi, "Properties and structures of glasses in the system Ge-S", Journal of the American Ceramic Society, **54** (1971) 131-135.

[60] Dennis Simons, PhD thesis, “Germanium gallium sulphide glasses for Pr-doped fiber amplifiers at 1.3μm”, 1995, Eindhoven University of Technology.

Chapter 7

Silver incorporation in germanium sulphide based glass by a photo-dissolution process

7.1 Introduction

A wide range of photo-induced phenomena exhibited by chalcogenide thin films enables them to be utilized in a variety of optical applications [1]. Among these phenomena optically-induced diffusion and dissolution (OIDD), also known in the literature as photo-doping or photo-dissolution of metals such as Ag, Zn, Cu or Cd into amorphous chalcogenide semiconductors has been extensively studied by many researchers [2-14] because of fundamental and technological interests. In the bi-layer or multi-layer metal/chalcogenide structure, light illumination induces fast migration of metal atoms into chalcogenides. Amorphous Ag/$As_{33}S_{67}$ and Ag/$Ge_{30}S_{70}$ films have recently been shown to be useful materials for fabrication of phase gratings and other diffractive optical elements with relief nanostructures [15-17]. There are also other related phenomena in Ag-rich chalcogenide glasses e.g. in ternary systems Ag-As-Se. Ag-As-S, Ag-Ge-S, which exhibit so-called photoinduced surface deposition of metallic Ag, i.e. photoinduced segregation of fine particles on the glass surface [18-23]. Furthermore, it was found that silver-containing chalcogenide film exhibits reversibility in optical writing and thermal erasing of the Ag patterns [24].

Another potential option in optical recording of information is to make use of glasses, or their films, with stoichiometric composition such as $AgAsS_2$ [25] and Ag-As(Ge)-S systems [26, 27]. Such glasses

are potentially applicable to phase-change optical recording based on a phase transition between amorphous and crystalline states [28]. Generally, such a transition can be induced by light exposure of a different energy to perform irreversible or reversible recording. The glasses of Ag-Ge-S, Ag-Ge-Se, Ag-As-S, and Ag-As-Se systems belong to the so-called super ionic conductors [29] and this quality has been demonstrated to be beneficial, e.g. in cell device applications [30].

Furthermore, The OIDD process allows the preparation of chalcogenide films with the silver content in a wide concentration range. Silver dissolution limits in different chalcogenides, made by OIDD process, are shown in Table 7.1 [31]. A silver concentration increase leads to a red shift of the optical absorption edge and the refractive indices increase with increasing silver content [4]. However, there is still no publication concerning waveguide fabrication by using this OIDD process. Therefore, an attempt to fabricate Ag-doped chalcogenide glass channel waveguides by using the OIDD process has been initiated.

Composition	**Diffusion Conc. Limits of Ag by OIDD (%)**
$As_{33}S_{67}$	30
$As_{30}S_{70}$	31
$As_{30}Se_{70}$	20
$Ge_{30}S_{70}$	25
$Sb_{33}S_{67}$	10
$Ge_{10}Sb_{30}S_{60}$	7

Table 7.1 Limits of the silver concentration obtained by OIDD in different chalcogenide systems

In this study, the germanium sulphide glass thin films were deposited on Schott N-PSK58 glass substrates by the CVD process. Channel structures were then formed by the photo-lithography process by patterning in photoresist, after which a 10nm thick layer of Ag was deposited on the germanium sulphide glass film by thermal evaporation. This was followed by the photo-dissolution process, after which the residual photo-resist was removed by acetone. Ag-doped germanium sulphide glass channel waveguides were demonstrated with a loss of 0.67± 0.05 dB/cm at 632.8nm.

7.2 Ag coating by thermal evaporation deposition

The Ag thin film coating on the germanium sulphide glass planar waveguide was prepared by thermal evaporation deposition. An Edward coater was used to carry out this deposition process. The raw material, Ag wire, was 99.99% pure from Agar Scientific. The Ag wire was wound around the tungsten filament and the germanium sulphide glass thin film was situated just above the Ag source in the vacuum chamber. Deposition took place under vacuum with a pressure about $1x10^{-6}$ mbar. The deposition was controlled by a film thickness monitor (gold coated quartz sensor, Z value=16.7 and density=10.5 for Ag) at a rate of 0.1nm/sec. Therefore a 10nm thick Ag layer can be achieved in 100 seconds.

7.3 Set-up for Ag photo-dissolution process

As for the OIDD mechanism suggested by D. Goldschmidt and P.S. Rudman [32], the light must be absorbed in the Ag metal and the photon absorption in the Ag layer generates hot electrons, which travel a distance of their mean-free path (several hundred Å). Then hot

electrons, surmounting the barrier between the chalcogenide and the Ag, enter the chalcogenide behind Ag^+ ions. Therefore, the generated electrostatic attraction enhances the transfer of Ag^+ to the chalcogenide. Inside the chalcogenide, transport of Ag^+ occurs either by diffusion or is enhanced by the electric field at the the doped-undoped interface.

The set-up for the Ag photo-dissolution process is shown in Figure 7.1. A white light (150W tungsten-halogen lamp) was used as the source, passing through an infrared filter (KG1 type glass, 350-700nm short-pass filter) to illuminate the Ag layer coated on germanium sulphide glass thin film. The infrared filter was used to reduce thermal effects. However, the OIDD process can be conducted without the infrared filter. The illumination time for the Ag to completely dissolve into the germanium sulphide glass film varied from one to several hours depending on the thickness of Ag layer.

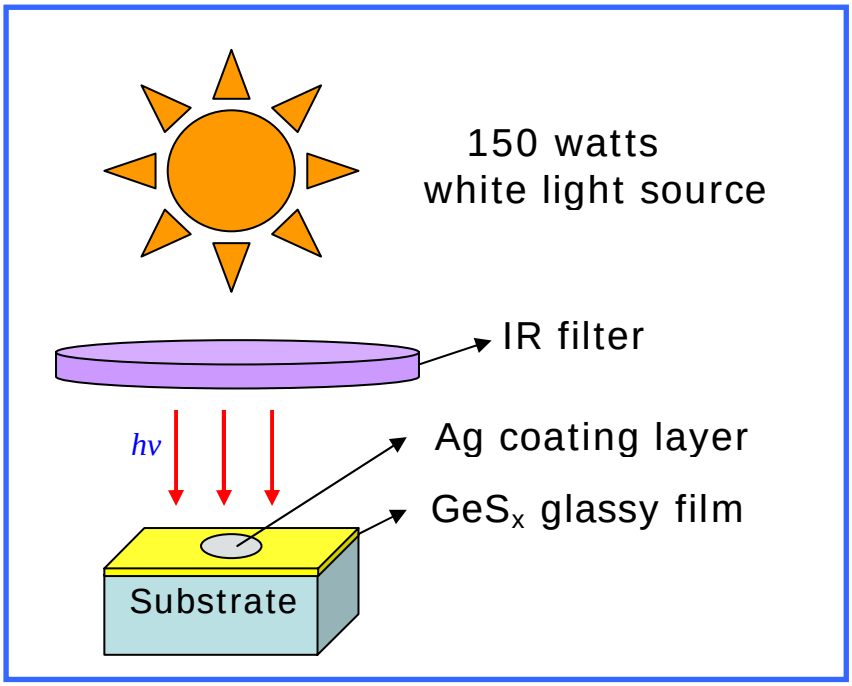

Fig. 7.1 Set-up for Ag photo-dissolution process

7.4 Refractive index change measurement

The refractive index (n) of germanium sulphide glass and Ag doped germanium sulphide glass waveguides were measured from the transmission spectra using a method suggested by Swanepoel [33]. The refractive index and film thickness of the germanium sulphide glass waveguide (run 35) have been measured by Swanepoel's method (details in Chapter 5).

In order to study the refractive index change of a Ag doped germanium sulphide film, for the first trial, a 42nm thick Ag layer was deposited on the germanium sulphide glass planar waveguide by thermal evaporation and this was followed by the photo-dissolution process. The refractive index of the Ag doped germanium sulphide glassy film was determined by the same single transmission method and compared with the original germanium sulphide glass thin film (Figure 7.2).

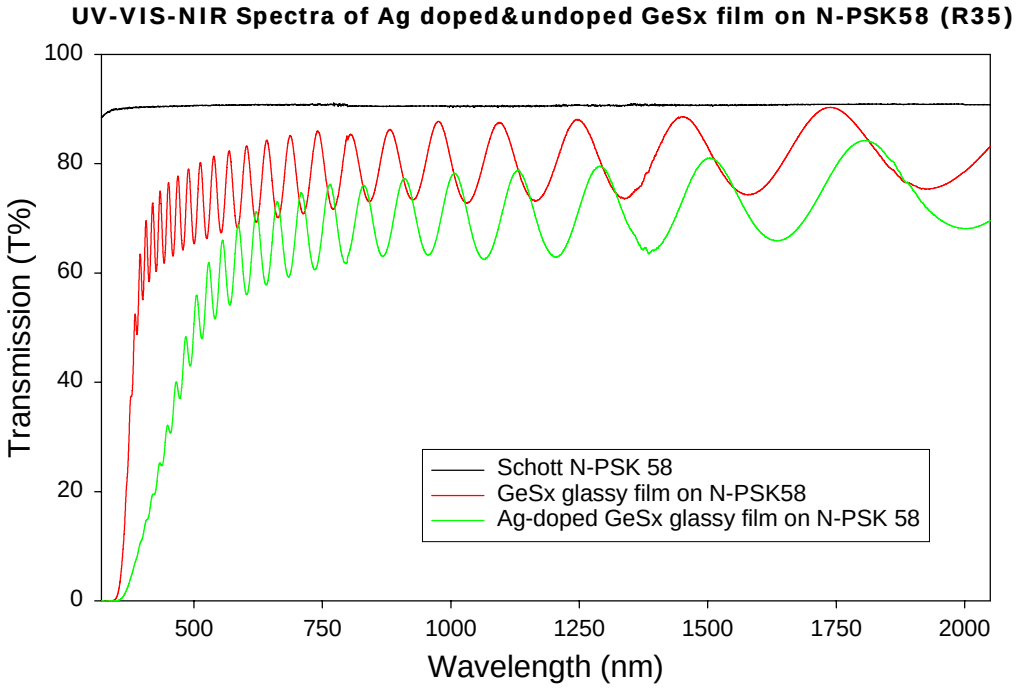

Fig. 7.2 UV-VIS-NIR spectra of germanium sulphide glass and Ag doped germanium sulphide glass planar waveguides

The refractive index of germanium sulphide glass and Ag doped germanium sulphide glass waveguides were shown in the Figure 7.3. As the results shown in Figure 7.3, the refractive index of Ag doped germanium sulphide glass film has been increased by the photo-dissolution process and the refractive index change (Δn) between Ag doped germanium sulphide glass and germanium sulphide glass waveguides is about 0.2.

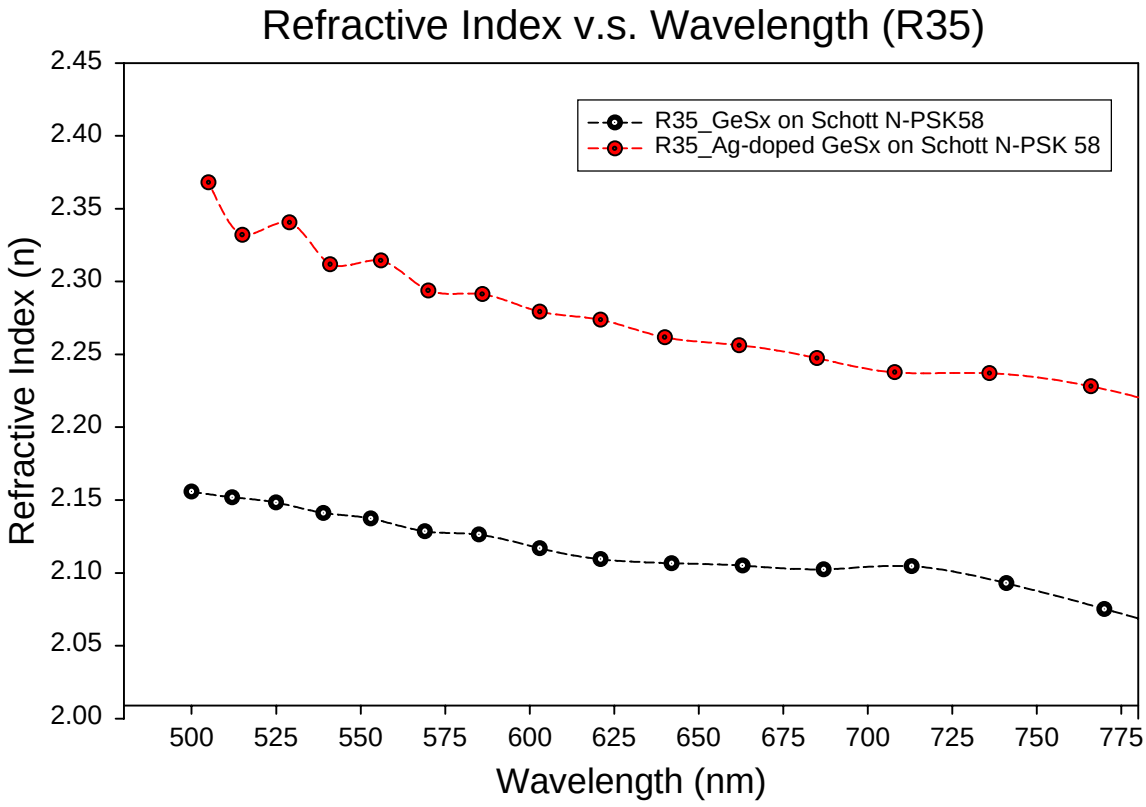

Fig. 7.3 Refractive index of germanium sulphide glass and Ag doped germanium sulphide glass planar waveguides (from 42nm thick Ag coated layer)

In order to reduce the refractive index change (Δn) between Ag doped germanium sulphide glass and germanium sulphide glass waveguides, a 10nm thick Ag coated germanium sulphide glass planar wavegude was prepared by the thermal evaporation process and

followed by the photo-dissolution process. As the results shown in Figure 7.4, the Δn has been reduced to a range from 0.02 to 0.05 depending on the wavelengths.

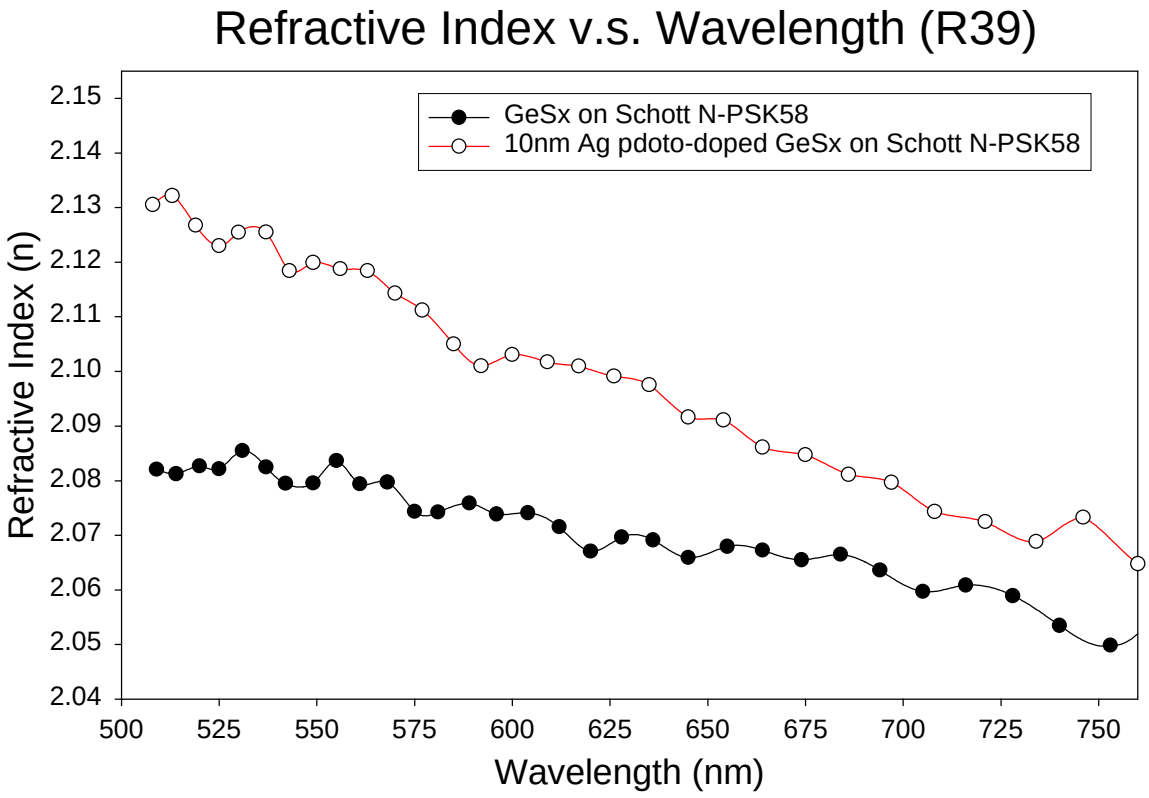

Fig. 7.4 Refractive index of germanium sulphide glass and Ag doped germanium sulphide glass planar waveguides (from 10 nm thick Ag coated layer)

7.5 Ag-doped channel waveguides

From the previous work on silver diffusion into planar films, we now have confidence that the Ag photo-dissolution process can be applied to locally increase the refractive index of a germanium sulphide thin film and thereby define channel waveguides in the glass. We

fabricated Ag doped germanium sulphide glass channel waveguides achieved by the photolithography process, then deposited a 10nm Ag layer on the germanium sulphide glass film. This was followed by the photo-dissolution process, and finally removal of residual photo-resist. The fabrication procedures are shown schematically in the Figure 7.5.

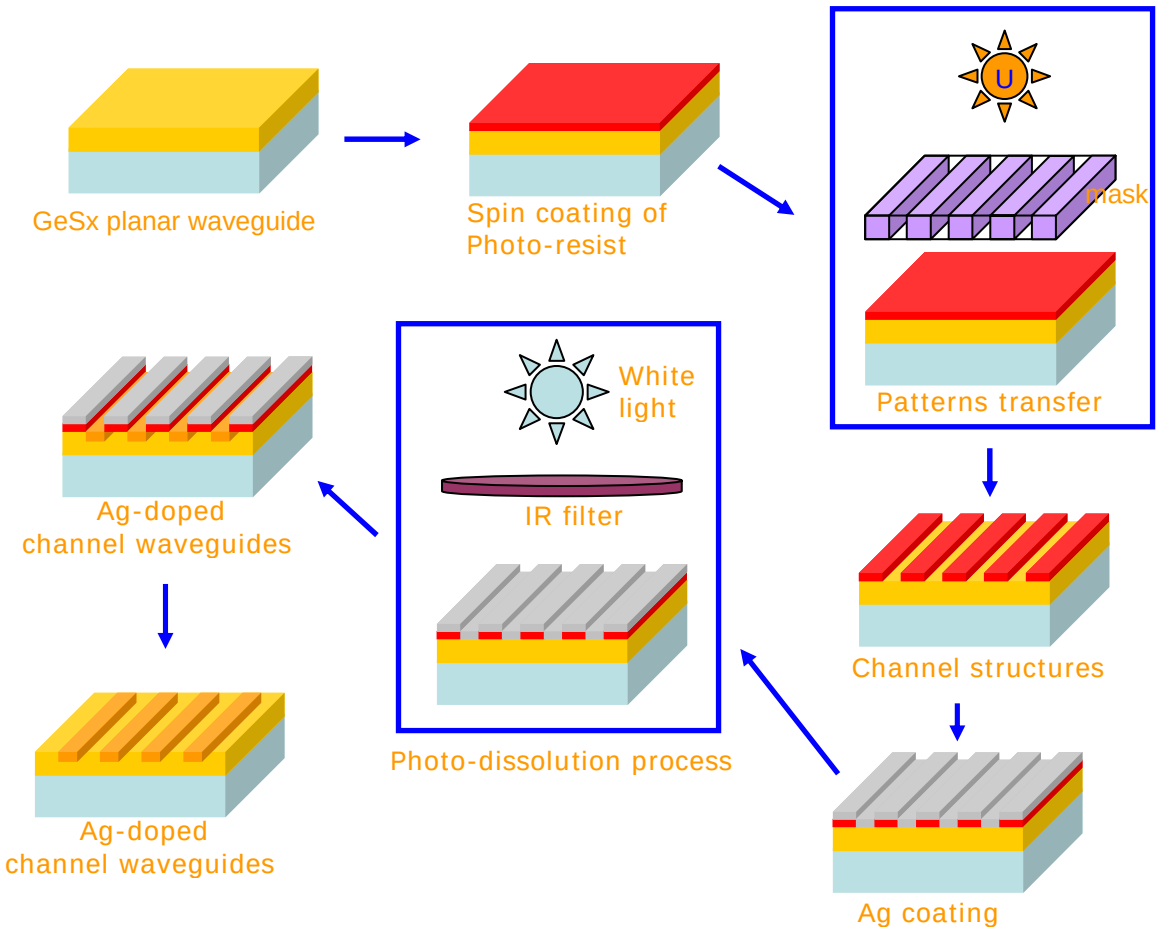

Fig. 7.5 Fabrication procedures for Ag doped germanium sulphide glass channel waveguides

The Ag doped germanium sulphide glass channel waveguides were initially evaluated by an optical microscope with a magnification of 20 and 40. As the photographs show in Figure 7.6, Ag doped germanium sulphide channel waveguides with a width of 5μm have been fabricated

by the CVD, photolithography, thermal evaporation, and photo-dissolution process.

Ag-doped channel GeS_x glass waveguides

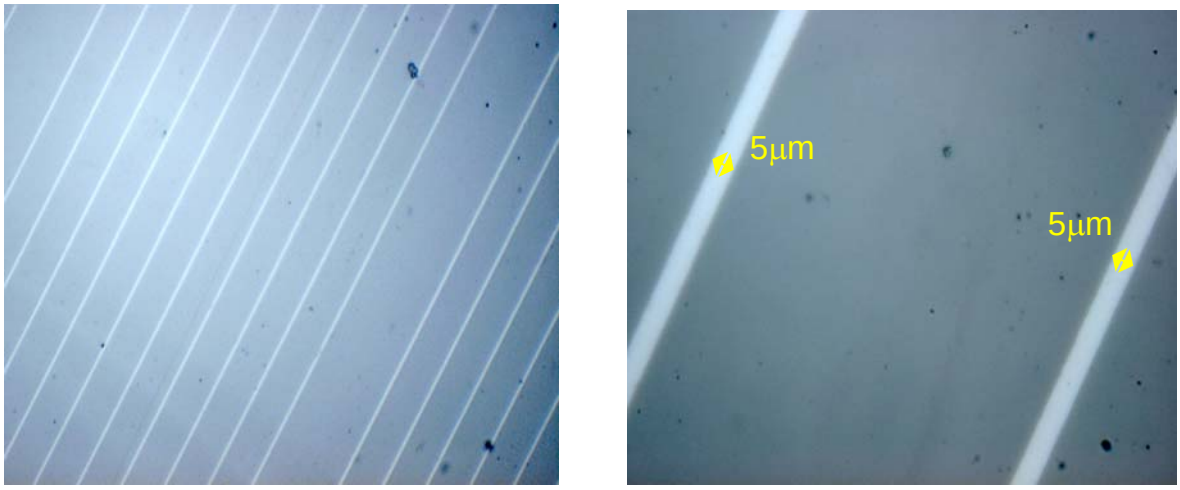

Fig. 7.6 Ag doped germanium sulphide glass channel waveguides

7.6 Waveguide attenuation

The attenuation of Ag doped germanium sulphide channel waveguides was measured by the fibre coupling technique with a He-Ne laser at the wavelength of 632.8nm as in the setup shown in Figure 7.7. The image taken by a CCD camera was converted to the pixel intensity along the length and the attenuation was fitted by linear regression. As the results show in Figure 7.8, the attenuation of Ag doped germanium sulphide glass channel waveguides was 0.67±0.05 dB/cm at 632.8nm.

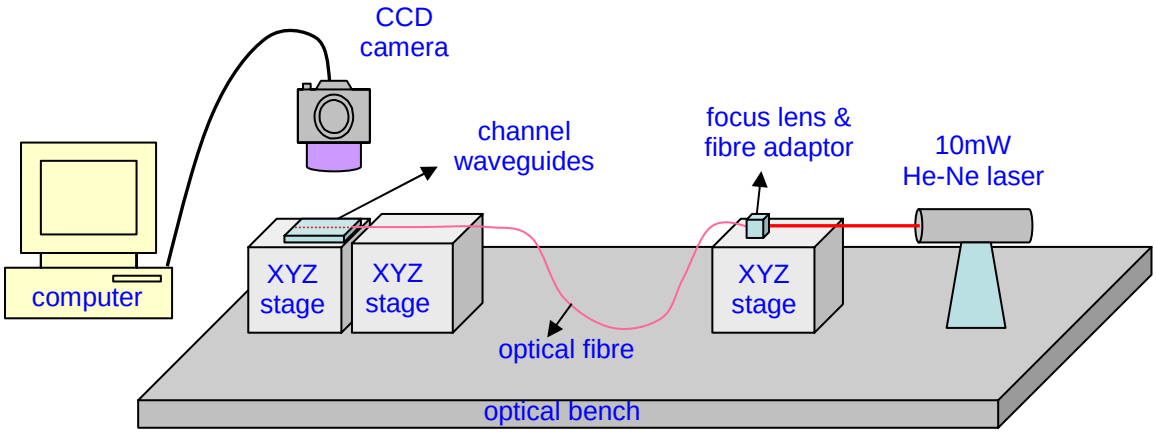

Fig. 7.7 Setup for waveguide attenuation measurement

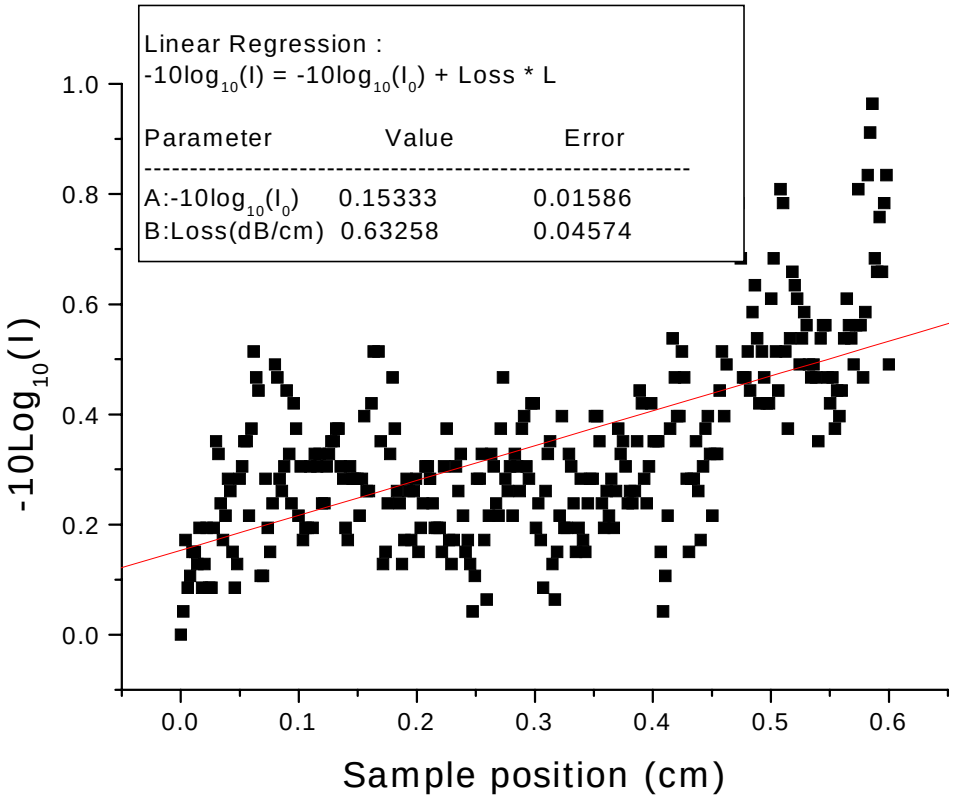

Fig. 7.8 Attenuation of Ag dope germanium sulphide glass channel waveguides at 632.8nm

7.7 Summary and future work

In this Chapter, the refractive index of germanium sulphide glass film was calculated directly from the transmission spectrum by UV-VIS-NIR spectroscopy. Also, the refractive index of germanium sulphide glass film can be modified by Ag incorporation by a photo-dissolution process.

Furthermore, Ag-doped germanium sulphide glass channel waveguides with the loss of 0.67±0.05 dB/cm at 632.8nm have been demonstrated by the CVD, photo-lithography, thermal evaporation, and photo-dissolution process.

The preliminary results indicate the potential for applications in optoelectronics, especially in integrated optic circuits and optical storage. However, the diffusion profile of silver doped channel waveguides still needs to be further investigated. A suggestion for the non-destructive measurement of the silver diffusion profile is the Rutherford backscattering spectrometry. Unfortunately we do not have this facility at the ORC. In addition, the influence of further thermal annealing of silver doped germanium sulphide channel waveguides also needs to be studied.

7.8 References

[1] Keiji Tanaka, “Photoinduced processes in chalcogenide glasses”, Current Opinion in Solid State & Materials Science, **1** (1996) 567-571.

[2] M. Mitkova, M.N. Kozichi, H.C. Kim, and T.L. Alford, “Thermal and photodissolution of Ag in S-rich GeS amorphous films”, Thin Solid Films, **449** (2004) 248-253.

[3] R. Wang, and J. H. Horton, “Photo-diffusion of silver in germanium sulfur compounds studied by AFM, nanoindentation, and RBS methods”, Phys. Chem. Chem. Phys., 2003, **5**, 4335-4342.

[4] T. Wagnar, J. Gutwirth, M. Krbal, Mir. Vlcek, Mil. Vlcek, and M. Frumar, “ Ag-Sb-S amorphous chalcogenide thin films prepared by optically induced dissolution and diffusion of silver”, Journal of Non-Crystalline Solids, **326&327** (2003) 238-242.

[5] V.Lyubin, M. Klebanov, A. Arsh, N. Froumin, and A.V. Kolobov, “Photoinduced diffusion of Zn in chalcogenide glassy films”, Journal of Non-Crystalline Solids, **326&327** (2003) 189-192.

[6] H.Y. Lee, J.K. Kim, and H.B Chung, “On Ag-doping in amorphous Sb_2S_3 thin film by HeNe and HeCd laser exposures and its optical characteristics”, Journal of Non-Crystalline Solids, **279** (2001) 209-214.

[7] E. Marquez, T. Wagner, J. M. Gonzalez-Leal, A. M. Bernal-Oliva, R. Prieto-Alcon, R. Jimenez-Garay, and P. J. S. Ewen, “Controlling the optical constants of thermally-evaporated $Ge_{10}Sb_{30}S_{60}$ chalcogenide glass films by photodoping with silver”, Journal of Non-Crystalline Solids, **274** (2000) 62-68.

[8] A. I. Stetsun, I. Z. Indutnyi, and V. G. Kravets, "Infrared absorption of Ag- and Cu-photodoped chalcogenide films", Journal of Non-Crystalline Solids, **202** (1996) 113-121.

[9] T. Kawaguchi and S. Maruno, "Composition dependence of Ag photodoping into amorphous Ge-S films", J. Appl. Phys., **71** (1992) 2195.

[10] C.A. Lucas, "X-ray scattering studies of the photodissolution of silver in chalcogenide glasses", J. Phys. Appl. Phys., **24** (1991) 928-936.

[11] A.Zekak, P.J.S. Ewen, C.W. Slinger, A.E. Owen, "The effect of heat on the metal photodissolution process in amorphous $As_{40}S_{60}$ films", Journal of Non-Crystalline Solids, **202** (1996) 122-127.

[12] J. Fernandez-Pena, J. B. Ramirez-Malo, J. J. Ruiz-Perez, C. Corrales, E. Marquez, P. Villares, R. Jimenez-Garay, "On the Ag-photodissolution phenomenon in $As_{0.35}S_{0.65}$ chalcogenide glass films", Journal of Non-Crystalline Solids, **196** (1996) 173-177.

[13] T. Wagner, G. Dale, P. J. S. Ewen, A. E. Owen, V. Perina, "Kinetics of the thermally and photoinduced solid state reaction of Ag with $As_{33}S_{67}$ films", Journal of Applied Physics, **87** (2000) 7758-7767.

[14] M. Jannai, "Photodissolution of silver in amorphous As_2S_3 films", Physical Review Letters, **47** (1981) 726-729.

[15] T. Wagnar and P.J.S. Ewen, "Photo-induced dissolution effect in $Ag/As_{33}S_{67}$ multilayer structures and its potential application", Journal of Non-Crystalline Solids, **266-269** (2000) 979-984.

[16] T.Wagnar, S. Schroeter, T. Glaser, and Mir. Vlcek, "Holographic grating preparation in $Ag/As_{30}S_{70}$ multilayer and bilayer

structures", Journal of Non-Crystalline Solids, **326&327** (2003) 500-504.

[17] T. Wagnar, G. Dale, P.J.S. Ewen, A.E. Ewen, and V. Perina, "Kinetics of the thermally and photoinduced solid state reaction og Ag with $As_{33}S_{67}$ films", Journal of Applied Physics, **87** (2000) 7758.

[18] T. Kawaguchi, S. Maruno, and S.R. Elliott, "Optical, electrical, and structural properties of amorphous Ag-Ge-S and Ag-Ge-Se films and comparison of photoinduced and thermally induced phenomena of both systems", J. Appl. Phys., **79** (1996) 9096.

[19] T. Kawaguchi, "Thermodynamic consideration for photoinduced surface deposition of Ag-As-S glasses", Jpn. J. Appl. Phys., **40** (2001) 567-568.

[20] T. Kawaguchi, "Photoinduced surface deposition of Ag-Ge-S films: its enhancement by addition of small amount of Au", Jpn. J. Appl. Phys., **37** (1998) 6318-6321.

[21] T. Kawaguchi, S. Maruno, "Photosurface deposition of Ag on Ag-rich Ag-Ge-S films:Analysis of change in the optical transmission spectra", Jpn. J. Appl. Phys., **36** (1997) L85-L88.

[22] T. Kawaguchi and S. Maruno, "Photoinduced surface deposition of metallic silver in Ag-As-S glass", Journal of Applied Physics, **77** (1995) 628-634.

[23] T. Kawaguchi and S. Maruno, "Kinetic study of metallic silver photoinduced surface deposition phenomenon", Jpn. J. Appl. Phys., **33** (1994) 3417-3418.

[24] T. Kawaguchi, and S. Maruno, "Reversible photowriting and thermal erasing of Ag patterns on Ag-rich Ag-GeS films", Jpn. J. Appl. Phys., **33** (1994) 6470-6474.

[25] T. Wagner, M. Frumar, S.O. Kasap, Mir Vlcek, Mil Vlcek, "New Ag-containing amorphous chalcogenide thin films-prospective

materials for rewriteable optical memories", Journal of Optoelectronics and Advanced Materials, **3** (2001) 227-232.

[26] T. Kawaguchi, "photoinduced surface deposition of ag on Ag-rich Ag-Ge-S films: Optimal Ag content and film thickness for application in optical recording devices", Appl. Phys. Lett., **72** (1998) 161.

[27] T. Kawaguchi and S. Maruno, "Photoinduced surface deposition of metallic silver: basic research for its application to optical recording devices", Jpn. J. Appl. Phys., **33** (1994) 4521-4525.

[28] T. Ohta, "Phase-change optical memory promotes the DVD optical disk", Journal of Optoelectronics and Advanced Materials, **3** (2001) 609-626.

[29] E. Robinel, "Silver sulphide based glasses (I). glass forming regions, structure and ionic conduction of glasses in GeS_2-Ag_2S and GeS_2-Ag_2S-AgI systems", Journal of Non-Crystalline Solids, **57** (1983) 49-58.

[30] M. Mitkova, M.N. Kozicki, "Silver incorporation in Ge-Se glasses used in programmable metallization cell devices", Journal of Non-Crystalline Solids, **299-302** (2002) 1023-1027.

[31] A.V. Kolobov, "Photo-induced meta-stability in amorphous semiconductors", WILEY-VCH, 2003.

[32] D. Goldschmidt and P. S. Rudman, "The kinetics of photo-dissolution of Ag in amouphous As_2S_3 films", Journal of Non-Crystalline Solids, **22** (1976) 229-243.

[33] R. Swanepoel, "Determination of the thickness and optical constants of amorphous silicon", J. Phys. E: Sci. Instrum., **16** (1983) 1214.

Chapter 8

Conclusion and future work

8.1 Conclusion

This thesis presents the research work of the development of germanium based sulphide glass waveguides and bulk glass by means of chemical vapour deposition (CVD).

Germanium sulphide glass films have been deposited on some selected substrates, including CaF_2, Schott N-PSK 58, silica on silicon, GeO_2/silica on silicon, and GeO_2 on silicon, by a hot-wall CVD process that was developed as part of this work. The thermodynamic analysis of the deposition of germanium sulphide glass from the reaction between $GeCl_4$ and H_2S indicates that this CVD process is feasible and that the yield would be better at higher temperatures. The parameters of the hot-wall CVD experiment have been optimized and the deposition temperature for germanium sulphide glass from the reaction between $GeCl_4$ and H_2S was typically set at 500 ^oC for a deposition efficiency of ~12μm/hr. This allows deposition of a thin film suitable for an OIC in ~ 15minutes. The reactive gas, H_2S, and the carrier gas for $GeCl_4$, argon, are delivered through the mass flow controllers (MFC) at the typical flow rate of 100 ml/min with the $H_2S/GeCl_4$ molar ratio of 2~3.

The composition and structure of germanium sulphide glass films investigated by micro-Raman and X-ray diffraction (XRD) certify that these films are in a glassy phase and free of crystalline and are of the composition of $GeS_{2\pm0.2}$. A scanning electron microscope (SEM)

technique was used to study the surface morphology of the germanium sulphide glass films which indicate that the films are homogeneous. The refractive index of germanium sulphide glass films studied by prism coupling and single transmission techniques show that this glass has a refractive index of ~2.1 at 632.8nm. Also, in this research work, the first chalcogenide glass planar waveguide fabricated by hot-wall CVD has been demonstrated with a propagation loss of 2.1±0.3 dB/cm at 632.8nm. In addition, germanium sulphide glass planar waveguides with channel structures have been fabricated by photolithography and dry-etching techniques.

A process of fabricating high purity germanium sulphide bulk glass by chemical vapour deposition and a conventional melt-quenching method has been developed at an efficiency of about 50%. The results for the purity of germanium sulphide glass measured by GD-MS show exceptionally low levels of transition metal impurities significantly better than the impurity levels achieved by a conventional method and by commercially available chalcogenides. The optical properties of this glass, studied by UV-VIS-NIR and FT-IR spectroscopy, indicate that the glass has a transmission range from 0.5 to 10.5μm (Table 6.3). Moreover, the thermal properties of germanium sulphide glass studied by DTA and TMA certify that this stable glass has a glass transition temperature (T_g) of 456 ^oC, a onset of crystallization temperature (T_x) of 620 ^oC, a melting temperature (T_m) of 715 ^oC, and a coefficient of thermal expansion (CTE) of $12.9x10^{-6}$ /^oC.

Furthermore, a process for Ag-doped germanium sulphide glass channel waveguides has been established by the CVD, photo-lithography, thermal evaporation, and photo-dissolution process. The refractive index of Ag incorporated germanium sulphide glass films has

been calculated directly from the transmission spectrum by UV-VIS-NIR spectroscopy. Also, the refractive index of germanium sulphide glass film can be modified by Ag incorporation by a photo-dissolution process. A Ag-doped germanium sulphide glass channel waveguides with a loss of 0.67±0.05 dB/cm at 632.8nm measured by the fibre coupling technique has been demonstrated.

8.2 Future work

Although some results have been achieved in this work, there is considerable scope for future work, which will be discussed in the following sections.

8.2.1 Direct writing

Germanium sulphide glasses similar to other chalcogenide glasses, are amorphous semiconductors and have a number of states in the bandgap, which reflect structural disorders. In chalcogenide glasses, due to their structural flexibility and strong electronic-lattice interaction, the defects take various forms which depend on their environments and many of the states in the bandgap consist of the defect states. The structural flexibility also enables chalcogenide glasses to have a many-minima structure in their potential energy and a high sensitivity to external stimuli such as light and heat. Therefore, by irradiation of the bandgap or sub-bandgap light, various photosensitive phenomena are induced in chalcogenide glasses [1-3]. Particularly, the photo-bleaching phenomenon has been reported in the germanium sulphide based glasses [4-6].

By exploiting this special photosensitive property of germanium sulphide glass, we can use a UV direct-writing or f-s laser writing techniques [7-13] to make channel waveguides and integrated circuit structures in germanium sulphide thin films on a selected substrate. From the UV-VIS-NIR spectrum shown in Figure 8.1, the absorption edge of germanium sulphide glass has been estimated at ~425nm (2.9 eV) which means that a 850nm f-s laser would be the best candidate tool to write these photosensitive structures, by means of two-photon absorption, which has been intensively studied by E. Mazur *et al.*[14].

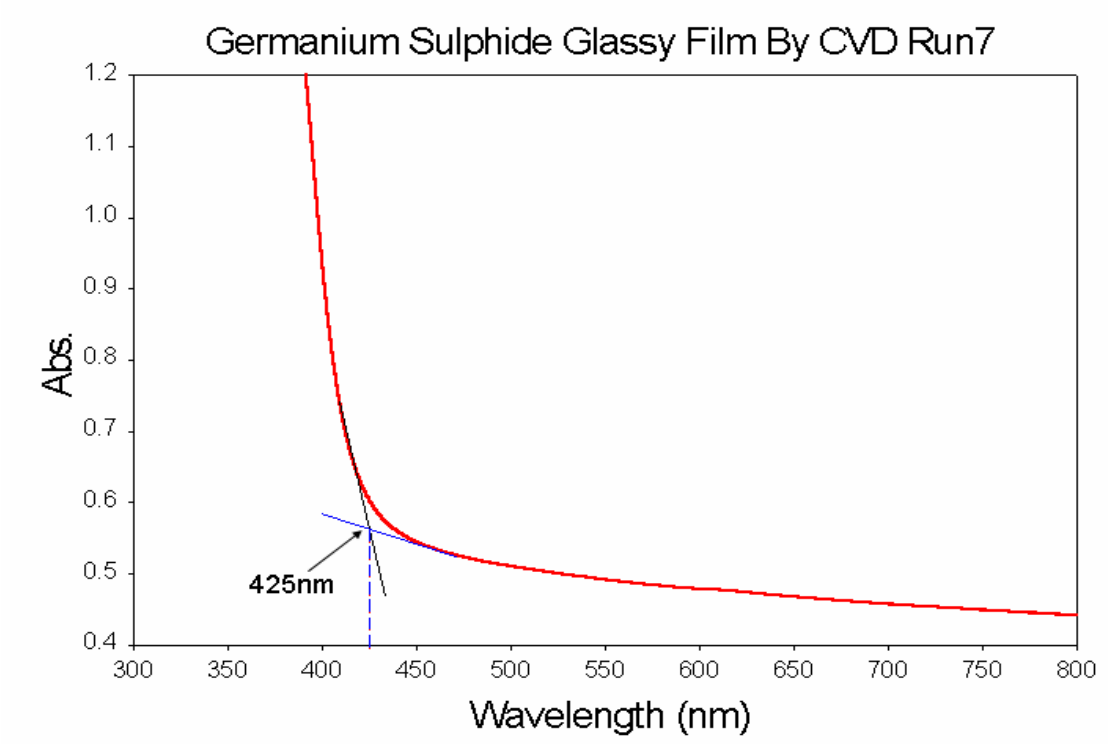

Fig. 8.1 UV-VIS spectrum of germanium sulphide glass by CVD run7

8.2.2 Cold-wall CVD

The main work in this research was conducted using a hot-wall CVD system. As described in chapter 4 and chapter 5, the deposition occurred on both the substrate and the inner wall of the reactor in the

hot-wall CVD system. A cold-wall CVD process was proposed in this section to provide a cleaner deposition of germanium sulphide glass on selected substrates as shown in Figure 8.2. The original cold-wall CVD reactor was made of borosilicate glass which would be safe below 550 ^{o}C. The heat coils from Elmatic Ltd [15] can be controlled by a temperature controller with a maximum temperature of 750±1 ^{o}C. With this cold-wall CVD system, we hope that a better quality of germanium sulphide glass film can be fabricated.

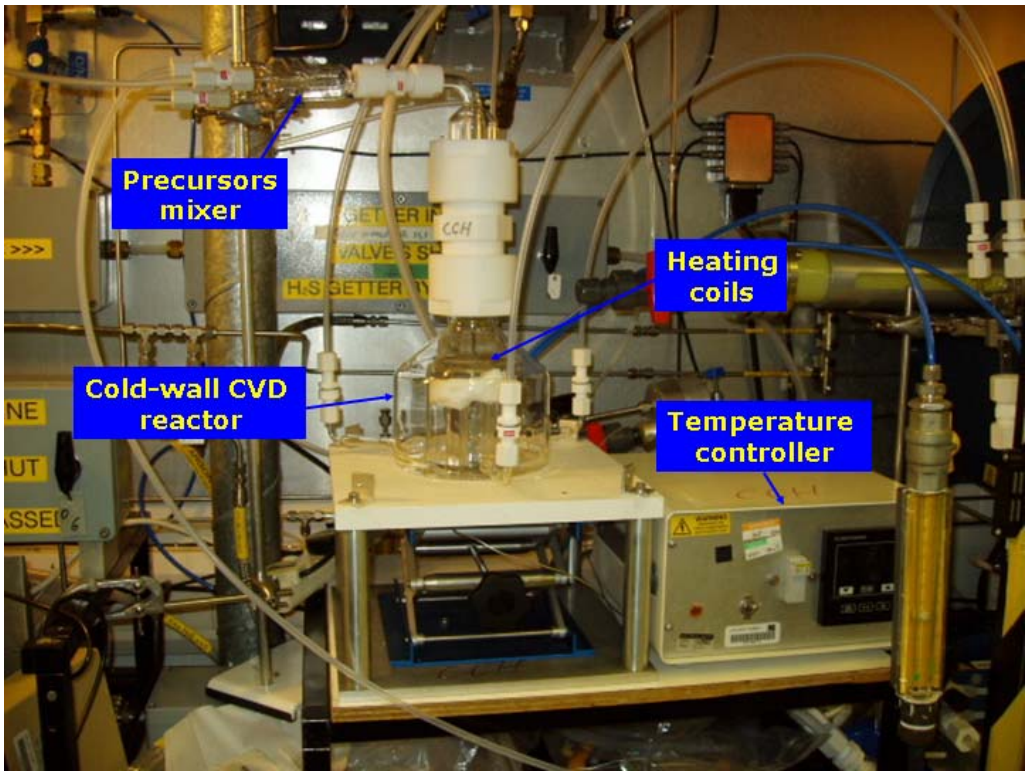

Fig. 8.2 Prospective cold-wall CVD system

8.2.3 Fibre fabrication

Although the high purity germanium sulphide bulk glass has been fabricated by the hot-wall CVD system and conventional melt-quenching, it would be more desirable to fabricate optical fibres from the fibre preform or crucible drawings [16, 17].

8.2.4 Modification of germanium based sulphide glasses

As described in the chapter 6, germanium sulphide glass can form stable ternary glasses with P, Sb, Ga, etc. For example, Sb can be used to increase the refractive index of germanium sulphide glass and form more stable Ge-Sb-S glasses. A proposed thermodynamic analysis of forming Sb_2S_3 from the reaction between $SbCl_5$ and H_2S (Eq.8.1) is presented in Table 8.1 (Gibb's free energy data from ref.18).

$$2\ SbCl_5 + 3\ H_2S \longrightarrow Sb_2S_3 + 6\ HCl + 2\ Cl_2 \qquad \text{(Eq. 8.1)}$$

	Room Temp.	500 K	800 K
ΔG (kJ/mol), Cl_2	0	0	0
ΔG (kJ/mol), HCl	-95.293	-97.158	-99.452
ΔG (kJ/mol), Sb_2S_3	-140.293	-136.844	-125.146
ΔG (kJ/mol), H_2S	-33.329	-40.179	-45.694
ΔG (kJ/mol), $SbCl_5$	-328.73	-288.697	-230.822
ΔG (kJ/mol), reaction of Sb_2S_3	45.396	-21.861	-123.132
Equilibrium constant (K)	1.098×10^{-8}	189.132	1.035×10^{8}

From the thermodynamic analysis, the formation of Sb_2S_3 from the reaction between $SbCl_5$ and H_2S is not spontaneous at room temperature, however as the temperature increased, the reaction becomes more and more favourable at higher temperatures. Therefore, if we introduced $GeCl_4$ and $SbCl_5$ precursors to react with H_2S at the same time, if would be possible to control the composition of Ge-Sb-S glasses in the CVD process.

8.3 References

[1] M. Seki, K. Hachiya, and K. Yoshida, "Photoluminescence and states in the bandgap of germanium sulphide glasses", J. Non-Cryst. Solids, **315** (2003) 107-113.

[2] O.M. Efimov, L.B. Glebov, K.A. Richardson, E.V. Stryland, T. Cardinal, S.H. Park, M. Couzi, J.L. Bruneel, "Waveguide writing in chalcogenide glasses by a train of femtosecond laser pulses", Optical Materials, **17** (2001) 379-386.

[3] Keiji Tanaka, "Sub-gap excitation effects in As_2S_3 glass", J. Non-Cryst. Solids, **266-269** (2000) 889-893.

[4] R. Todorov, Tz. Iliev, K. Petkov, "Light-induced changes in the optical properties of thin films of Ge-S-Bi(Tl,In) chalcogenides", Journal of Non-Crystalline Solids, **326&327** (2003) 263-267.

[5] Q. Liu, and F. Gan, "Photobleaching in amorphous GeS_2 thin films", Materials Letters, **53** (2002) 411-414.

[6] E. Marquez, A. M. Bernal-Oliva, J. M. Gonzalez-Leal, R. Prieto-Alcon, R. Jimenez-Garay, "On the reversible photo-bleaching phenomenon in obliquely-evaporated GeS_2 glass films", Journal of Non-Crystalline Solids, **222** (1997) 250-257.

[7] D. Homoelle, S. Wielandy, A. L. Gaeta, N. F. Borrelli, and C. Smith, "Infrared photosensitivity in silica glasses exposed to femtosecond laser pulses", Optics Letters, **24** (1999) 1311-1313.

[8] A.K. Mairaj, P. Hua, H.N. Rutt, D.W. Hewak, "Fabrication and characterization of continuous wave direct UV (λ=244nm) written channel waveguides in chalcogenide (Ga:La:S) glass", Journal of Lightwave Technology, **20** (2002) 1578-1584.

[9] J.W. Chan, S.H. Risbud, J.S. Hayden, D.M. Krol, "Waveguide fabrication in phosphate glasses using femtosecond laser pulses", Applied Physics Letters, **82** (2003) 2371-2373.

[10] R. Osellame, S. Taccheo, M. Marangoni, R. Ramponi, and P. Laporta, "Femtosecond writing of active optical waveguides with astigmatically shaped beams", J. Opt. Am. B, **20** (2003) 1559-1567.

[11] R. Osellame, S. Taccheo, G. Cerullo, M. Marangoni, D. Polli, R. Ramponi, P. Laporta, S. De Silvestri, "Optical gain in Er-Yb doped waveguides fabricated by femtosecond laser pulses", Electronics Letters, **38** (2002) 964-965.

[12] D. M. Krol, "Waveguide fabrication in glasses using femto-second laser pulses", Glass Science and Technology, **75** (2002) 164-180.

[13] O.M. Efimov, L.B. Glebov, K.A. Richardson, E. Van Stryland, T. Cardinal, S.H. Park, M. Couzi, J.L. Bruneel, "Waveguide writing in chalcogenide glasses by a train of femtosecond laser pulses", Optical Materials, **17** (2001)379-386.

[14] Mazur group (http://mazur-www.harvard.edu)

[15] ELMATIC (CARDIFF) LIMITED (http://www.elmatic.info)

[16] Jas S. Sanghera and Ishwar D. Aggarwal, "Infrared Fiber Optics", CRC Press, USA, 1998.

[17] Toshio Katsuyama and Hiroyoshi Matsumura, "Infrared Optical Fibers", IOP publishing Ltd, 1989.

[18] Ihsan Barin, "Thermochemical Data of Pure Substances", 3rd edition, VCH, 1995.

Appendix I

Publications:

[1] C. C. Huang, D. W. Hewak, J. V. Badding, "Deposition and characterization of germanium sulphide glass planar waveguides", Optics Express, **12** (2004) 2501-2505.

[2] C.C. Huang, D.W. Hewak, "High purity germanium sulphide glass for optoelectronic applications synthesized by chemical vapour deposition", Electronics Letters, **40** (2004) 863-865.

[3] C.C. Huang, D.W. Hewak, and J.V. Badding, "Direct synthesis of germanium sulphide glass planar waveguides by chemical vapour deposition (CVD)", CLEO/IQEC 2004 San Francisco 16-21 May 2004.

[4] R.J. Curry, A.K. Mairaj, C.C. Huang, R.W. Eason, C. Grivas, J.V. Badding, D.W. Hewak, "Chalcogenide glass thin films and planar waveguides", Journal of American Ceramic Society, 2004 (accepted).

[5] R.J. Curry, C.C. Huang, A.K. Mairaj, R.E. Simpson, D.W. Hewak, "Advancing the application of planar chalcogenides", AcerS. Glass & Optical Materials Div., Fall 2004 Meeting Florida Nov 2004.

[6] A.K. Mairaj, C.C. Huang, R.J. Curry, R.W. Eason, C. Grivas, J.V. Badding, D.W. Hewak, "Through thick and thin: recent developments with chalcogenide films", The American Ceramic

Society: Glass and Optical Materials Division Fall Meeting Corning 12-15 Oct 2003 (invited).

[7] C. C. Huang, D. W. Hewak, J. V. Badding, "Properties and application of germanium sulphide glass", PREP 2003 Exeter 14-16 Apr 2003.

Patents:

[1] D.W. Hewak, C.C. Huang, J.V. Badding, "Synthesis of germanium sulphide and related compounds", (filed).

Appendix II: Optimization of germanium sulphide parameters by CVD

	Precursors	Carrier Gas & Flow Rate	Reactive Gas & Flow Rate	Furnace Temp. (^oC)	Run Time (mins)	Film Thickness (μm)	Deposition Rate (μm/hr)	Molar Ratio $H_2S/GeCl_4$	SEM-EDX GeS_x, x
CVD run1	$GeCl_4$	Ar (100 mL/min)	Ar (100mL/min) H_2S (100mL/min)	450	77	0.9	0.7	~9.7	1.66±0.01
CVD run2	$GeCl_4$	Ar (100mL/min)	Ar (100mL/min) H_2S(100mL/min)	500	64	8	7.5	~9.7	1.69±0.01
CVD run3	$GeCl_4$	Ar (40mL/min) + H_2S(20mL/min)		500	283	67.9	14.4	~3.5	1.72±0.02
CVD run4	$GeCl_4$	H_2S(50mL/min)		800	180	No Deposition on Reactor	Nil	~10.4	Nil
CVD run5	$GeCl_4$	H_2S(50mL/min)		600	150	crystalline	Nil	~10.4	Nil
CVD run6	$GeCl_4$	H_2S(50mL/min)		550	120	74.8	37.4	~10.4	3.5 ?
CVD Run7	$GeCl_4$	H_2S(50mL/min)		575	60	Crystalline on substrates	Nil	~10.4	Nil
CVD Run8	$GeCl_4$	H_2S(50mL/min)		550	50	Rough glassy film on substrates (not transparent)	Nil	~10.4	Nil
CVD Run9	$GeCl_4$	H_2S(50mL/min)		500	60	Rough glassy film on substrates (not transparent)	Nil	~10.4	Nil
CVD Run10	$GeCl_4$	H_2S(50mL/min)		520	60	Crystalline on CaF_2 substrates (not transparent)	Nil	~10.4	Nil
CVD Run11	$GeCl_4$	H_2S(50mL/min)		450	60	Rough glassy film on substrates (not transparent), 0.77-0.99μm	0.77-0.99	~10.4	Nil
CVD Run12	$GeCl_4$	H_2S(50mL/min)		350	150	Crystalline on substrates (not transparent)	Nil	~10.4	Nil
CVD Run13	$GeCl_4$	H_2S(50mL/min)		400	120	Crystalline on substrates (not transparent)	Nil	~10.4	Nil
CVD Run14	$GeCl_4$	Ar (50mL/min)	H_2S(150mL/min)	450	110	Yellow film on substrates?	Nil	31.26	Nil
CVD Run15	$GeCl_4$	Ar (50mL/min)	H_2S(150mL/min)	400	120	Crystalline on substrates (not transparent)	Nil	31.26	Nil
CVD Run16	$GeCl_4$	Ar (50mL/min)	H_2S(150mL/min)	800 / RT*	45	Ge & S crystalline	Nil	31.26	Nil
CVD Run17	$GeCl_4$	Ar (40mL/min) + H_2S(20mL/min)		500	40	Germanium sulphide glass on quartz (7.09μm) & CaF_2 substrate(9.04μm)	10.64μm/hr on quartz & 13.56μm/hr on CaF_2	~3.5	Quartz, 1.74±0.01 CaF_2,1.75±0.01
CVD Run18	$GeCl_4$	Ar (90mL/min) + H_2S(10mL/min)		500	23	Germanium sulphide glass 3.87 & 4.84μm on CaF_2 substrate1 & 2	10.1 & 12.36 μm/hr of CaF2 substrate 1 & 2	0.97	S1,1.71±0.01 s2,1.72±0.01
CVD Run19	$GeCl_4$	Ar (80mL/min) + H_2S(20mL/min)		500	30	Germanium sulphide glass 6.96 & 8.62μm on CaF_2 substrate1 & 2	13.92 & 17.23 μm/hr of CaF2 substrate 1 & 2	2.32	Nil
CVD Run20	$GeCl_4$	Ar (80mL/min) + H_2S(20mL/min)		500	113	Germanium sulphide glass 24.5 & 22.4μm on CaF_2 substrate1 & 2	13.03 & 11.91 μm/hr of CaF2 substrate 1 & 2	2.27	Nil
CVD Run21	$GeCl_4$	Ar (80mL/min) + H_2S(20mL/min)		475	20	Germanium sulphide glass 1.94 & 2.19 & 2.42μm on CaF_2 substrate1 & 2 & 3	5.82 & 6.58 & 7.27 μm/hr of CaF2 substrate 1 & 2 & 3	2.10	1.71±0.01
CVD Run22	$GeCl_4$	Ar (80mL/min) + H_2S(20mL/min)		500	150	Semi-transparent germanium sulphide glassy films	Nil	2.80	Nil

*RT: room temperature